UNIVERSITY OF OKLAHOMA

GRADUATE COLLEGE

THERMAL PERFORMANCE OF SANDSTONE RESERVOIRS FOR THERMAL ENERGY STORAGE: AN INTEGRATED EXPERIMENTAL AND ANALYTICAL STUDY.

A DISSERTATION

SUBMITTED TO THE GRADUATE FACULTY

In partial fulfillment of the requirements for the

Degree of

DOCTOR OF PHILOSOPHY

By

CESAR VIVAS

Norman, Oklahoma

2023

THERMAL PERFORMANCE OF SANDSTONE RESERVOIRS FOR THERMAL ENERGY STORAGE: AN INTEGRATED EXPERIMENTAL AND ANALYTICAL STUDY.

A DISSERTATION APPROVED FOR THE

MEWBOURNE SCHOOL OF PETROLEUM AND GEOLOGICAL ENGINEERING

BY THE COMMITTEE CONSISTING OF

Dr. Saeed Salehi, Chair

Dr. Hamidreza Karami

Dr. Mashhad Fahes

Dr. Reza Foudazi

© Copyright by CESAR VIVAS 2023
All Rights Reserved.

Acknowledgment

What a wonderful time I spent at the University of Oklahoma!! I want to express my deepest gratitude to my advisor, Dr. Saeed Salehi, for his unwavering support, guidance, and patience in helping me complete my research and other projects. Dr. Salehi has been with me from day one and has provided me with the necessary support, time, sponsorship, and feedback that has motivated me to learn and grow beyond what I thought possible. I am sincerely thankful and will forever be in your debt.

I am also grateful to my committee members, Dr. Hamidreza Karami, Dr. Mashhad Fahes, and Dr. Reza Foudazi, for their valuable feedback. I am thankful to the University of Oklahoma and the Mewbourne School of Petroleum and Geological Department for the opportunity to learn and grow as a professional and individual and for allowing me to connect with exceptional individuals.

I sincerely thank those who participated in my experimental research, especially Esteban Ugarte and Zeming (Christal) Hu, wonderful teammates, and forever friends. I am particularly grateful for the assistance given by Jeff McCaskill and Gary Stowe for the laboratory support during my experimental research. I would not have been able to achieve the results without your unwavering support.

I extend my appreciation to the U.S. Department of Energy's Office of Energy Efficiency and Renewable Energy (EERE) under the Geothermal Program Office for funding all my research.

I also want to thank my friends and teammates for their support and motivation, and my family, especially my wife Lina and my sons Martin and Tomas, for your unwavering love. You are my greatest motivation, strength, and support. I love you deeply. Finally, I extend my thanks to my mother for her guidance in my journey thus far; I am indebted to her for everything.

Table of Contents

List of Figures

List of Tables

Abstract

With the global plans of decarbonization in motion, major energy players and large oil and gas (O&G) companies are moving towards increasing energy generation from non-fossil sources. The implementation of renewable energy has a critical constraint, the intermittent nature of the renewables. Energy storage systems help overcome the seasonal intermittence of renewable power generation sources. Besides, thermal energy storage (TES) systems can optimize renewable energy management, providing equilibrium between energy generation and demand. For utility-scale projects, the TES systems must be capable of storing an extensive amount of heat.

The thermal capability of subsurface rocks to store heat makes them an optimal option for energy storage. A subsurface thermal energy storage can store the energy surplus generated by solar and wind plants. The energy excess is used to heat a heat transfer fluid; then, this fluid is injected into the geothermal sedimentary reservoir. When solar or wind cannot generate energy or the demand is higher than production, the energy stored in the thermal battery is extracted for thermal direct use or power generation. Subsurface TES can store a considerable quantity of energy at a reasonable cost. Sedimentary formations in oil and gas basins offer multiple advantages for being TES solutions. O&G basin sands are i) deep enough to store water at high pressure, ii) usually offer higher porosity (storage capacity) and higher permeability (flow capacity) than volcanic rocks or shales, iii) the water stored is confined by sealing rocks, and iv) the sedimentary reservoirs frequently offer large volumes to store the hot water.

This dissertation aims to evaluate the thermal performance of sandstone reservoirs for thermal energy storage applications. The research encompasses a comprehensive experimental analysis of 30 sandstone samples, encompassing petrophysical and thermal rock properties, rock

mineralogy, and rock texture analyses. The specific objectives are: i) establish connections between the porosity, permeability and density of sandstone rocks and their thermal behavior, with a focus on thermal energy storage applications, ii) Establish correlations between the mineralogy and other rock properties, such as thermal properties and textural features, to comprehend the influence of mineral composition on the sandstone's behavior and performance iii) understand the relationships between textural properties and thermal properties, and iv) evaluate the impact of the natural heterogeneity of sandstone properties in the thermal energy storage reservoir performance.

1. Introduction

1.1 Background

Recently, the interest in increasing renewable energy generation has been growing rapidly. The downside is that these sources of energy are affected by weather and seasonal factors, limiting their capability to provide baseload power generation (Vivas et al., 2020). **Figure 1** depicts the seasonality of solar and wind energy generation. The installed capacity of these renewable power generation energy sources has strong and steady growth. However, the energy generated shows a component of variability that affects their ability to provide energy steadily in all-year seasons.

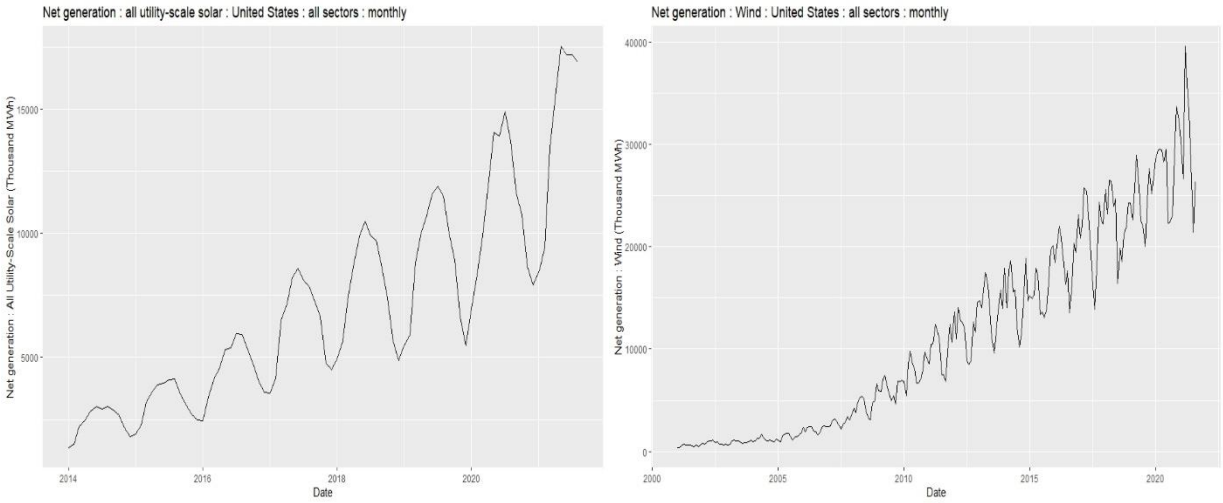

Figure 1. Historical generation of utility-scale solar power (2014-2021) [left], and wind power (2001-2021) [right] generated with information from the EIA.

Wind and solar energy are intermittent renewable energy sources that cannot be stored but must be used as they become available to avoid losing their energy potential. These renewable sources provide instantaneous energy that needs to be changed into another form of energy to be stored (Evans et al., 2012). The variable nature of renewable energy supply sources and conditional variations in the quantity of energy consumed over time have highlighted the need for energy storage systems (Suberu et al., 2014). TES systems support energy management by storing the surplus of

energy produced from renewable energy sources in the form of heat. When solar or wind cannot generate enough energy, the heat stored in the geothermal battery is extracted to produce energy.

High temperature subsurface thermal energy storage has 50 years of development. The International Energy Agency's (IEA) Storage program launched the first research tests to combat rising fuel prices following the 1973 oil crisis (Fleuchaus et al., 2020). This technology has been termed in various technical names: underground thermal energy storage -UTES- (Gluyas et al., 2020), high temperature subsurface thermal energy storage -HSTES- (Zheng, 2014), geologic thermal energy storage -GeoTES- (Neupane et al., 2020), aquifer thermal energy storage -ATES- (Mindel and Driesner, 2020) which is the most common name found in the literature. From now, in the present study the sedimentary reservoir thermal energy storage -SRTES- term will include all the above mentioned systems and refers to the thermal energy storage where the heat transfer fluid is stored in a subsurface sedimentary reservoir.

SRTES systems have been proposed as complement of solar systems. SRTES offers opportunities to store solar energy from daily cycles to seasonal cycles (Alva et al., 2018; Bauer et al., 2010; Cruickshank and Baldwin, 2016; Xu et al., 2014).

Sedimentary basins offer large reservoir volumes to store heat, and they are available in extensive areas throughout the US (Idaho National Laboratory, 2006). The concept of storing heat in sedimentary reservoirs was considered for reducing the impact of the seasonal variation of solar energy's capacity factor since the 70s (Collins, 1977; Molz et al., 1980, 1976; Rabbimov et al., 1971; Tsang et al., 1977).

Sedimentary reservoir thermal energy storage projects for elevated to high temperatures (HT-SRTES) in shallow sedimentary aquifers have been developed since the early 80s', but most of them are not operative. The SRTES projects have proven the feasibility of the concept; however,

further research is needed to move from low-medium temperatures storing systems to high temperatures large-scale applications (Vangkilde-Pedersen and Kallesøe, 2019).

There are some conditions that affect the performance of the SRTES. Experimental research has established that hot water production generates mineral deposits that affect the aquifer porosity and permeability (Bershaw et al., 2020; Bonte et al., 2013; García-Gil et al., 2016; Jin et al., 2022; Neupane et al., 2021; Rosenbrand et al., 2014). The potential reduction of reservoir transmissibility can affect enthalpy production in the long term. The duration of the storage period is essential to have an efficient TES system in the long time (Nordell, 1994).

A good formation with the potential to be a TES reservoir needs to offer enough volume to contain a large volume of the working fluid. The rock must let the heat transfer fluid flow across the reservoir during the injection and production stages, and the reservoir pressure must be enough to contain the heat transfer fluid in liquid phase or in supercritical conditions (Green et al., 2021).

Despite the promising results in SRTES studies, more research is still required to analyze the feasibility of TES systems in sedimentary basins. This study will evaluate the influence of different sandstones in SRTES performance. For TES implementation in sedimentary formations, sandstones offer better thermal properties than shales, claystones, and shales. Besides, sandstones usually offer better permeability than other sedimentary rocks. Through extensive experimentation and analysis, this study aims to provide valuable insights for leveraging sandstone reservoirs in thermal energy storage applications, contributing to the sustainable and efficient utilization of geothermal energy. The aim is to understand the influence of sandstone properties in TES systems' performance.

1.2 Problem Statement and Motivation

Despite the general interest in SRTES projects to improve the capability of renewable energy sources to produce a sustainable baseload power supply, the overall implementation can still be considered low. The concept of storing heat in underground reservoirs come from the early 70's (Rabbimov et al., 1971). Today, the global TES installed capacity is 234 gigawatt-hour (DOE, 2023), less than 0.01% of the solar and wind energy combined global installed capacity of 3427 terawatt-hour (Energy Institute, 2023).

SRTES projects can play a vital role in effectively managing and utilizing surplus energy generated from renewable sources, while also meeting peak energy demands. While SRTES has shown promise at smaller scales, its widespread implementation at utility scales has been limited. One of the most important barriers to the successful utility-scale SRTES implementation is the insufficient understanding of rock properties (Kallesøe et al., 2019). Utility-scale TES requires suitable geological formations capable of storing and efficiently releasing thermal energy. The lack of comprehensive data on rock properties hinders the identification of suitable reservoirs for large-scale SRTES (Matos et al., 2019).

There are several technical barriers to the SRTES implementation, especially related to the underground reservoir properties that can be summarized as follows: i) The first and foremost technical barrier is the geological suitability of the site. For SRTES, the subsurface should have appropriate geological formations that can store and retrieve thermal energy efficiently (Winterleitner et al., 2018). This includes suitable permeability, porosity, thermal conductivity, and thermal capacity of the geological formations. Unsuitable geological conditions can severely limit the effectiveness of SRTES systems. ii) Thermal interference between different boreholes in close proximity is another major technical issue (Llanos et al., 2015). The operation of multiple SRTES

systems in close proximity can lead to overlapping thermal plumes, which can reduce the efficiency of energy storage and recovery. Thermal interference can result in increased energy losses and reduced system performance (Mindel and Driesner, 2020; Zhou et al., 2016). iii) SRTES systems can have significant impacts on local hydrogeology. These impacts can include changes to groundwater flow patterns, which can affect thermal energy storage and recovery (Shi et al., 2016). And iv) the long-term performance of SRTES systems can be affected by non-uniformities in the thermal properties, due to heterogeneity in the geology, that can lead to thermal breakthroughs and preferential flow paths that reduce system performance and lead to decreased system performance over time (Bridger and Allen, 2014). The understanding of the interaction between mineralogy, petrophysics, and thermal properties of sandstone rocks, as SRTES reservoir rocks, have impact in the described technical barriers.

The mineralogy and petrophysics of sandstone rocks can affect their permeability, porosity, thermal conductivity, and thermal capacity, which are crucial factors in determining the suitability of a site for SRTES systems. Sandstone rocks with high porosity and permeability can provide adequate space for thermal energy storage and retrieval, while rocks with low thermal conductivity may require additional materials to enhance heat transfer. The thermal properties of sandstone rocks can affect the efficiency of energy storage and recovery in SRTES systems. Rocks with high thermal conductivity can help to reduce thermal interference between boreholes, while rocks with low thermal capacity may require additional thermal energy storage materials. The properties of sandstone rocks can affect the impact of SRTES systems on local hydrogeology. Rocks with high permeability can lead to changes in groundwater flow patterns, which can affect thermal energy storage and recovery. The mineralogy and petrophysics of sandstone rocks also affect the long-term performance of SRTES systems.

For improving the reservoir characterization of thermal energy storage reservoirs, there are some research gaps in the understanding of the rock properties:

- Lack of representation of heterogeneity: In laboratory research, it has been observed that porosity and permeability significantly influence rock thermal properties, resulting in high heterogeneity. Failure to adequately represent the heterogeneity of both petrophysical and thermal properties limits the understanding of rock properties for thermal energy storage reservoir characterization.
- Limited integration of rock properties: the overlook of the interrelationship between mineralogy, texture, petrophysical and thermal properties of rocks hinder the ability to accurately characterize thermal energy storage reservoirs.
- Absence of focus on sandstone reservoirs: while various rock types have been analyzed in laboratory research on rock properties, there is a notable absence of studies specifically targeting sandstone reservoirs with an extensive sample. Understanding the unique characteristics and behavior of sandstone reservoirs is crucial, as sandstones offer multiple advantages in TES implementations.

1.3 Study Objectives

In this dissertation, the interaction between mineralogy, petrophysical and thermal properties in sandstone rocks for SRTES is analyzed. Following are the specific objectives:

- Investigate the reservoir type more adequate for SRTES.
- Using experimental laboratory tests to acquire the mineralogy, petrophysical and thermal properties of 30 rock samples.
- Analyze the interrelations between properties and their influence on the SRTES performance.

- Understand the influence of morphology and textural rock properties in the thermal properties of the sandstones analyzed.
- Use the experimental results to build a 3D model with heterogeneous petrophysical and thermal properties to perform sensitivity analysis to analyze the factors that affect SRTES performance.

This dissertation presents (i) an analysis of the reason choosing sandstone rocks as ideal sedimentary reservoirs for utility scale thermal energy storage; (ii) an experimental research for calculating mineralogy, petrophysical and thermal properties of the 30 sandstone rock samples; (iii) a data analysis and interrelationships between the rock properties evaluated; (iv) textural properties of rocks extracted from SEM images and their relationship with thermal properties of rocks; and (v) simulation of a 3D model generated with the data obtained in the experimental study to evaluate how heterogeneity, seasonal cycling and temperature affects the efficiency of the SRTES.

1.4 Research Hypotheses

The research hypotheses are based on the available studies in literature discussing underground thermal energy storage. The following hypotheses are considered in this research study:

- Sandstone rocks have better thermal conductivity and thermal diffusivity compared with shales and carbonates.
- Rocks with higher quartz content will have better thermal conductivity. Quartz has one of the highest thermal conductivities among common rock-forming minerals, so rocks with more quartz will conduct heat more efficiently.
- Sandstone rocks have higher storage capacity and transmissibility capacity compared with shales and carbonates.

- Uniform thermal properties throughout the reservoir TES for even heat distribution are ideal, however, sedimentary rocks are very heterogeneous.

1.5 Research Scope and Methodology

This study consists of four main parts to cover the work scope and attain the main objectives of this study. These parts include a comprehensive literature review, experimental study, data analysis and SEM study. The workflow of this study is shown in **Figure 2**, and the scope of each part is discussed in the following sections.

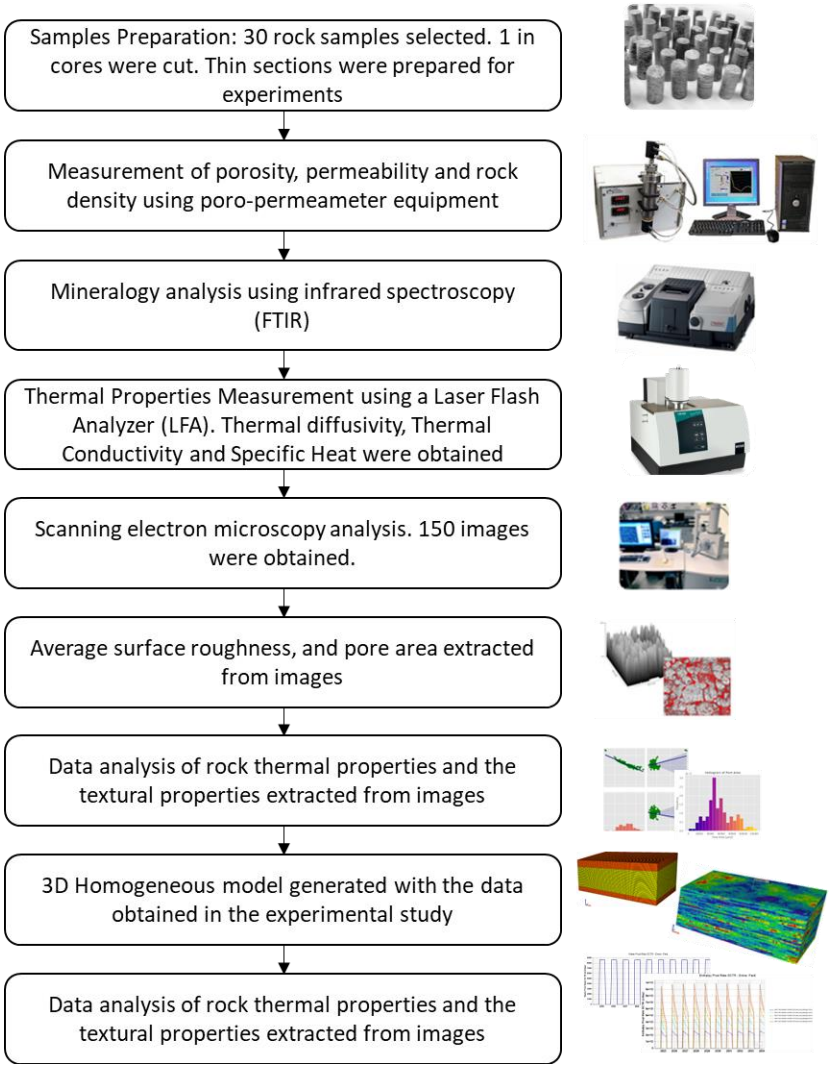

Figure 2. Workflow of the research

i. ***Literature Review***: The primary objective of this task is to examine the mechanisms involved in thermal energy storage within sedimentary rocks, summarize the laboratory experimental studies and discusses the criteria for evaluating the suitability of subsurface rocks for thermal energy storage. The section also examines various SRTES configurations, well setups, thermal cycles, and other factors that impact the performance of sedimentary thermal energy storage. The objective is to identify the challenges and current gaps related with the understanding of sedimentary rocks properties for thermal energy storage evaluation.

ii. ***Experimental Study***: In this task, three phases of experiments were conducted to evaluate the rock properties that impact the SRTES reservoir performance. In the first phase samples of sandstone rocks were prepared to obtain porosity, permeability, and density. In the second phase of experiments, mineralogy of the rocks was analyzed using FTIR equipment. In the third phase of experiments, thin sections of the samples were extracted to obtain their thermal properties using a LFA equipment.

iii. ***Data Analysis Study***: In this task the data generated is used to analyze the rock properties and mineralogy together with thermal properties. In this section the results per mineral and per core sample are examined and study the individual patterns between properties. The benefit of analyzing the thermal properties of rocks by individual minerals is that each mineral has different thermal properties. Thermal properties such as thermal conductivity, heat capacity, and thermal diffusivity can vary widely depending on the mineral composition of the rock. By analyzing the thermal properties of individual minerals, we can gain a better understanding of the thermal behavior of the rock as a whole.

iv. ***SEM Study***: In this task, scanning electron microscopy (SEM) was used to analyze the 30 sandstone rock samples and compare their thermal properties based on their texture. The

intention is to analyze if rock textural properties influence their thermal properties. Surface roughness and the presence of pores and cracks are analyzed using image segmentation techniques. Then the results are compared with the measured thermal properties to evaluate the intercorrelations between the images and the experimental values.

v. ***3D Seasonal Thermal Storage Simulation***: In this task a three-dimensional (3D) model that captures the heterogeneity of porous media for SRTES applications was built. The properties required for constructing the model, such as porosity, permeability, thermal conductivity, and volumetric heat capacity, were obtained through laboratory experiments conducted on the set of 30 sandstone rock samples. The model was built using CMG-STARS (Steam, Thermal and Advanced processes Reservoir Simulator), an advanced reservoir simulation software. This software enables the integration of the acquired data and the generation of accurate representations of the subsurface medium. Part of the task is to simulate multiple scenarios to understand how the heterogeneity, temperature change and seasonal cycling affect the efficiency of the SRTES.

2. Overview of Thermal Energy Storage Systems

This chapter presents how the industry has been addressing the thermal energy storage in sedimentary basins. Case studies in the thermal energy storage in underground reservoirs were reviewed. Besides, a review of applied solutions in the field will be presented.

2.1 Initial research about thermal energy storage systems in subsurface rocks

The principles of storing heat in sedimentary rocks were initially analyzed to support the extraction of hydrocarbons. Marx and Langerheim (1959) proposed the injection of hot fluids in sedimentary reservoirs as an enhanced recovery method for extracting hydrocarbons. The authors proposed a mathematical approach to estimate the thermal invasion based on the thermal conductivity and thermal diffusivity of rocks and the specific heat capacity of the working fluid. In the 50s, 60s, and 70s, the oil and gas industry researched the heat transfer in sedimentary rocks for secondary and tertiary recovery and Steam-Assisted Gravity Drainage (SAGD) processes (Diaz-Munoz and Farouq Ali, 1974; Miller and Seban, 1955; Somerton, 1958).

In the '70s, the concept of storing heat in sedimentary reservoirs was considered to moderate the effect of the seasonal variation of solar energy's capacity factor. Rabbimov et al. (1971) proposed to store the surplus of solar energy in a gravel ground. Collins, (1977) suggested that sedimentary rocks provided an ideal solution to store solar energy. The large surface-to-volume ratio of the solid matrix of any porous sedimentary rock leads to the nearly instantaneous local thermal equilibrium of the rock matrix with the fluids contained in the rock pores. However, sedimentary rock's low thermal conductivity leads to a very slow heat loss to adjacent rocks not permeated by injected hot fluids (Collins, 1977). The maximum solar energy availability during the middle of the day or during

the summer season does not match the time of the maximum heating needs (at night in a daily cycle or winter in a seasonal cycle). The TES provides a solution to have a uniform solar energy demand curve (Wyman, 1979).

Molz et al. (1980) presented the results of an experimental study of storing heat in a shallow confined aquifer (40 to 62 meters) in Mobile, Alabama. In that study, 54,784 m^3 of water at 55ºC were injected in an aquifer with an ambient temperature of 20ºC. The water was injected during 80 days, stored in the TES for 51 days, then 55,345 m^3 where produced during 40.5 days (**Figure 3**). The **Figure 4** shows how the heat envelope did not shrink dramatically during the almost 2 months of storage, with a recovery factor of the project of 65%. (Molz et al., 1976; Rabbimov et al., 1971; Tsang et al., 1977). Somertom (1958) experimentally evaluated the thermal properties of sedimentary rocks pressurized and saturated with water. The results showed that the heat capacity of saturated rocks increased with pressure. Besides, the researcher concluded that thermal conductivity is higher in rocks with a high quartz concentration than in rocks with a high feldspar and clay mineral composition. Experimental research has found that rocks with high quartz content had greater thermal conductivities than shales, claystones, and siltstones (Blackwell and Steele, 1989; Labus and Labus, 2018a). The thermal conductivity and heat capacity of sedimentary rocks are affected by their porosity (Blackwell and Steele, 1989; Fuchs, 2018; Robertson, 1988; Somerton, 1958).

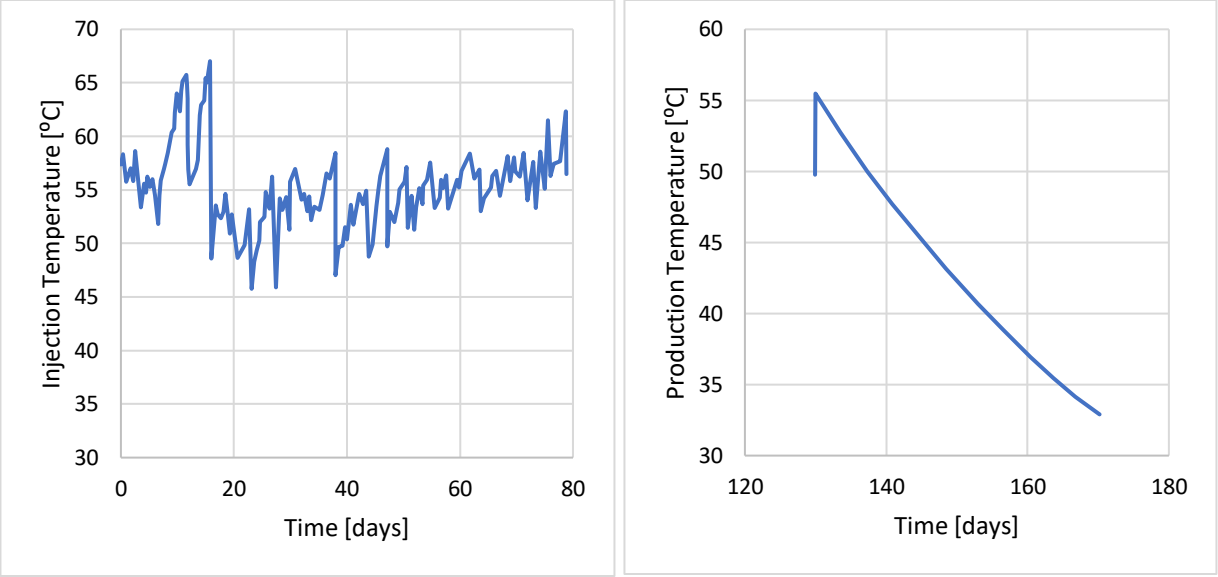

Figure 3. Temperature of the water injected [left] and the water produced [right] from the first stage of the TES (Plot built with information from Molz et al., 1980)**.**

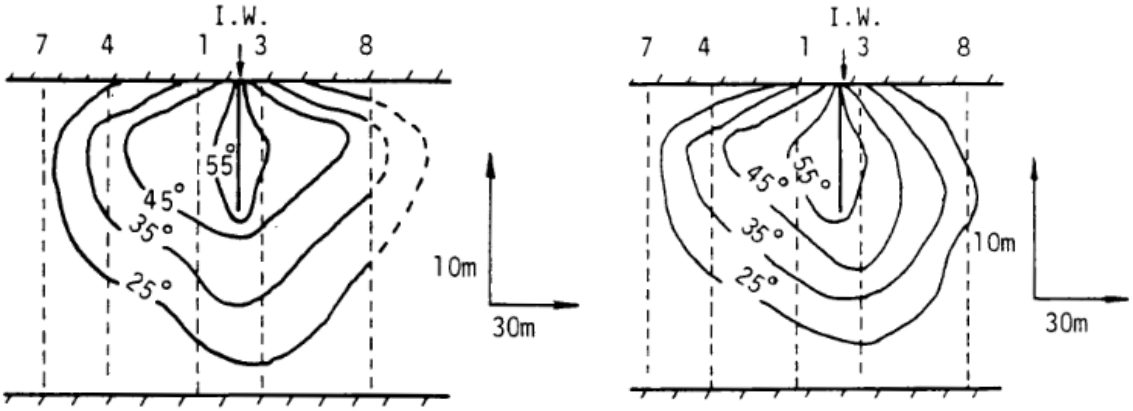

Figure 4. Temperature distribution in a transversal representation of the TES reservoir near the end of the injection phase [left], and near the end of the storage period (Molz et al., 1980)**.**

2.2 Summary of Sedimentary Reservoir Thermal Energy Storage Projects

SRTES projects for elevated to high temperatures in shallow sedimentary aquifers have been developed since the early 80s', but most of them are not operative (**Table 1**). The listed projects have proven the feasibility of the concept; however, further research is needed to progress from low-

medium temperature to high-temperature heat-storing systems for large-scale applications (Vangkilde-Pedersen and Kallesøe, 2019).

Table 1. Underground TES projects in shallow sedimentary aquifers projects (After Sanner and Knoblich, 1999; Vangkilde-Pedersen and Kallesøe, 2019)**.**

Project	Country	Year	Max. Temp.	Remarks	Status	Reference
SPEOS, LAUSANNE-DORIGNY	Switzerland	1982	69ºC	Waste incineration, Aquifer TES, closed	Closed	(Saugy et al., 1988)
HØRSHOLM	Denmark	1982	100ºC	Waste incineration, Aquifer TES, closed	Closed	(Sanner and Knoblich, 1999)
UNIVERSITY OF MINNESOTA, ST. PAUL	USA	1982	150ºC	Aquifer TES, experiment, aquifer at 180-240m depth, closed	Closed	(Sanner and Knoblich, 1999)
LULEÅ TECHN. UNIVERSITY., LULEÅ.	Sweden	1982	65ºC	Borehole heat store (120,000 m3 rock volume). Depth 150m. Industrial Waste Heat, 121 wells, inoperative	Closed	(Gehlin and Nordell, 2006; Nordell, 1994; Sanner and Knoblich, 1999)
GRONINGEN	Netherlands	1984	50ºC	Solar Heat, 360 Borehole Heat Exchangers	Closed	(Sanner and Knoblich, 1999)
PLAISIR, THIVERVAL-GRIGNON,	France	1987	180ºC	Aquifer TES, experiment, aquifer at 500 m depth, inoperative	Closed	(Sanner and Knoblich, 1998)
DE UITHOF, UTRECHT UNIVERS. UTRECHT,	Netherlands	1991	90ºC	Waste heat from heat and power co-generation	Closed	(Sanner and Knoblich, 1999)
HOSPITAL "HOOGE BURCH", GOUDA	Netherlands	1998	90ºC	Waste heat from co-generation	Closed	(Sanner and Knoblich, 1999)
AMORBACH, NECKARSULM	Germany	1998	70ºC	Solar Heat, 168 Borehole Heat Exchangers	Closed	(Sanner and Knoblich, 1999)
REICHSTAG BUILDING AND OFFICES, BERLIN.	Germany	1999	70ºC	Waste heat from heat and power co-generation	Operative	(Sanner and Knoblich, 1999)
NEUBRANDENBURG	Germany	2004	80ºC	Combined heat and power	Operative	(Vangkilde-Pedersen and Kallesøe, 2019)
GEOSTOCAL	France	2009	95ºC	Waste Combustion	Explorative	(Vangkilde-Pedersen and Kallesøe, 2019)
DUIVEN	Netherlands	2015	140ºC	Waste Combustion	Feasibility study	(Vangkilde-Pedersen and Kallesøe, 2019)

2.3 Thermal Energy Storage Technologies

Thermal energy storage involves heating or cooling a heat transfer fluid (HTF) to use the energy stored when it is required. In TES systems, the energy cycle starts with energy charging; then, energy is stored for a specific time and finally discharged when needed (Ortega and Gutiérrez, 2020). The system must meet a series of conditions to be efficient; the storage material must have a high energy density, adequate thermal conductivity, be mechanically and chemically stable, and have small thermal losses while the HTF is stored (Tamme et al., 2012). Thermal energy may be stored in three ways: by utilizing the sensible heat of the materials, the latent heat from a substance's matter state transitioning, and the energy applied in a chemical reaction (Ortega and Gutiérrez, 2020) (**Figure 5**).

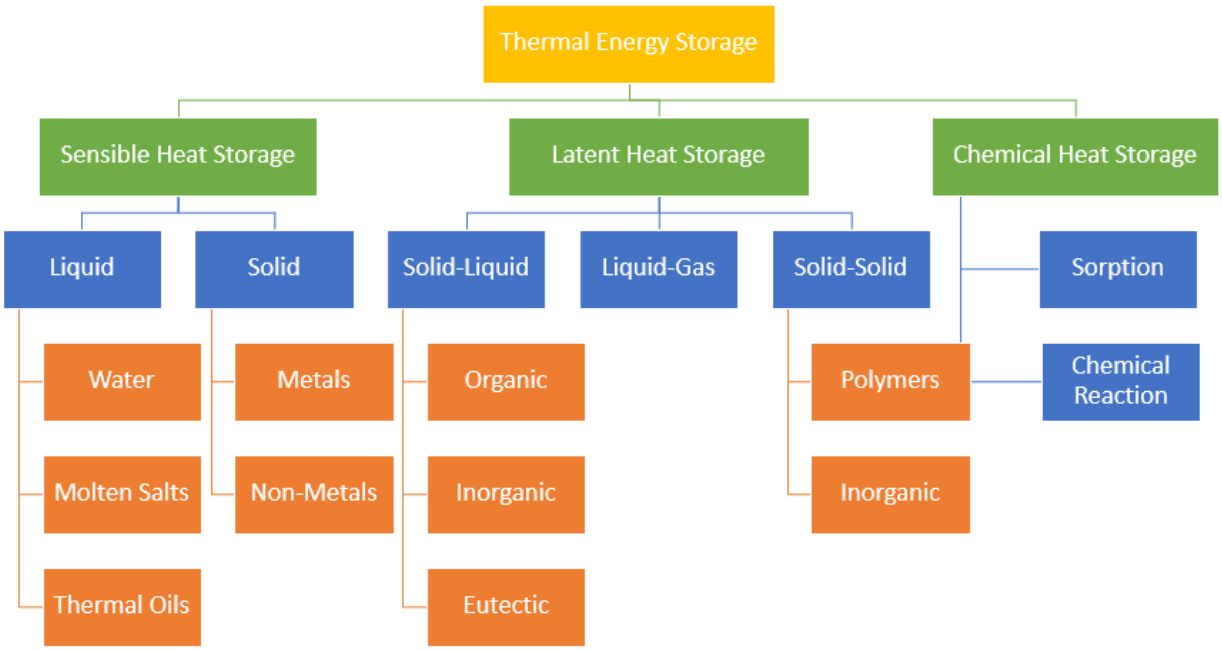

Figure 5. General classification of TES technologies (After Podara et al., 2021).

2.3.1 Sensible Thermal Energy Storage

The most basic, straightforward process to store heat in a sensible heat storage system. In this system, the thermal energy is stored by heating or cooling a heat transfer fluid. Underground sensible heat storage systems are suitable to store a large amount of energy for large-scale projects (Sarbu and Sebarchievici, 2018). The main advantages of this storage system are that it is a cheap option to store representative amounts of heat and does not involve using toxic or harmful materials.

The most implemented fluid to heat storing in thermal energy storage systems is water. Water is considered as a sensible heat storage fluid (Alva et al., 2018). Materials with high heat capacity are the most adequate for sensible heat storage (cp) (Khare et al., 2013). The materials with higher heat capacity are the best suited for sensible heat thermal energy storage systems. The definition of the thermal energy stored in terms of heat capacity is given by the equation below (Zhang et al., 2016):

$$Q = m \int_{T_L}^{T_H} C_p \, dT = mC_p(T_H - T_L) \text{ when CP ~ constant} \quad (1)$$

Where Q represents the thermal heat stored, m represents the mass, and dT is the temperature increase during the charging process (the difference between high temperature and low temperature). In this case, the mass, the heat storage capacity, and the temperature increase have a direct relation with the amount of heat stored. As water has a high heat capacity, is easy to access, relatively inexpensive, and easy to handle, the usage of this fluid in TES is reasonable.

2.3.2 Latent Thermal Energy Storage

In latent heat storage systems, the heat generates a phase change in the storage substance. The processes in this system include evaporation, condensation, sublimation or solidification (Ortega

and Gutiérrez, 2020). Latent heat storage benefits from phase change materials (PCM), being water one of the most typical materials utilized. PCM are materials that have a phase change in a little temperature change. Heat transfer in latent systems is the product of phase change (Jouhara et al., 2020). This phase change is connected to the absorption or discharge of heat at a steady temperature. Therefore, the heat added or discharged is not perceived and seems to be latent (EASE-EERA, 2017).

The equation below represents the thermal energy stored in terms of latent heat (Mehling and Cabeza, 2008; Zhang et al., 2016):

$$Q = m \int_{T_L}^{T_m} C_{ps}\, dT + m\Delta H_m + m \int_{T_m}^{T_H} C_{pl}\, dT \qquad (2)$$

Where T_m represents the melting point of the phase change material, C_{ps} represents the specific heat for the solid phase, C_{pl} represents the specific latent heat for the liquid phase and ΔH_m represents the enthalpy during state change. Due to the dependence on mass, the materials transitioning from solid to solid systems are capable store a significant quantity of energy with minor volume changes. Another advantage of these systems is that they do not need to be enclosed and are not susceptible to leakage (Fallahi et al., 2017; Jouhara et al., 2020). In liquid-to-gas systems, during the phase transition, a higher amount of latent heat can be generated. Nevertheless, the drastic change in storage material volume is a concern that limits the usage of liquid-to-gas systems (Cárdenas and León, 2013). Solids and liquids systems are most used latent heat systems (Zhang et al., 2016).

2.3.3 Chemical Thermal Energy Storage

A chemical heat storage system is based on the internal fluctuation of the storage substance caused by chemical reactions. In this system, the thermal energy is stored from a reversible chemical reaction; the heat causes an endothermic reaction in the charging phase, and an exothermic reaction

with the energy is discharged (Ortega and Gutiérrez, 2020). The chemical heat storage systems have a range of operation from 200°C to 400°C and are the systems with the highest density of energy storage capacity per mass and volume (Alva et al., 2018). Chemical reactions allow storing heat for long periods with limited enthalpy losses, making this a high-efficiency solution (Zhang et al., 2016). The **Figure 6** depicts the process where a solid substance (A) is exposed to heat, and in an endothermic reaction, it produces a solid (B) and a gas (C) (charging phase). Then the gas (C) is stored independently. Once the heat is required, the gas (C) is combined with the solid (B), generating an exothermic reaction, where the solid (A) is produced (discharging phase). The heat discharged can be used to generate power.

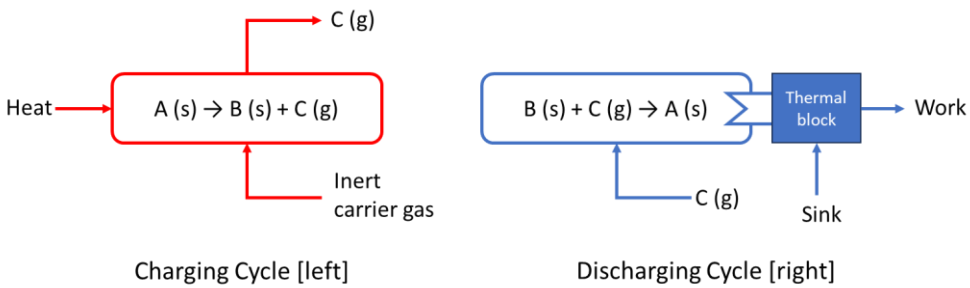

Figure 6. Description of the reversible reaction for chemical thermal energy storage systems (modified from Zhang et al., 2016)**.**

Chemical energy storage systems have presented promising results. However, some factors affect their implementation, such as the time required to charge the system or the chemical reactions that generate solids that affect the medium permeability. This storage system has been proved on a laboratory scale, but large-scale implementation requires further research (Alva et al., 2018).

2.3.4 Discussion of the thermal energy storage technologies

In utility-scale thermal energy storage solutions, the heat must be stored in the storage medium for periods that can variate from hours to months. Latent and chemical heat storage technologies offer

higher energy density, but these technologies are immature (Error! Reference source not found.). B esides, latent and chemical storage required the use of a confined container, which limits the volume of the system(Zhang et al., 2016). More research is still needed about the scalability of these technologies and their implications in terms of required infrastructure and costs. Sensible heat storage technology that uses a heat transfer fluid has less energy density than the rest of the storage systems. However, the scalability, high maturity, and flexibility of sensible heat systems make this technology more suitable for storing heat for long periods in large-scale volumes.

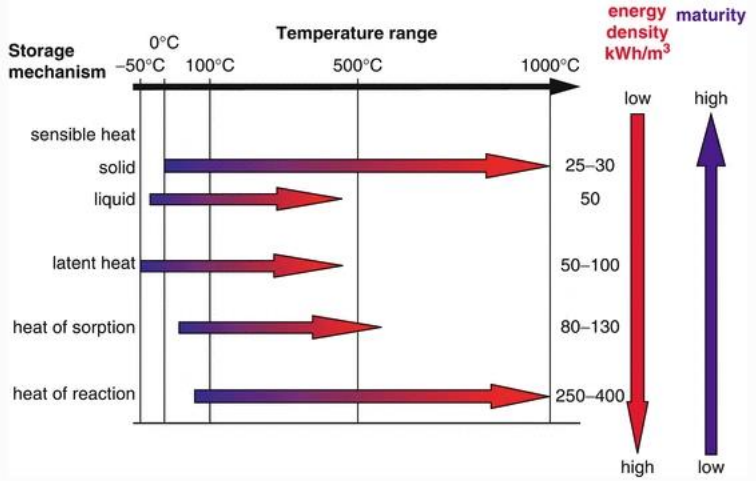

Figure 7. Operational ranges, energy density and maturity of the TES systems (Tamme et al., 2012).

2.4 Subsurface Thermal Energy Storage Systems

At the surface, the periodic climate variations generate seasonal fluctuations in temperature. In contrast, temperatures below 10 to 15 meters are not influenced by the weather and are more steady. In the summer, the shallow subsurface temperatures are lower than the surface temperatures. In winter, the opposite occurs; subsurface temperatures are higher than surface temperatures (Lee, 2013). The subsurface reservoirs offer the conditions to store heat, working as a thermal battery.

2.4.1 SRTES (Sedimentary Reservoir Thermal Energy Storage)

A sedimentary reservoir thermal energy storage is an open system that stores heat (or cool) through the groundwater. An SRTES comprises a single or multiple wells connected to the sedimentary groundwater reservoir (Stryi-Hipp, 2015). SRTES store heat by injecting hot water into aquifers in shallow and deep sedimentary reservoirs. The hot fluid is stored and produced again when required. The aquifers might be composed of fractured rock formations, unconsolidated sand units, or other sedimentary rocks. The depth of the reservoir limits the temperature storage capability. The higher the temperature, the deeper the reservoir (Kallesøe et al., 2019). Medium temperature SRTES systems can store heat at temperatures from 30-60ºC (Pedersen et al., 2014). High temperature systems can store water above 60ºC (Kallesøe et al., 2019; Mahon et al., 2022). SRTES systems components will be discussed in deep in the following chapters.

2.4.2 BTES (Borehole Thermal Energy Storage)

BTES stores thermal energy by using the intrinsic heat capacity of a vast volume of subterranean soil or rock. In a BTES typical system, a series of vertical boreholes into the ground are drilled. The storage volume is defined by the geological formation, which impacts the thermal capacity of the system. Typically, rocks or soils saturated with water provide a good thermal storage reservoir (Rad and Fung, 2016). The basic idea behind BTES is to heat and cool the BTES reservoir by circulating the heat transfer fluid via u-tube pipes inserted in many near-spaced closed-loop borehole heat exchangers (BHE). The interval between boreholes is generally 2 to 5 meters, and BTES is often restricted to boreholes of around 20-200 meters in depth (Kallesøe et al., 2019). A set of BHEs is linked to form a circuit that follows an essentially circular direction halfway through the storage. To optimize the charging temperatures, limit BTES heat loss, and minimize collector inlet temperature,

the BTES is charged from the center to the outer end in the loading phase and from the outer end to the center in the discharge phase. Several parallel circuits are employed to disperse the flow into the BTES reservoir uniformly. (Sibbitt and McClenahan, 2014). **Figure 8** depicts a BTES arrangement and the BHE cross-section.

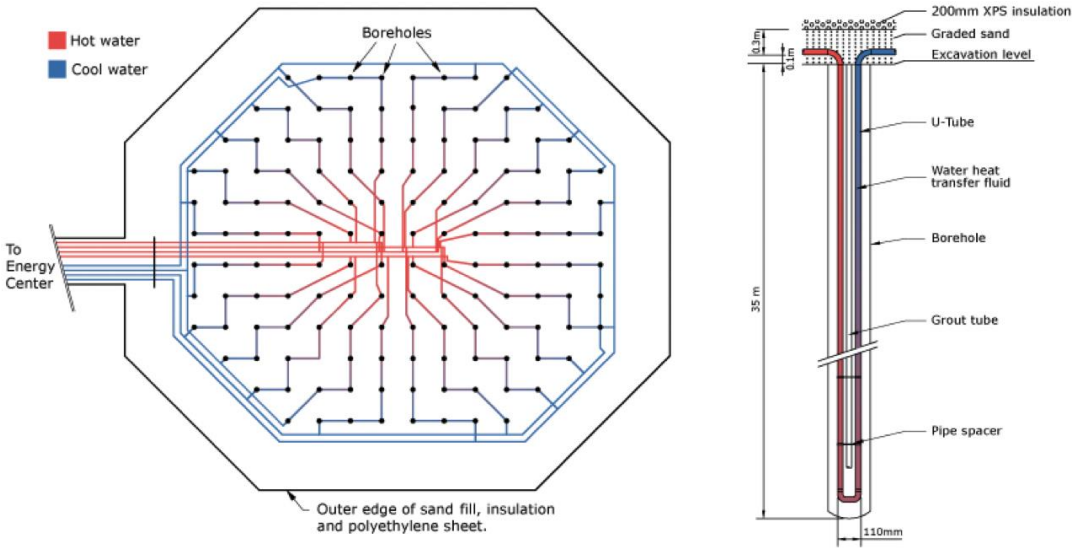

Figure 8. Example of a BTES layout and a BHE cross-section (Sibbitt and McClenahan, 2014)**.**

The thermal losses are determined by: the subsurface's thermal and hydraulic parameters, the form, size, and volume of the storing reservoir, the local aquifer flow (advection losses), and surface losses. (Kallesøe et al., 2019).

BTES performance varies depending on the quantity and depth of the BHEs, borehole spacing, ground type, thermal conductivity, and volumetric heat capacity. In the Drake Landing BTES project, 144 BHEs were placed at 35 m depth to support a community of 52 houses in Oktokos, Canada (Malmberg, 2017; Mesquita et al., 2017). The charging temperature ranged from 50 to 65°C, and the injection and extraction power were 2,530 and 1,370 GJ, respectively, for an efficiency of 54.1%. In Crailsheim, Germany, a BTES comprised 80 BHEs at 55 m depth. The

charging temperature was 90°C, and the injection and extraction power was 780 and 382 MWh, respectively, for an efficiency of 49% (Schneider, 2013). A BTES in Brædstrup, Denmark, has 48 BHEs placed at 45 m depth to complement a solar plant (Gehlin, 2016; Sørensen et al., 2013). The charging temperature of the system was 80°C, and the injection and extraction power was 444 and 163 MWh, respectively, for an efficiency of 36.7%.

2.4.3 PTES (Pit Thermal Energy Storage)

In a PTES, excavated ground with waterproof liners or artificial stores made of concrete or stainless steel is used to store the heat from solar heating or other renewable systems (Chang et al., 2017; Novo et al., 2010; Xiang et al., 2022). The sidewalls and the floor are usually coated with a polymer liner; however, they can alternatively be built of concrete. PTES can hold 90°C of storing temperature, providing the adaptability to district heating energy systems as other TES (Kallesøe et al., 2019). The PTES system in Dronninglund, Denmark, is associated with a solar district with 37,600 m^2 solar collectors (Dahash et al., 2020). The volume of the PTES is 60,000 m^3, with a total capacity of 5,400 MWh. The injection and extraction power were 38,093 and 33,038 MWh/a, respectively, for an efficiency of 89.5%. In Gram, Denmark, a PTES system is associated with a solar district with 44,800 m^2 solar collectors. The volume of the PTES is 122,000 m^3, with a total capacity of 8,630 MWh. The injection and extraction power were 12,997 and 6,534 MWh/a, respectively, for an efficiency of 50.3% (Kallesøe et al., 2019). The difference in efficiency is attributed to an insulation damage. Besides, for scalability purposes, for large pit storage volumes is understandable to face difficulties in insulation materials, and other problems related to control heat losses.

2.4.4 MTES (Mines Thermal Energy Storage)

An MTES system for a large-scale project requires a considerable quantity of mine water volume to store the heat. Besides, the system needs to be dependable high energy efficient with the ability to connect it to the energy distribution infrastructure. In addition, an HT-MTES needs to be operational for 40 to 50 years to meet the associated financial needs (Bartels et al., 2019; Kallesøe et al., 2019).

Hahn et al. (2018) examined the Prosper-Haniel HT-MTES prospect in Germany. The project benefits from the large volume of the subsurface infrastructure of a recently abandoned coal mine. The coal mine surface has 167 km2, with 141 km length of underground galleries with a maximum depth of 1,159 m. The recorded rock temperatures range from 30 to 50ºC (Leonhardt, 1983). Based on numerical simulations, storing 252,000 m3 of water in one coal mine sector at 90ºC during 6 months can deliver 12.8 GWh/a with an efficiency of 84%. Include the results from (Hamm et al., 2021). Several authors have evaluated the prospectively of MTES in abandoned subterranean mines (Bücken et al., 2022; Hahn et al., 2019; Moeck et al., 2021; Passamonti et al., 2020; Poulsen et al., 2019). The vast capability of MTES to store water offers an auspicious opportunity for utility-scale TES. The limitation of massifying this technology is that it is restricted to regions with access to abandoned mines (most of the studies found are placed in Europe). Besides, the mines must be located nearby the potential end-users, industrial o residential.

2.4.5 Discussion about the sensible heat storage system for utility-scale systems

For a utility-scale solution, where large amounts of heat need to be stored, the following characteristics are desired:

- Thermal energy storage systems that can be placed near the renewable energy generation source (for instance, solar energy plants, or wind farms), and

- Large-volume TES are required for utility-scale applications.

MTES have large volumes to store the heat transfer fluid, however its main limitation is that this TES can be developed in places with access to mines, minimizing the flexibility of this system to be implemented as complement with current renewable power generation projects. PTES system offer the flexibility to be placed near the renewable power plant, but it is limited in the amount of volume. Besides, it is still needed the availability to a large surface area, and the storing temperature is limited to 90ºC. If water is intended to be used in this system (and this makes sense, because using and engineered HTF in a large volume is cost prohibitive), the system is limited to the temperatures below the water boiling point (100ºC). Going beyond the boiling point required a pressurized system, which reduces the technical and economic feasibility of the project. BTES system have similar limitations as PTES for utility-scale applications.

As the intention is to explore a solution to integrate renewable sources like solar or wind with thermal energy stage systems that enhance the dependability of the system in large-scale projects, the deep aquifer thermal energy storage provide an adequate solution. The sedimentary storage uses large volume reservoirs that are placed downhole, so the surface footprint is limited to the wells location. Directional drilling allows to reduce the surface area and provide additional flexibility to the surface location. Using sedimentary reservoirs offers different challenges that are going to be explored in the following chapters of this study.

2.5 Thermal Energy Storage Heat Transfer Fluids

Heat transfer fluids can be used to transfer or store the heat in a TES (El Alami et al., 2020; Gil et al., 2010; Medrano et al., 2010). Water is the most common and commercial heat storage medium, with a variety of residential and industrial applications (Sarbu and Sebarchievici, 2018). Water is a

sensible heat storage fluid that has easy accessibility, is relatively inexpensive and easy to handle (Alva et al., 2018). Water has high specific heat and heat capacities (4190 J/kg K and 4.174 MJ/m^3K respectively) (Ataer, 2009; Esence et al., 2017). In addition to water, there is a wide variety of HTFs whose selection is defined by the type of application. (Heller, 2013) summarized the different characteristics highly desirable for a heat transfer fluid. HTFs should have low solidification and high evaporation temperature; solidification affects the HTFs capability to serve as a medium to transport the heat, and evaporation reduces the HTF's heat transfer coefficient. Other desirable properties are low toxicity, viscosity, and high heat capacity and density. **Table 2** present the thermal properties of different HTFs used in TES.

Table 2. Properties of different heat transfer fluids used in TES (El Alami et al., 2020)**.**

	Chemical Composition	Density	Specific Heat C_p	Heat Capacity	Thermal Conductivity	Dynamic Viscosity	References
		kg/m^3	J/kg K	MJ/m^3K	W/m K	mPa.s	
SYNTHETIC OIL	**Therminol VP-1 [73.5% diphenyl oxide and 26.5% biphenyl]**	815	2319	1.89 at 250 °C	0.106 at 250 °C	0.29 at 250 °C	(Eastman, 2022a, 2020; Hoffmann, 2015)
	Therminol 55 [Synthetic hydro-carbon mixture]	868	2720	2.36	0.1017	0.488	(Ataer, 2009; Eastman, 2022b; Gil et al., 2010)
	Therminol 66 [Terphenyl, hydro-genated]	750–845	2100–2380	1.57–2.01	0.106	0.57	(Ataer, 2009; Eastman, 2022c; Gil et al., 2010)
	Dowtherm A [Diphenyl Oxide/Biphenyl Blend]	859	2218	1.90	0.1019	0.28	(Ataer, 2009; Dow, 2022; Kuravi et al., 2013)
	Jarytherm DBT [Dibenzyl-toluene]	870	2350	2.04	0.11	0.47	(Esence et al., 2017)
MINERAL OIL	**Caloria HT 43**	695	2700	1.87		0.68	(Ataer, 2009; Esence et al., 2017)
VEGETAL OIL	**Colza [Fatty acid]**	787.7	2492	2.02	0.139 at 250 °C	2.5 at 250 °C	(Hoffmann, 2015)
MOLTEN SALT	**Solar salt [60% $NaNO_3$+40% KNO3]**	1720–1910	1495–1550	2.57–2.96*	0.50–0.55	1.03–3.50	(Gil et al., 2010; Heller, 2013; Kearney et al., 2003; Pacio and Wetzel, 2013)

	Chemical Composition	Density	Specific Heat C_p	Heat Capacity	Thermal Conductivity	Dynamic Viscosity	References
	Hitec [7% $NaNO_3$ + 40% $NaNO_2$ +53% KNO3]	1690–1980	930–1560	1.57–3.08*	0.24–0.44	1–20	(Esence et al., 2017; Heller, 2013; Herrmann and Kearney, 2002; Kearney et al., 2003)
	Hitec XL [45% KNO_3+7% $NaNO_3$+48% Ca(NO3)2]	1992	1447	2.88	0.52	6.3	(Esence et al., 2017; Kearney et al., 2003)
	Carbonate salts	2100	1800	3.78	2		(Gil et al., 2010; Kuravi et al., 2013)
	Liquid sodium	850	1300	1.105	71		(Heller, 2013; Kuravi et al., 2013)
OTHERS	**air [21% O_2 and 78% N_2]**	0.22–0.934	1075–1220	1.14×10^{-3}	0.0314–0.0966	0.0219–0.0582	(Gil et al., 2010; Heller, 2013; Kadoya et al., 1985; Kuravi et al., 2013)
	Water [H_2O]	900–1000	4187–4190	4.174	0.64	0.58	(Ataer, 2009; Esence et al., 2017)

Synthetic oils have a wide range of operational temperatures, from -3ºC to 345ºC, without phase change (Eastman, 2022c). This wide range allows the storage of synthetic oils at high temperatures, increasing the efficiency of the TES system (Bouguila and Said, 2020). Lower viscosities at high temperatures are also beneficial for using synthetic oils.

Molten salts have high thermal stability at high temperatures; however, solidification temperatures are also high. Commonly, molten salts are solidified at 140ºC; however, in some high-performance molten salts, values of 65ºC have been reported (Raade and Padowitz, 2011). The high solidification temperature limits the applicability of molten salts for utility-scale projects. Molten salts are as well very expensive, representing around 20% of the total capital costs of a TES project integrated with a concentrated solar power plant (Angelini et al., 2014; Herrmann and Kearney, 2002).

Other working fluids are considered in geothermal systems. Supercritical CO_2 has been proposed as heating transfer fluid (Brown, 2000). One of the main advantages that CO_2 has over water is their high compressibility capacity and the high buoyancy effect. The impact is the significant reduce in the energy required to circulate this HTF through the entire geothermal system (Pruess, 2006). Other advantages of CO_2 is it low viscosity, which can result in faster flow velocities than water, and their low capability to dissolve minerals, which reduce the problems associated to minerals precipitation and scaling (Brown, 2000). CO_2 presents a lower heat capacity than water (0.8457 and 4,190 J/(kg*K) respectively). Although, due to their lower viscosity and buoyancy factor, the lower heat capacity of CO_2 can be compensated with the an increased production (Pruess, 2006). Sun et al. (2018) presented a numerical study where CO_2 is used in abandoned horizontal wells as working fluid. Chen et al. (2019) analyzed the usage of CO_2 as working fluid finding that the pre-saturating the CO_2 reservoir before heat extraction enhances the heat production. Buscheck et al. (2017) presented a concept of CO_2 capture, utilization and storage (CCUS), with the geothermal battery concept, in an innovative approach for thermal energy storage with simultaneous CO_2 sequestration.

2.5.1 HTFs Discussion

Water is selected as an adequate HTF for utility-scale applications for this study. Water has higher heat capacity, and specific heat than the other HTFs evaluated. Other important factors are that water is easy to access and has a low cost. These factors are critical to large-scale projects. The weak point of using water is its low boiling point, 100ºC. This value restricts the charging temperature of a TES that use water as HTF, lowering the system efficiency. To increase the water boiling point, increasing the TES confining pressure is necessary. To achieve this, reservoirs in the region of 1,000 m depth provide a pore pressure of 9,800 kPa (with a normal pore pressure gradient). At those

conditions, the boiling temperature of water increases up to 310ºC. In this case, deep aquifers offer good conditions for a high-temperature, utility-scale TES.

The concept of storing heat using CO_2 is appealing. The combination of thermal energy storage, and carbon capture provide an ingenious environmental solution. This technological approach is still in an early research phase and is going to be further analyzed in the future (not in this study). The focus of this study is to analyze the application the implementation of water usage as the HTF.

2.6 Mechanisms of Thermal Energy Storage in Sedimentary Rocks

The concept of thermal energy storage in sedimentary reservoirs requires the understanding of the heat transfer mechanisms in porous media and the thermal properties of sedimentary rocks and the fluid used to transport the heat to the reservoir, store it and transport the heat back to the surface. The production and injection cycles in thermal energy storage require analyzing the evolution of temperature and heat flux in the reservoir battery. Temperature and heat are associated through rocks' thermal properties and heat transfer fluid stored in the poral space. Volumetric heat capacity, thermal conductivity, and thermal diffusivity are the most critical thermal properties. Volumetric heat capacity indicates the amount of heat needed to increase the temperature of a specific volume of rock by one unit of temperature. Thermal conductivity represents where and how much heat flows product of the reservoir temperature differences. Thermal diffusivity defines how fast the thermal front moves across the reservoir (Chekhonin et al., 2012).

2.6.1 Thermal Conductivity

Thermal conductivity (λ) specifies the quantity of heat that moves over a unit of distance through a reservoir section, per temperature change unit, per time unit (Clauser, 2011). This property is defined

by the fourth law of Fourier, where λ_{ij} represents the thermal conductivity tensor, $\frac{\partial T}{\partial x_j}$ represents the temperature gradient, and q_i the heat flow per unit of area.

$$q_i = -\lambda_{ij} \frac{\partial T}{\partial x_j} \qquad (3)$$

Thermal conductivity in sedimentary rocks is highly anisotropic. This property is affected by the burial history of sediments, the reservoir's depositional environment, and the rock's mineralogy (MidttØmme and Roaldset, 1999). Distinct quantities of heat flux are produced by temperature variations along orthogonal pairings of opposing sides of a rock block. (**Figure 9**). In materials deposited in layers, like sedimentary rocks, the thermal conductivity parallel to the layers is commonly higher than the thermal conductivity perpendicular to them (Chekhonin et al., 2012).

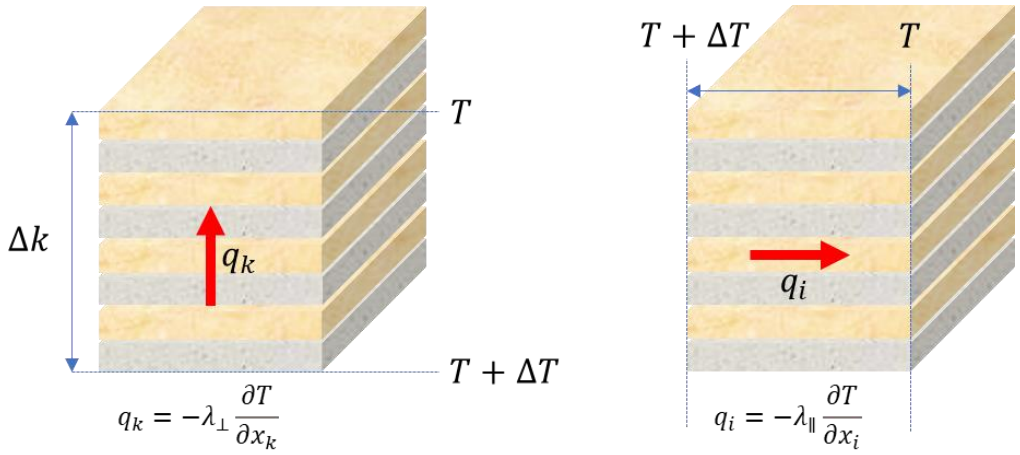

Figure 9. Graphical representation of anisotropic thermal conductivity (Adapted from Chekhonin et al., 2012)**.**

2.6.2 Thermal diffusivity

Thermal diffusivity (κ) defines how fast a material responds to a temperature variation (Labus and Labus, 2018a). Thermal diffusivity controls transient heat diffusion, and corresponds to the ratio of

thermal conductivity (λ) to heat capacity, or the ratio of heat flow over the side of a cubic meter of volume, and the heat stored in a cubic meter of volume per second in SI units (Clauser, 2011).

$$\kappa = \frac{\lambda}{\rho * c} \tag{4}$$

Thermal diffusivity in the sedimentary reservoir describes the velocity of the thermal front throughout the reservoir (Chekhonin et al., 2012). The thermal diffusivity of a rock affects the depth of penetration and speed of temperature adaptation in a changing thermal ambient (Korte et al., 2017).

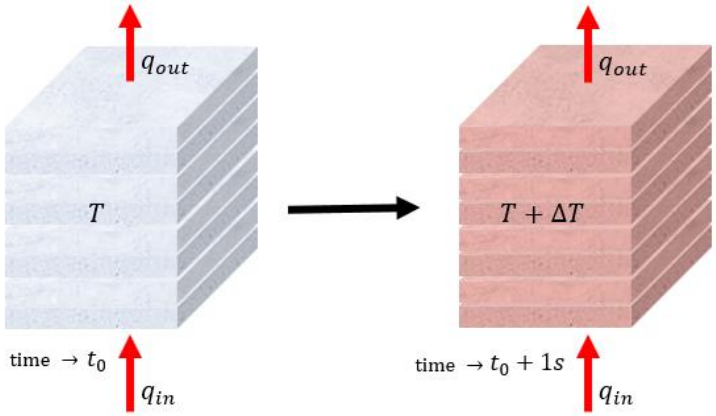

Figure 10. Graphical representation of thermal diffusivity (adapted from Chekhonin et al., 2012)**.**

2.6.3 Specific Heat Capacity

The specific heat capacity (c) defines the quantity of sensible heat that may be stored (temperature increase) or extracted (temperature decrease) per mass of rock and temperature change at constant pressure. Thermal capacity or volumetric heat capacity is the result of the specific heat capacity and density (Clauser, 2011). The heat capacity of the fluid is, similarly to the sedimentary rocks, a thermal property computed in heat units per temperature and mass. Materials with the ability to absorb heat energy with a relatively small increase in temperature have a high heat capacity.

Conversely, materials that are heated with only a small heat input they have a low heat capacity (Alva et al., 2018).

2.6.4 Thermal and Petrophysical Properties of Rocks

Sedimentary thermal energy storage is a sensitive heat system where the heat is stored in sedimentary rocks. Indeed to gain a better understanding of the sedimentary TES system's thermal performance, it is beneficial to understand the effect of all properties and various aspects of the storage material, the sedimentary rocks, and their interaction with the heat transfer fluid in the TES reservoir. As observed in equation 4, the thermal conductivity, thermal diffusivity and specific heat are mutually correlated.

In **Table 3** there is presented the thermal capacity, which is the product of specific heat and rock density ($\rho * C_P$). As the property defines the amount of heat required to elevate the temperature of a cubic meter of the rock in one ºC, the higher the specific heat, the more heat is needed to increase the temperature of a particular volume of that rock. As observed in the **Table 3**, clays has the more specific heat than sandstones.

Table 3. Thermal capacity of common minerals (After Clauser, 2011; Petrunin et al., 2004; Waples and Waples, 2004)**.**

Rock Type/Mineral	Density [kg/m^3]	Specific Heat Capacity [J/(kg*K)]	$\rho * C_P$ [kJ/(m^3*K]
Albite	2540–2560	755–780	1922–1991
Amphibole	3010	700–1134	2110–3410
Anhydrite	2950–2960	590–940	1740–2780
Anorthite	2740	800	2202
Basalt	2870	880–900	2526–2583
Clay	2680	860	2300
Coal	1350	1300	1760
Diabase	2790	731–860	2040–2400
Dolomite	2800	900	2520
Gabbro	2970–3000	650–1000	1950–2970
Gneiss	2700	770–979	2080–2640
Granite	2620–2650	600–1172	1590–3070

Rock Type/Mineral	Density [kg/m³]	Specific Heat Capacity [J/(kg*K)]	$\rho * C_P$ [kJ/(m³*K]
Gypsum	2370	1010	2390
Limestone	2760–2770	680–880	1880–2430
Peridotite	2740–3190	705–1005	1930–3210
Pyroxenite	3190–3240	660–1000	2140–3190
Quartzite	2640	731–1013	1930–2670
Rock Salt	2160	880	1900
Sandstone	2640	775	2050
Schist	2770–2900	790–1096	2190–3180
Serpentinite	2270–2540	730–1005	1660–2550
Siltstone	2680	910	2449
Slate	2770–2780	740–1113	2060–3080
Syenite	2820	460	1300
Talc	2780	1000	2780
Tuff	2750	1090	3000

Anand et al. (1973) evaluated the thermal conductivity of different sandstones (Error! R eference source not found.). The rocks were tested dry and saturated with water, silicone oil and a solvent has different heat transfer fluids. The samples saturated with water presented the highest thermal conductivity in all cases, regardless the different porosity, permeability and density values.

Table 4. Thermal conductivity of sandstones saturated with different fluids (Anand et al., 1973)**.**

Sample	Density	Porosity	Resistivity Factor	Perm	Thermal Conductivity at 20ºC [10^{-3} Cal/cm*s*ºC]			
	[gr/cc]	[v/v]		[md]	Dry	Water	Silicone oil	Solvent
Berea	2.10	0.162	13.0	190	5.37	12.40	10.54	8.18
Bandera	2.10	0.208	13.0	38	4.05	8.52	7.85	6.49
Boise	1.80	0.292	7.9	2513	3.31	7.36	5.04	4.92
Ss No. 1	2.22	0.160	18.5	152	5.79	12.24	6.82	0.00
Ss No. 2	2.00	0.250	10.9	557	4.55	13.48	-	-
Ss No. 3	2.26	0.149	12.0	34	3.72	-	-	-
Venango	2.30	0.122	35.9	437	9.88	-	-	-
Gatchell	2.04	0.227	13.3	858	4.55	-	-	-

Robertson (1988) evaluated the thermal conductivity of sedimentary rocks with different content of quartz. **Figure 11** and **Figure 12** show the variation of thermal conductivity with squared solidity (1-porosity) at different quartz content in sandstones dry and water saturated respectively. In the plots it is observed: a) the content of quartz affects positively the thermal conductivity, b) the increase in solidity (or decrease in porosity) increases the thermal conductivity of the system sandstone-dry and sandstone-water, and c) the thermal conductivity in the sandstone saturated with water are higher than the thermal conductivity in the dry sandstone. **Figure 13** and **Figure 14** present the variation of thermal conductivity with squared solidity at different quartz content in shales saturated in air and water respectively. The same interpretations are observed compared with the experiments of sandstones, where the thermal conductivity increases with quartz content, solidity, and the water saturated samples with higher values than the dry samples. It is also observed that the thermal conductivity of sandstones-water systems are higher than the shale-water system (the same happens with dry samples). The higher thermal conductivity of sandstone-water systems has better heat transfer rate, enhancing the heat exchange, which results in better thermal efficiency.

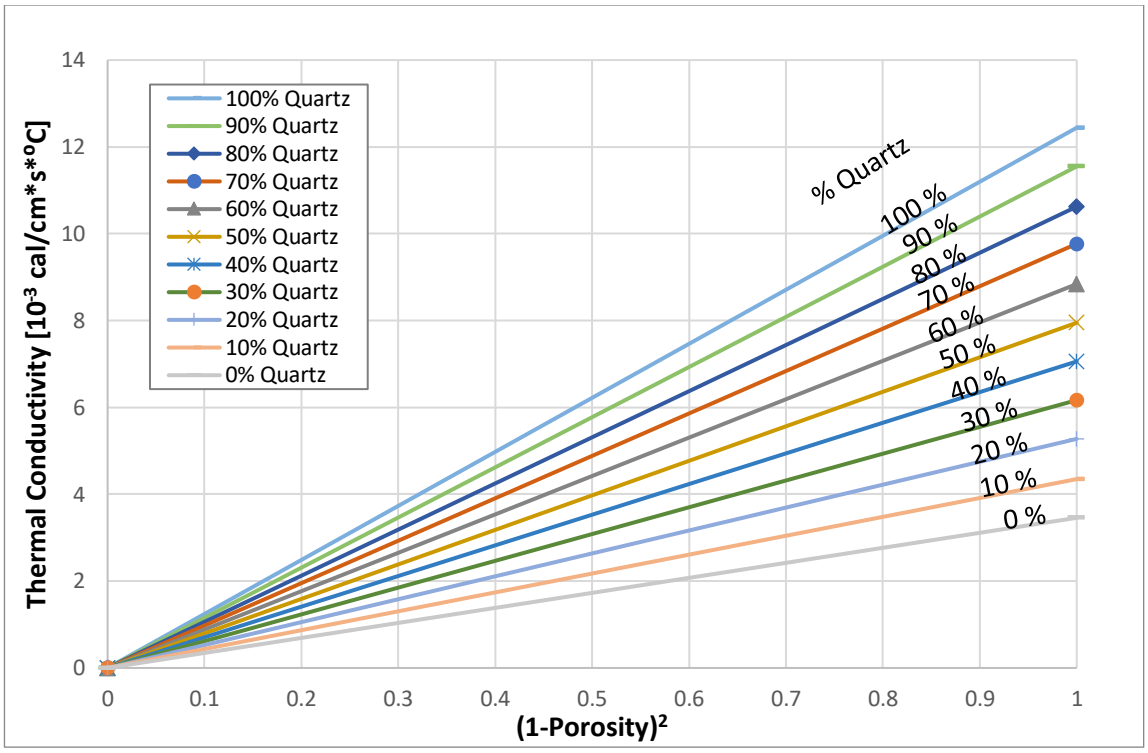

Figure 11. Thermal conductivity of dry sandstones, showing variation with solidity and quartz content (After Robertson, 1988)**.**

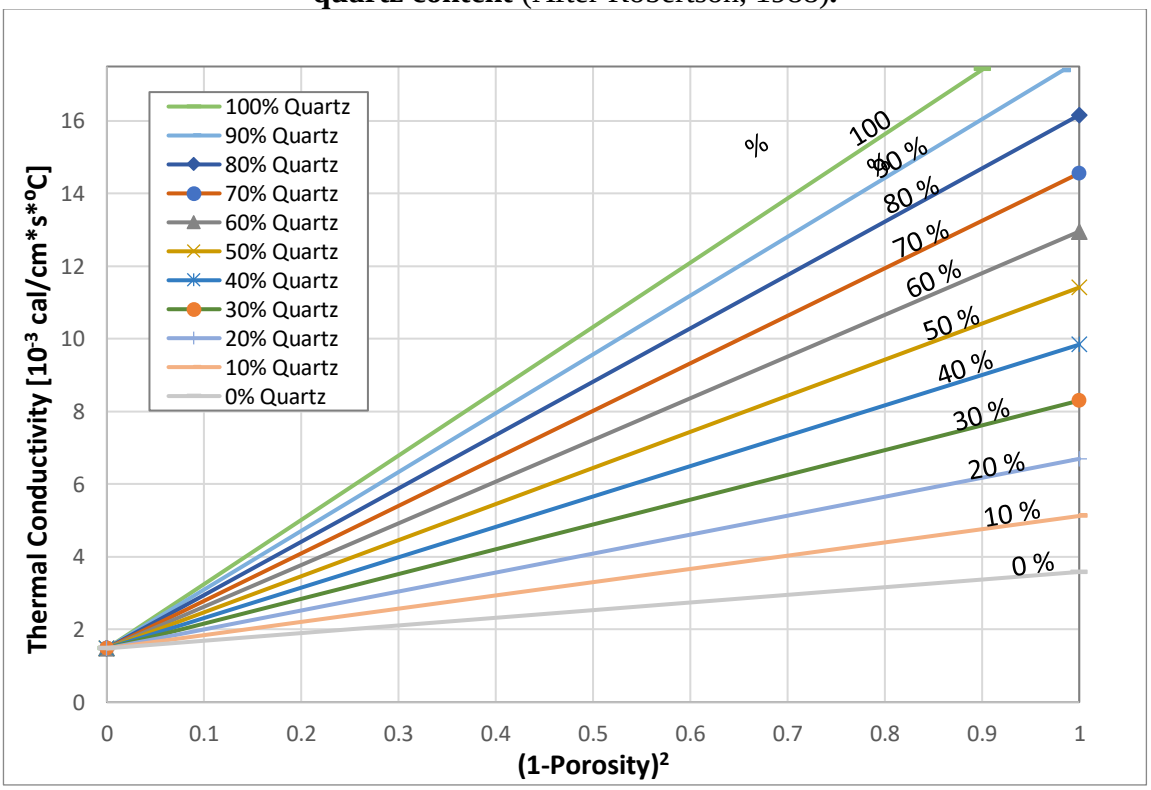

Figure 12. Thermal conductivity of sandstones saturated with water, showing variation with solidity and quartz content (After Robertson, 1988)**.**

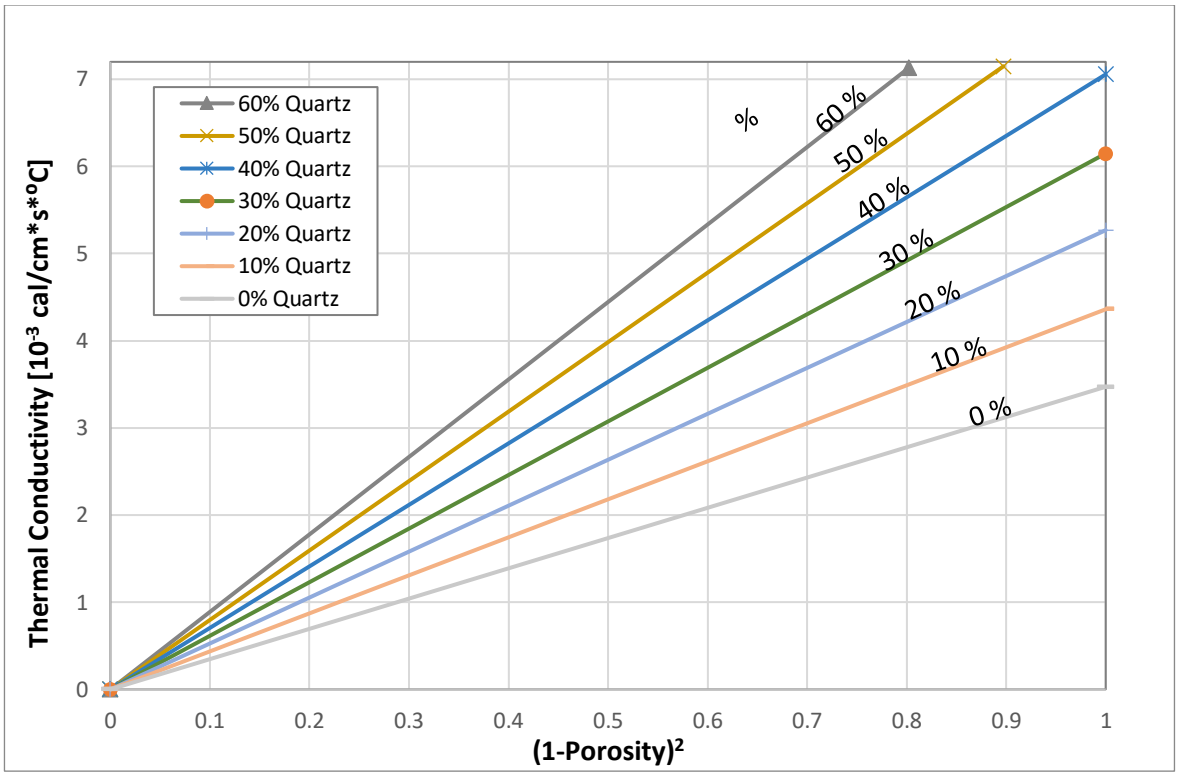

Figure 13. Thermal conductivity of dry shales, showing variation with solidity and quartz content (After Robertson, 1988)**.**

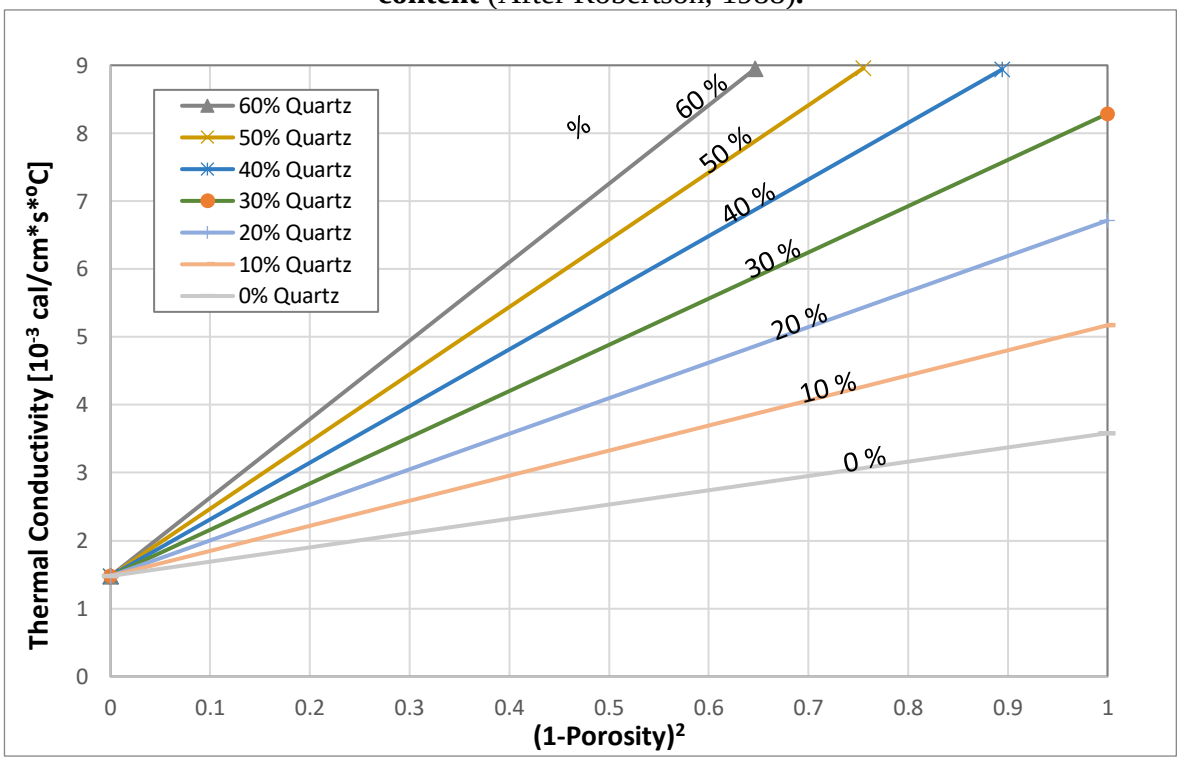

Figure 14. Thermal conductivity of shales saturated with water, showing variation with solidity and quartz content (After Robertson, 1988)**.**

Anand et al. (1973) evaluated the effect of temperature in two types or sandstones (Berea and Boise sandstones) and a shale. The results of the study are presented in **Figure 15**, where it is observed than sandstones tend to decrease their thermal conductivity with temperature. In contrast, the thermal conductivity of shales tend to increase with temperature. Regardless of the results, the thermal conductivities of sandstones are higher than the shales in the temperature range of 110-150ºC, which is the operational range of high temperature sedimentary thermal energy storage systems.

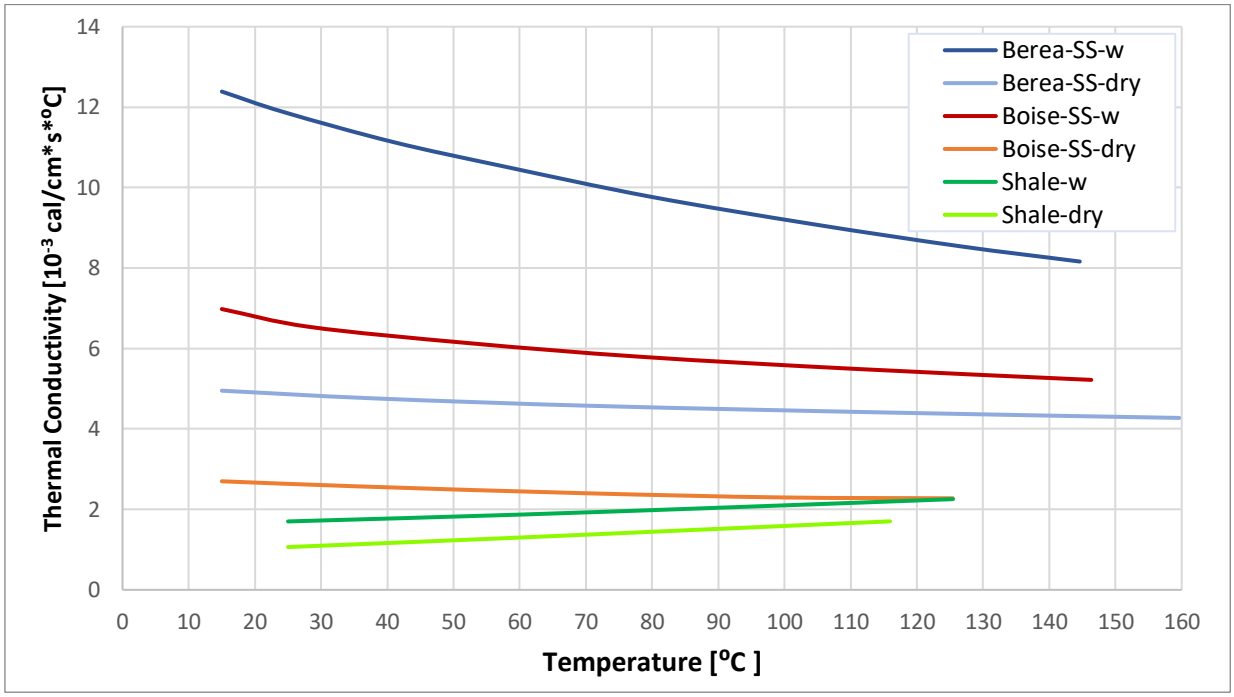

Figure 15. Effect of temperature in thermal conductivity of shales and sandstones saturated with water (w) and air (a) (after Anand et al., 1973)**.**

Thermal diffusivity variates among rock types. (Fuchs et al., 2021) evaluates experimentally the speed of heat propagation in sedimentary rocks. The authors evaluated the relationship between thermal diffusivity of different sedimentary rocks saturated in water. Results show that quartz sandstones have more thermal diffusivity than the claystones and carbonates analyzed **Figure 16**. Besides, the thermal diffusivity tends to decrease with the porosity increase as seen in the **Figure**

16. These results confirms the influence of mineralogy and porosity in the thermal diffusivity of sedimentary rocks.

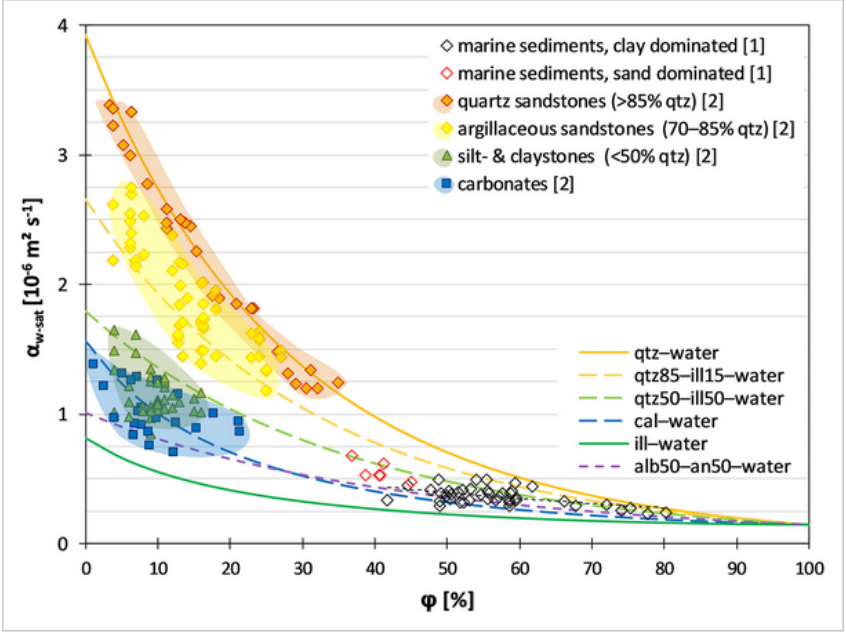

Figure 16. Thermal difussivity of diferent sedimentary rocks saturated in water (Fuchs et al., 2021)**.**

2.6.5 Influence of rock wettability on the thermal properties of a SRTES

There is limited literature directly addressing the influence of rock wettability on heat transfer capabilities. A fundamental understanding of which intrinsic rock properties impact wettability is needed. Factors determining whether a rock is hydrophobic or hydrophilic include salinity, ionic composition, mineralogy, surface roughness, and surface charge. Salinity and ionic composition can affect the wettability of rocks (Fathi et al., 2010). The mineralogy of the rock, along with its surface roughness and surface charge, indirectly govern preferential water attraction or repellence at the pore-scale (Borysenko et al., 2009).

- Grain/mineral composition: The adhesion forces between minerals and fluids can impact wettability. Some minerals may have a stronger affinity for certain fluids, leading to preferential wetting or non-wetting behavior (Rucker et al., 2019). Certain minerals like quartz tend to be more water-wetting compared to calcite or clay minerals, whose wetting properties depend more on composition. In waterflooding research on sandstone reservoirs, Saeed et al. (2022) observed that the presence of kaolinite in the sandstone reservoir resulted in decreased water-wettability compared to the other clay minerals studied, such as chlorite, illite, montmorillonite, and smectite.
- Surface roughness: In independent experimental studies conducted by AlRatrout et al. (2018) and Sari et al. (2020) in rock-oil-brine systems, it was observed that the contact angle consistently decreases (indicating a shift towards greater water-wettability) as the surface roughness increases, regardless of the salinity level.
- Surface charge: The surface charge of minerals in the rock can attract or repel ions present in the fluid. This interaction can affect the wetting behavior of the rock. If the rock surface has a negative charge, it can attract positively charged ions in the fluid, leading to a more water-wet condition (Hou et al., 2021).
- Pore structure: The shape and geometry of the pores can impact wettability. Irregular or complex pore geometries can create trapping or corner effects, affecting fluid distribution and wetting behavior. Additionally, the presence of preferential flow paths or channels can influence the wetting characteristics of the rock (Wang et al., 2020). The shape and geometry of the pores can impact wettability. Irregular or complex pore geometries can create trapping or corner effects, affecting fluid distribution and wetting behavior. Additionally, the presence

of preferential flow paths or channels can influence the wetting characteristics of the rock (Jahanbakhsh et al., 2021).

The factors mentioned above not only influence the rock's wettability but also influence the rock's thermal properties. On the other hand, the wettability of a rock surface can affect the flow of fluids within the rock's pore network. When a rock is water-wet, water spreads and flows more easily through the pores, enhancing heat transfer. On the other hand, if the rock is hydrophobic, water may have flow resistance and reduce heat transfer efficiency. In hydrophobic rocks, water may preferentially flow through interconnected hydrophilic pathways or fractures, bypassing the hydrophobic regions. This can result in uneven flow distribution and reduced overall water flow through the rock (Vidler et al., 2021). Consequently, as water is the heat transfer fluid, this hinders the performance of the SRTES.

It is important to note that the specific effects of wettability on rock thermal properties can vary depending on factors such as rock composition, intrinsic properties, and fluid properties. Therefore, further research and analysis are often required to fully understand the relationship between wettability and rock thermal properties in the SRTES performance.

2.6.6 Convection and conduction phenomena in thermal energy storage reservoirs

In thermal energy storage systems involving the injection of hot water into a sandstone reservoir, both convection and conduction are important mechanisms for heat transfer. The dominance of one mechanism over the other depends on various factors, including the specific design and operating conditions of the system.

In general, during the initial stages of the injection process, convection tends to be the dominant mode of heat transfer (Vidal et al., 2022a). As hot water is injected into the reservoir, it displaces

the cooler surrounding water and creates a convective flow. This convective flow helps distribute the thermal energy throughout the reservoir, allowing for efficient heat transfer to a larger volume of the sandstone (Gao et al., 2023). Convection plays a significant role in rapidly distributing the heat and ensuring that it reaches a larger portion of the reservoir.

However, as time progresses and the hot water comes into contact with the sandstone matrix, conduction becomes increasingly important (Qi et al., 2023). Heat is transferred from the hot water to the adjacent rock particles through conduction. The thermal conductivity of the sandstone determines the rate of heat transfer by conduction. Conductive heat transfer through the solid sandstone matrix would also occur concurrently on a smaller scale, propagating heat ahead of and behind the convecting fluid front. Over longer time periods after injection ceases, conduction would dominate as the dominant residual heat transfer mechanism as the reservoir gradually cools and stabilizes. The efficiency of a SRTES system increases when heat conduction leads over heat convection (Vidal et al., 2022a).

The relative importance of convection and conduction can vary depending on factors such as the flow rate of the injected hot water, the temperature difference between the injected water and the reservoir, the porosity and permeability of the sandstone, and the geometry of the system. These factors influence the efficiency and effectiveness of heat transfer mechanisms.

Nusselt number

The Nusselt number (*Nu*) is a is a dimensionless parameter used in heat transfer analysis to characterize the convective heat transfer between a solid surface and a fluid. It represents the ratio of convective heat transfer to conductive heat transfer across a boundary layer (Cengel, 1997).

The average Nu is obtained as:

$$Nu = \frac{\bar{h}d}{\lambda} \quad (5)$$

Where, *Nu* is defined as the ratio of the convective heat transfer coefficient ($\bar{h}$) to the conductive heat transfer coefficient represented by the ratio of thermal conductivity (λ) and the characteristic length (*d*).

In the context of seasonal thermal energy storage in sedimentary rocks, the Nusselt number provides useful insights. During the loading phase, a high Nusselt number (*Nu* >> 1) indicates that convective heat transfer via fluid motion is efficiently transporting and distributing heat throughout the reservoir, rather than slower conductive processes (Nagano et al., 2002). In a highly efficient system the hot water fully saturate the rock and enables fast charging of the storage medium via convection currents.

Prandtl number

The Prandtl number (*Pr*) is a dimensionless number that compares the relative importance of thermal diffusivity and momentum diffusivity (kinematic viscosity) for a fluid.

$$Pr = \frac{\nu}{\kappa} = \frac{\mu C_p}{\lambda} \quad (6)$$

Where ν represents thermal kinematic viscosity, which is the ratio of dynamic viscosity (μ) and density, and κ represents the thermal diffusivity.

The Prandtl number has a direct impact on the convective heat transfer rate within the sedimentary reservoir. The *Pr* number is heat transfer fluid's intrinsic property. Fluids with low Prandtl numbers

are characterized by high thermal conductivity and fluidity, making them excellent choices for efficient heat conduction (Rapp, 2016).

Rayleigh number

The Rayleigh number is a dimensionless parameter that represents the ratio of buoyancy forces to viscous forces in a fluid (Nield and Bejan, 2017).

$$Ra = \frac{\beta \rho g h C_p k \Delta T}{\mu \lambda} \qquad (7)$$

Where, β is the coheficient of thermal expansion, g is the acceleration of gravity, C_p is the heat capacity, and *k* is permeability. The Rayleigh number dictates the occurrence and intensity of natural convection within the SRTES aquifer (Spitler et al., 2016). Natural convection arises when buoyancy forces resulting from temperature differences drive fluid motion. Higher Rayleigh numbers indicate stronger buoyancy forces and are associated with more vigorous natural convection (Sheikholeslami and Ganji, 2017). This can lead to enhanced heat transfer rates within the aquifer.

2.6.7 Discussion of rock thermal properties

In section 2.6, there were presented how thermal conductivity, thermal diffusivity, and heat capacity affect different sedimentary rocks and different heat transfer fluids. Among sedimentary rocks, sandstone showed the best thermal conductivity and diffusivity values in samples saturated in water. These optimal thermal properties, combined with favorable petrophysical properties (high storage and flow capacities), make sandstones an ideal candidate for SRTES reservoirs for utility-scale applications. A reservoir delimited with shales not only provides a sealed vessel, besides the lower thermal conductivity of shales allows for reduced heat losses. The heat transfer fluid that better

complements sandstones is water. Moreover, water is abundant, easily accessible, and cheap, ideal for large-scale thermal energy storage projects.

2.7 Thermal Energy Storage Sedimentary Reservoir Configuration

The previous chapters contextualize the applicability of thermal energy storage in sedimentary aquifers for utility-scale projects. This chapter explores the different components of the subsurface sedimentary TES, and factors that impact the implementation of them in large-scale projects.

2.7.1 TES Reservoir

Similar to an ideal oil & gas reservoir, the thermal energy storage reservoir is a permeable porous rock confined by seal rocks (cap-rock and base-rock with minimal to no permeability) (Allen, 1979). Other desirable properties for ideal thermal storage are low thermal conductivity of cap and base rocks, access to a large volume aquifer, and the capability to store water under high pressures (Allen, 1979; Green et al., 2021; Tsang et al., 1977; Xu et al., 2014). Choosing a proper reservoir for thermal energy storage is essential to a successful TES system. The capacity of an aquifer to receive or store water restricts the production rate that may be employed in a TES plant. Furthermore, the sedimentary reservoir's porosity influences the reservoir volume aquifer needed to hold a particular volume of hot or cold water. This condition will constrain the size of the TES field. The size, form, and functioning of the TES system are also affected by the direction and velocity of groundwater flow and the thermal characteristics of water and sedimentary rock. (Bakr et al., 2013).

In **Figure 17** it is depicted the configuration of a subsurface thermal energy storage system. In a TES system, the surplus of energy generated by other renewable resources is used to heat water (or the selected heat transfer fluid). Then the heated HTF is injected into the reservoir. The sedimentary reservoir keeps the water during a certain amount of time (this time is defined by the

energy cycle required). Then the water is produced to generate energy. The hot water and the steam produced are used to generate power, or in a direct use application to provide heat and cooling to buildings.

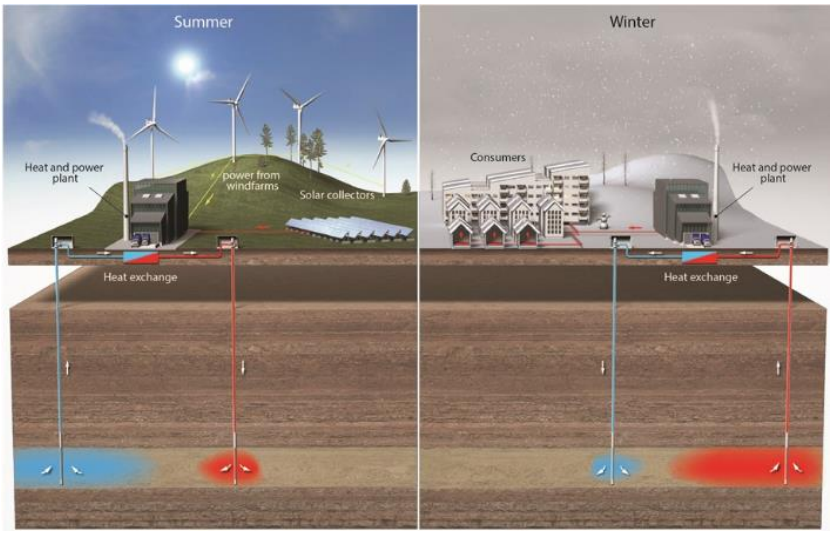

Figure 17. Subsurface thermal energy storage system in summer [left] and in winter [right] (Kallesøe et al., 2021)

Reservoir volume available in sedimentary sands throughout the US offers petrophysical conditions that facilitate the implementation of large-scale TES (Idaho National Laboratory, 2006).

The US offers large sedimentary areas that can be potential candidates for the sedimentary reservoir thermal energy storage implementation (Anderson, 2013). Using sedimentary formations has significant advantages; among them, the wells are significantly easier to drill, shallower, faster, and less expensive (Idaho National Laboratory, 2006). Moreover, TES projects can benefit from O&G infrastructure (wells and pipelines) or information to characterize the reservoir (well logs, regional studies) (Salehi et al., 2022). Many upfront reservoir and development costs can be decreased, and the current infrastructure can be adjusted to power generation (Idaho National Laboratory, 2006).

Various authors have evaluated using sedimentary formations for thermal energy storage implementation (Buscheck et al., 2016; El Alami et al., 2020; Green et al., 2021; Wendt et al., 2019). Using sedimentary formations has significant advantages, among them, the well are significantly easier to drill, shallower and faster and less expensive (Wendt et al., 2019). Winterleitner et al. (2018) evaluated the geological, petrophysical and thermal properties of a shallow aquifer near Muscat, Oman, for the implementation of a SRTES. The sandstone reservoir is located 250 m of depth, has a reservoir pressure of 3.88 MPa and can store water at 70°C for seasonal storage (up to 180 days) with an injection rate of 6.4 l/s. Wendt et al. (2019) simulated a thermal energy storage sedimentary reservoir at 1,220 m with a porosity of 0.15 and a horizontal permeability of 100mD. The system is intended to store solar thermal heat in a daily cycle process. With a temperature injection of 250°C and a water extraction production of 40 kg/s for 8 hours per day, the system can deliver 40 MW_e. Panja et al. (2020) performed a sensitivity study using a commercial simulator (CMG-STARS), simulating a huff and puff daily cycle (8 hrs for injection, 10 hrs for production, and 6 hrs shut-in). Sensitivity analysis in various porosities (5%, 10%, 15%, and 20%) and permeabilities (10, 20, 50, and 100 mD) showed an insignificant impact on pressure and temperature profiles. In contrast, formation thickness and injection rate showed an apparent effect on temperature and pressure profiles. Numerical simulations have shown that energy recovery is potentially high in the long term. However, the thermal front in the reservoir requires a charging time to expand inside the TES reservoir. In this case, optimal well spacing is critical to efficiently recover the stored heat (Green et al., 2021; Panja et al., 2020; Wendt et al., 2019).

In **Figure 18**, it is observed a map of the sedimentary basins in the continental United States. This illustrates the areas where the concept of using sedimentary rocks for storing heat can be applied.

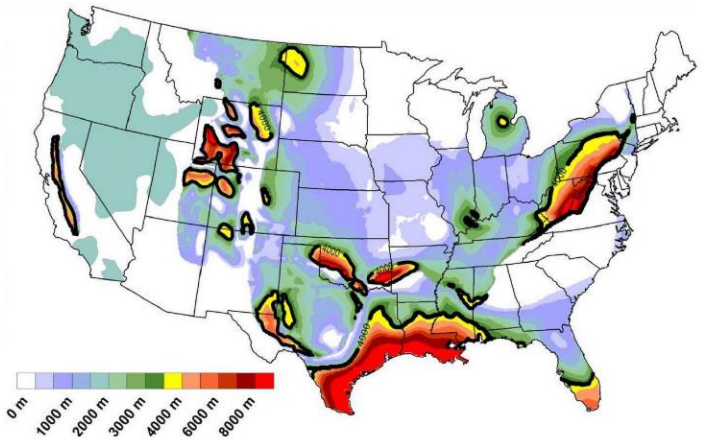

Figure 18. Sediment thickness in the continental United States (Idaho National Laboratory, 2006)**.**

An optimal sedimentary formation with the potential to be a thermal energy storage reservoir needs to meet three conditions. Firstly, the reservoir has to have sufficient volume capacity to store the heat transfer fluid. Secondly, the rock has to let the HTF flow through the reservoir during the injection and production stages. Finally, the reservoir pressure has to be enough to contain the working fluid in a liquid phase (Green et al., 2021). The petrophysical properties that evaluate the storage capacity and the transmissibility capacity are the porosity and the permeability. In the **Figure 19** it is presented the porosity and permeability of different basins throughout the U.S. that can be potential candidates for thermal energy storage implementation (Anderson, 2013). Those areas have known geological and petrophysical information from O&G exploration and development. SRTES projects can benefit from the subsurface knowledge generated in O&G, which will be represented in lowering the costs of gathering reservoir characterization data. Besides, inactive O&G infrastructure, like existing wells that have ended their productive cycle, can enable access to sedimentary reservoirs that otherwise are cost-prohibitive for SRTES projects (Salehi and Nygaard, 2011).

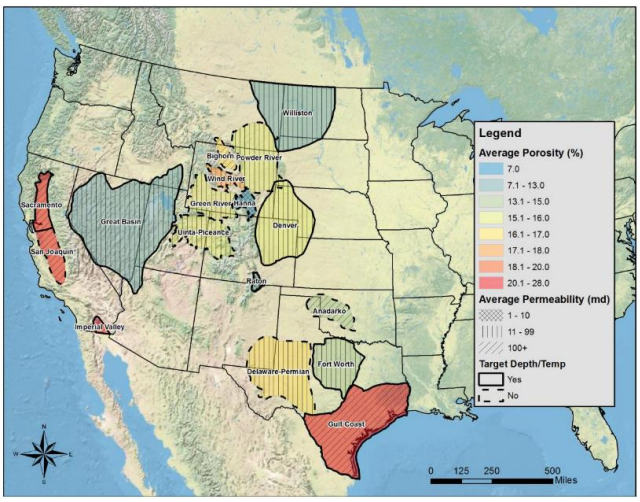

Figure 19. Map with sedimentary regions with high flow and storage capacity in the United States (Anderson, 2013)**.**

2.7.2 Well Configurations

The wells configuration plays an important role in the TES performance. Deficient TES design leads to a high surface area vs. volume proportion of the layout form, entitling substantial conductive heat losses and lowering storage efficiency significantly (Skarphagen et al., 2019). A number of authors have analyzed the influence of well configuration in terms of sweep efficiency (Green et al., 2021; Panja et al., 2021; Sanyal and Butler, 2005; Vidal et al., 2022b). This section of the study will focus on the influence of the well configuration in terms of enthalpy efficiency.

Llanos et al. (2015) comparative performance of 3 system configurations: duplets, 4-spot and 5-spot using the information from Cooper Basin, Australia. The authors performed a numerical simulation forecasting the temperature evolution with the different layouts, finding that with the same water production (35 kg/s), the flowing wellhead temperature was better in the duplet system, showing a better thermal efficiency (**Figure 20**). Zhou et al. (2016) evaluate the performance of different well configurations using horizontal wells systems (**Figure 21**). The authors concluded that the thermal breakthrough time or cumulative water production at the thermal breakthrough time

in horizontal well doublet systems with longitudinal fractures or multi-stage orthogonal fractures is proportional to the product of well spacing, horizontal section length, and well spacing squared. The optimal reservoir design in horizontal well doublet systems with longitudinal or multi-stage orthogonal fractures has the longest modeled horizontal section length and the smallest well spacing value that satisfies the imposed constraint of a thermal breakthrough.

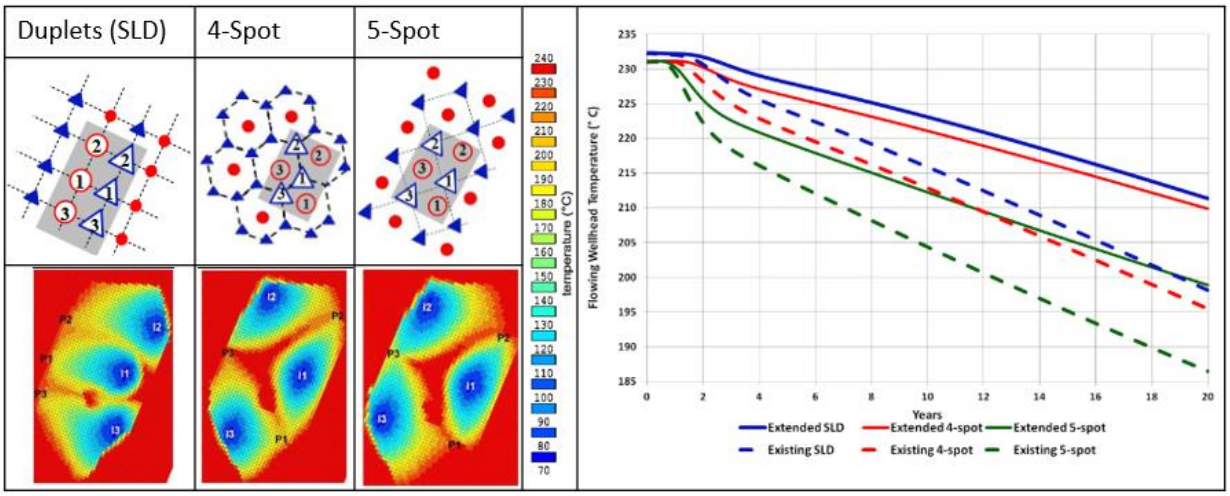

Figure 20. Temperature and cold front of different layouts (After Llanos et al., 2015)**.**

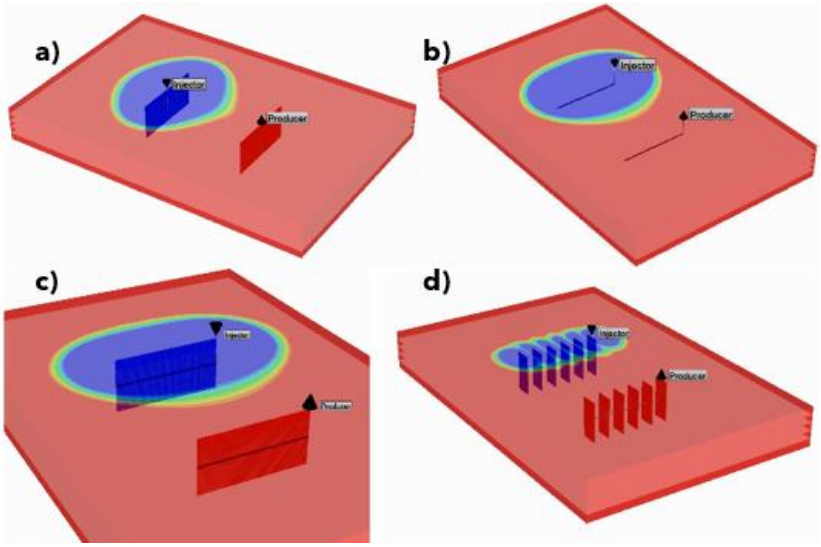

Figure 21. [a] vertical duplet, [b] horizontal doublet completed in open hole, [c] horizontal duplet stimulated with fractures parallel to well axis, and [d] horizontal duplet stimulated with fractures perpendicular to well axis (After Zhou et al., 2016)**.**

Mindel and Driesner (2020) evaluated numerically the effect of the well pattern in the performance of a TES for a design project using the information of an aquifer located in Geneva, Switzerland. The authors evaluated 3 layouts, a single well, a doublet, and a 5-spot (**Figure 22**). The simulations revealed that the doublet and 5-spot patterns routinely beat the single well pattern, which also mimics the scenario wherein auxiliary wells must travel a great distance to provide pressure support. In contrast, the 5-spot pattern only occasionally performs slightly better than the doublet. From a perspective of techno-economical, the duplet pattern seems to be superior (Mindel and Driesner, 2020).

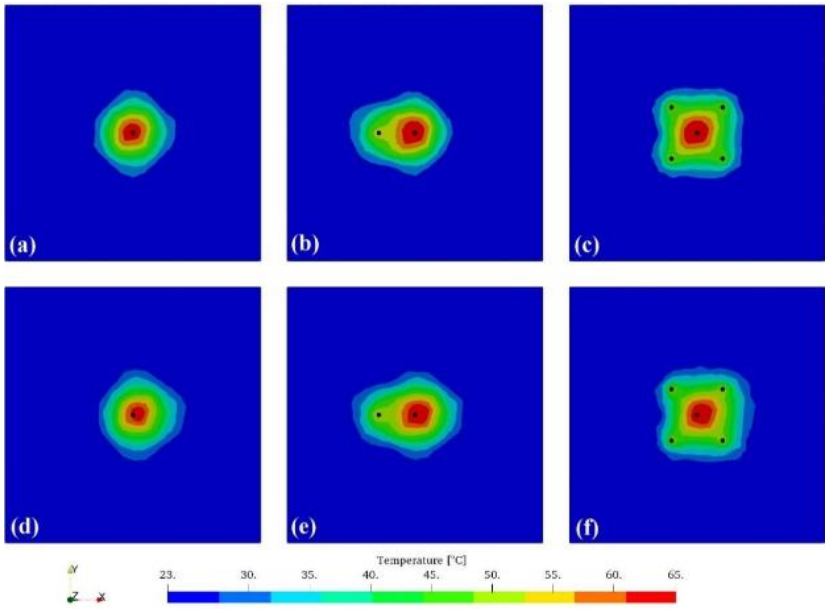

Figure 22. Temperature and cold front of different layouts at the end of the simulation with groundwater flow effect [a, b, and c] and without groundwater flow effect [d, e, and f] (Mindel and Driesner, 2020)**.**

Bakr et al. (2013) evaluated the effect of interference evaluating 19 TES systems in a sedimentary TES in The Hague, Netherlands. Each system contained different amounts of wells, production and injection rates, wells spacing, and configurations. As the wells are placed in the same region, they offered an excellent opportunity to compare the influence of wellbore layout and

performance with real-life data. The efficiency of each TES was evaluated for 10 years. **Figure 23** depicts the 76 wells and 19 TES systems that were analyzed. Clusters of wells are from 2 wells (single duplet -injector-producer) and up to 10 wells (5 injectors, 5 producers). The effect of interference was analyzed in terms of energy interference.

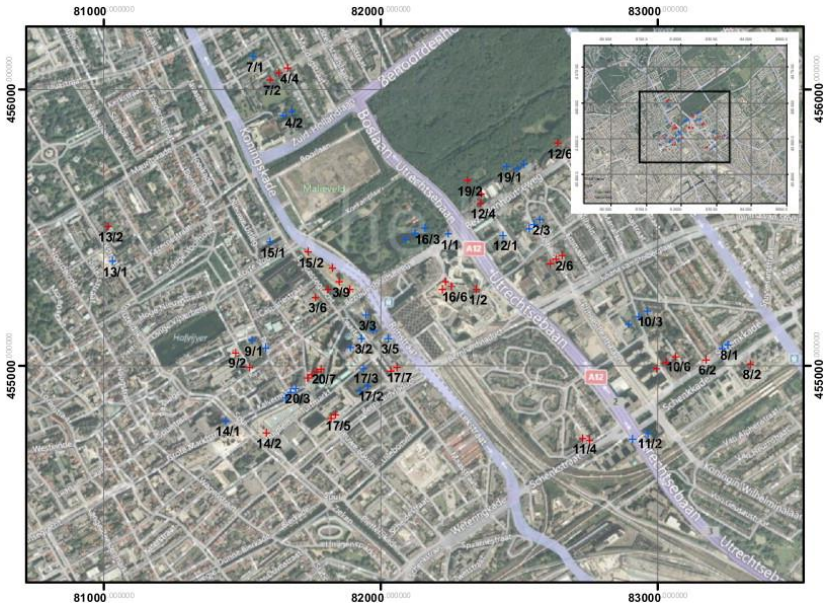

Figure 23. Map with 76 wells (blue marks for cold and red marks for warm) in 19 TES systems (Bakr et al., 2013)**.**

Bakr et al. (2013) observed that the effect of the interference variates among the wells; in some wells, the interference has a positive impact on the efficiency (up to +20%). In other wells, interference has a negative impact on efficiency (up to -25%). The authors concluded that the overall impact of interference was positive at +3.2%. As the paper offers some data about the efficiency in the different TES, that data was analyzed to understand the impact of different configuration variables. **Table 5** summarizes the data from 76 well that were extracted from the Bakr et al. (2013) paper using digital tools.

Table 5. Summary of data extracted from the The Hague TES project, used in the data analysis.

TES System	# Wells per TES system	Average Prod per well pair [m^3/ day]	Total Prod per TES [m^3/ day]	Avg Distance Inj-Prod well [m]	Efficiency [%]
	No_Wells	Total_Per_Well	Total_Prod	Dx_I-P	Efficiency
S01	2	730.6	730.6	224.9	87.1
S02	6	547.9	1643.7	147.2	84.2
S03	10	566.2	2831	217.0	85.1
S04	4	547.9	1095.8	157.8	84.9
S06	2	200.9	200.9	72.0	77.9
S07	2	526.0	526	106.2	82.3
S10	6	730.6	2191.8	190.8	86.7
S11	4	712.3	1424.6	193.0	84.7
S12	6	749.5	2248.5	150.4	85.3
S13	2	305.9	305.9	124.4	81.3
S14	2	1424.7	1424.7	152.2	83.8
S15	2	1369.9	1369.9	143.5	81.9
S16	6	599.1	1797.3	221.1	86.6
S17	7	626.2	2191.8	129.7	78.6
S18	2	949.8	949.8	91.2	73.5
S19	2	949.8	949.8	152.9	81.1
S20	7	302.7	1059.3	105.1	80.7

This analysis aims to understand the influence of well configuration parameters, such as the number of wells per system and distance from the injector and producing wells, on the performance of the TES. **Figure 24** presents a scatter plot where the relationship between the number of well in the TES (No_Wells), average production per producing well (Total_Per_Well [m3/day]), total production of the TES system (Total_Prod [m3/day]), the average distance between injectors and producers (Dx_I-P [m]), and efficiency [%] is presented. The plot shows that the average distance between injection and producing wells is strongly positively correlated with the TES efficiency. The tendency shows that the longer the distance, the better the efficiency. The number of wells per TES as well as a positive influence, but this influence seems to be connected to the amount of production. More wells increase the overall production, and overall TES production is positively correlated with efficiency. Another finding is that systems with 7 wells are less efficient than systems with 6 and 10

wells. A potential reason could be the un-even ratio between injectors and producers (in this case, the systems S17 and S20 have more producers -4- than injector wells -3-). The rest of the systems have the same amount of injectors and producers.

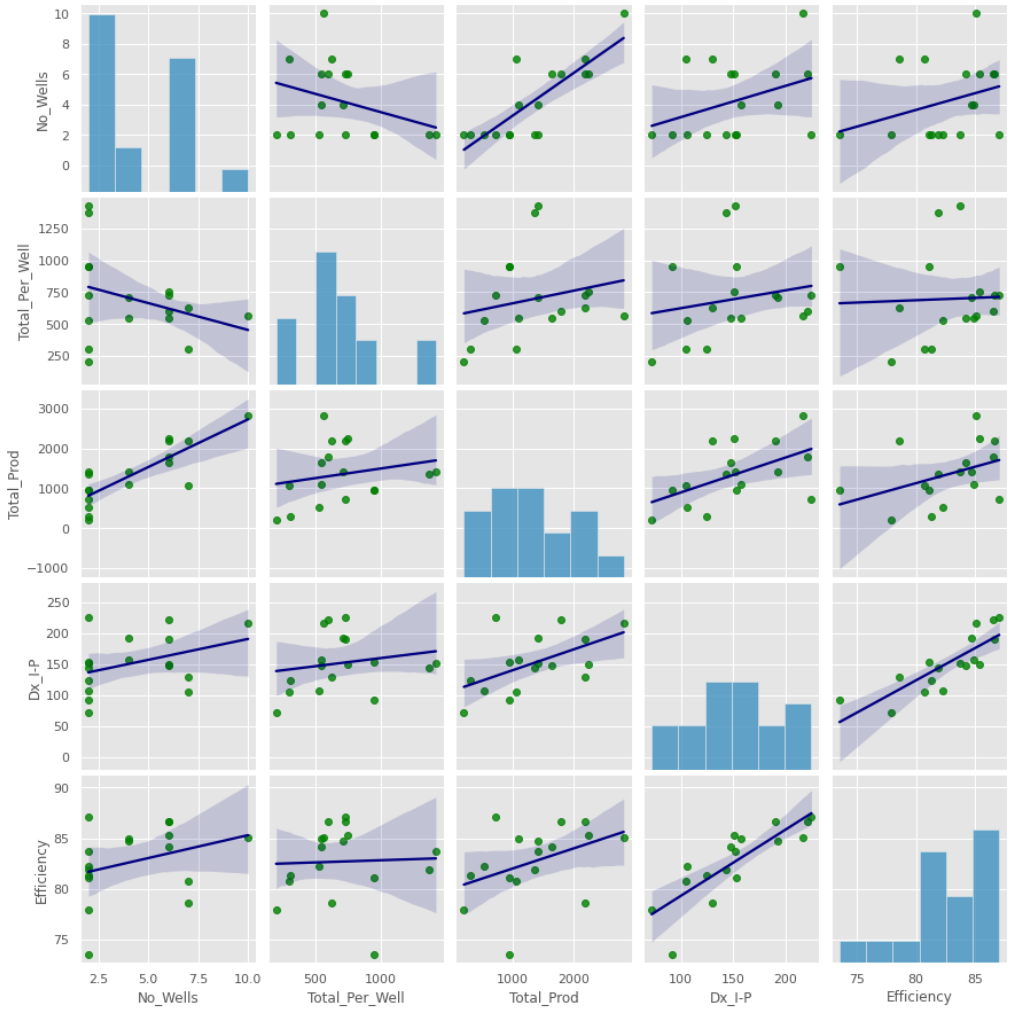

Figure 24. Scatter plot comparing the correlation between the number of well in the TES (No_Wells), average production per producing well (Total_Per_Well [m^3/day]), total production of the TES system (Total_Prod [m^3/day]), average distance between injectors and producers (Dx_I-P [m]), and Efficiency [%].

Figure 25 shows how the different variables evaluated correlate with the TES efficiency. The Pearson correlation coefficient was the method used to calculate the level of correlation between variables. The values closer to 1 (positive correlation) or -1 (negative correlation) indicate that the

variables are correlated. Values closer to zero indicate that the variables are not related (uncorrelated). The results confirm that the efficiency is strongly correlated with the distance between wells. In contrast, the efficiency seems uncorrelated with the average production per well (Total_Per_Well). The correlation between total production and efficiency is less strong than the wells' distance.

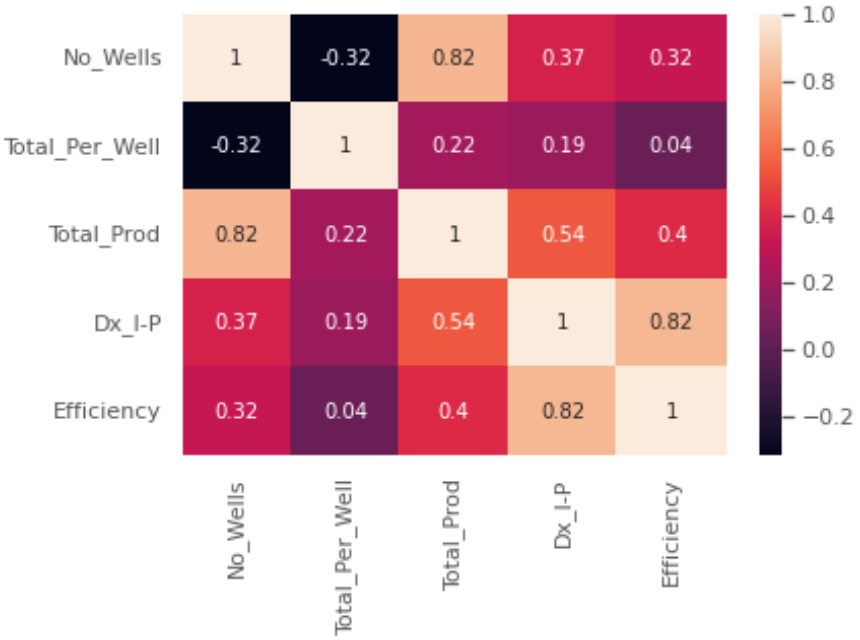

Figure 25. Heat map presenting the correlation between the analyzed variables vs TES efficiency.

The spacing between injection and production wells must be optimized to enable the maximum amount of energy to be stored (Jenne et al., 1992). The injection temperatures in relation to the natural ground-water temperatures determine if any influence from the warm side on the temperatures on the cold side (or vice versa) is wanted. Thermal breakthrough is unwanted if the injection temperatures on the warm and cold sides of the reservoir TES are such that the natural ground-water temperature resides among those values. In contrast, if the injection temperatures on

the warm and cold sides are upper or lower than the average ground-water temperature, then some thermal breakthrough is desired (Jenne et al., 1992).

2.7.3 Thermal Losses in the Wellbores

Ramey (1962) established a mathematical model for the heat transfer in the wellbore, and defined an overall heat transfer coefficient including the heat resistance of the annulus. Heat can be lost through the wellbore walls due to conduction, where heat is transferred from the hot fluid inside the wellbore to the surrounding formation (Kallesøe et al., 2019). Convective heat losses occur when there is fluid flow inside the wellbore. As the fluid moves, it can carry heat away from the desired storage zone, leading to thermal losses (Vangkilde-Pedersen and Kallesøe, 2019). Radiation losses occur when heat is transferred through electromagnetic radiation from the wellbore to the surrounding environment. This can happen if the wellbore is not properly insulated, resulting in energy losses. (Zhou et al., 2015) summarized the heat transfer in wellbores for heat production:

Thermal Conduction:

Thermal conduction occurs in the annulus of the well, unless there is no temperature difference between the tubing outside and the casing inside.

Fourier's Law is used to describe thermal conduction, which states that the energy increment in the direction of r, φ, and z is proportional to the thermal conductivity and the temperature gradient.

$$q = \lambda_a \frac{\Delta T}{\Delta r} \qquad (8)$$

Where λ_a represents the thermal conductivity of the annular material, ΔT is the differential temperature of the casing internal wall and the tubing external wall, and Δr is the difference between the casing internal radius amd the tubing external radius.

The fluid density through the annulus is inversely proportional to the radius, but the fluid flow rate remains constant.

Thermal Radiation:

Thermal radiation occurs when the annulus is filled with gas or vacuum. Radiation is the transfer of heat without a medium and is dependent on the temperature and emissivity of the materials. The radiative heat transfer coefficient can be calculated using the Stefan-Boltzmann Law and depends on factors such as temperature, surface finish, view factors, and the sizes of the tubing and casing. (Hasan and Kabir, 2002) defined the heat transfer coefficient by radiation as follows:

$$h_r = \frac{\psi(T_{tbg}^2+T_{csg}^2)(T_{tbg}+T_{csg})}{\frac{1}{\varepsilon_{tbg}}+\frac{r_{tbg}}{r_{csg}}\left(\frac{1}{\varepsilon_{tbg}}-1\right)} \qquad (9)$$

Where h_r represents the radiation heat transfer coefficient, T_{tbg} and T_{csg} denote the external temperature of the tubing and the internal temperature of the casing respectively, ε represents the emissivity of the casing and tubing, r is the radius of the casing and tubing, and ψ is the Stefan-Boltzmann constant.

Natural Convection:

Natural convection occurs when the annulus is filled with gas or liquid. It is caused by fluid motion resulting from the variation of density with temperature. The proportion of natural convection in the total heat transfer depends on factors such as temperature, annulus size, and the properties of the filling materials. Dimensionless parameters like the Prandtl number and the Grashof number are used to describe natural convection. The convective heat transfer coefficient can be estimated using different methods, such as the Dropkin and Somercales method (Dropkin and Somerscales, 1965).

$$h_c = \frac{0.049 Ra^{1/3} Pr^{0.074} \lambda_a}{r_{tbg} ln\left(\frac{r_{csg}}{r_{tbg}}\right)} \quad (10)$$

Where h_c represents the convective heat transfer coefficient, Ra is the Rayleg number, and Pr is the Prandtl number.

2.7.4 Thermal Energy Storage Cycles

The cycle of heat injection to energy harvest can be performed from hours to months. To compensate the intermittence of renewables, when the systems are generating a surplus of energy, this energy is converted into heat. Water is used to transport the heat to charge the reservoir. Then the heat is stored in the reservoir until needed. In a daily cycle, for instance, in applications that combine solar energy with the TES, the surplus of solar energy generated during the off-peak hours is used to heat water that is injected in the reservoir. Then, the energy is produced during the peak of usage hours when the solar energy generated is not enough to satisfy the demand (Green et al., 2021). **Figure 26** depicts a daily cycle of a TES linked with solar energy.

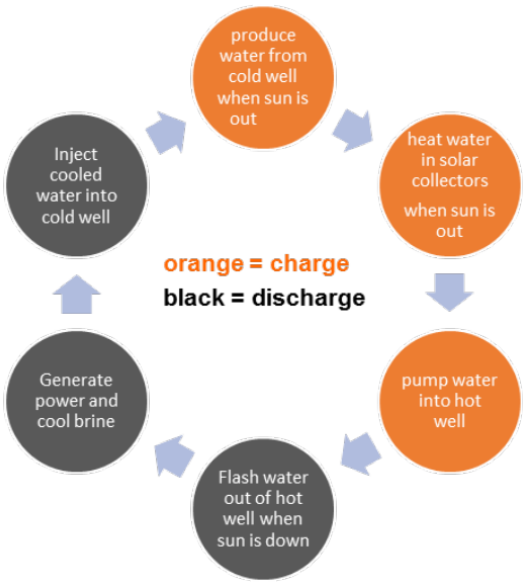

Figure 26. Sedimentary reservoir TES operation cycle (Wendt et al., 2019)**.**

In seasonal cycles (or annual cycles), the process consists in capturing additional heat energy in the summer and storing it for use in the winter (Sheldon et al., 2021). Green et al. (2021) present a numerical study where wellbore temperatures were simulated for daily cycles of injection, storage and production. In **Figure 27** it is depicted how the bottom hole temperature tends to stabilize with the time and cycles.

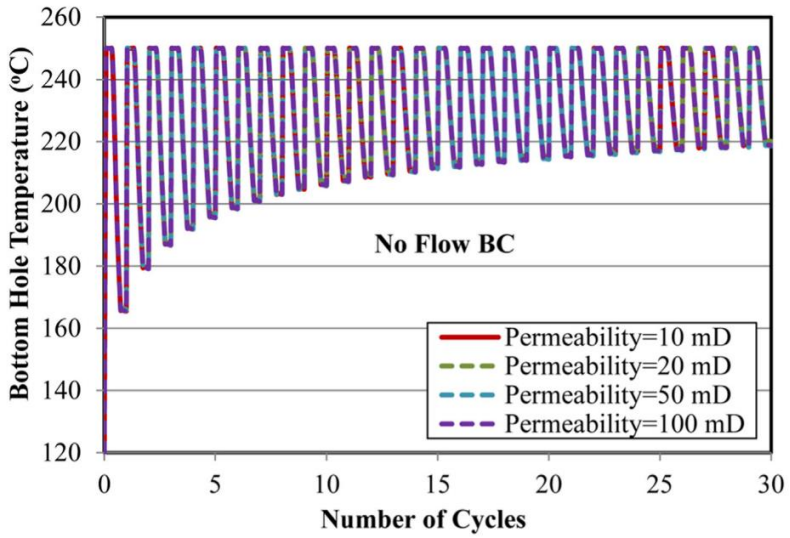

Figure 27. Bottom hole temperature of 30 daily cycles at two different initial reservoir temperatures (Green et al., 2021)**.**

Sheldon et al. (2021) evaluated the recovery efficiency (the ration between the heat injected to the heat recovered) in daily and annual cycles. The daily cycle is divided into 4 parts, for charging, storage, production and rest, which corresponds to 8 hours, 4 hours, 8 hours and 4 hours respectively. The annual cycle has the same four sections (charging, storage, production and rest), and each section lasts 3 months. The results indicated that the daily storage is more efficient in terms of energy recovered, with efficiencies ranging in the different scenarios simulated from 63% to 93%. In contrast, the annual cycle obtained results ranging from 11% to 88%. **Figure 28** shows the temperature profiles of different scenarios at the end of the injection and at the end of storage for the daily cycle (left), and the annual cycle (right). The white lines represent the boundaries of the

reservoir (cap-rock and base-rock). The images for the annual cycle shows that the hot front has more radial distance inside the reservoir than the daily cycle. However, in the annual cycle simulation it is observed that an important portion of the heat was transferred to the cap-rock and the base-rock. As the latter rocks are impermeable, the hot stored is not completely recovered, impacting negatively the TES efficiency.

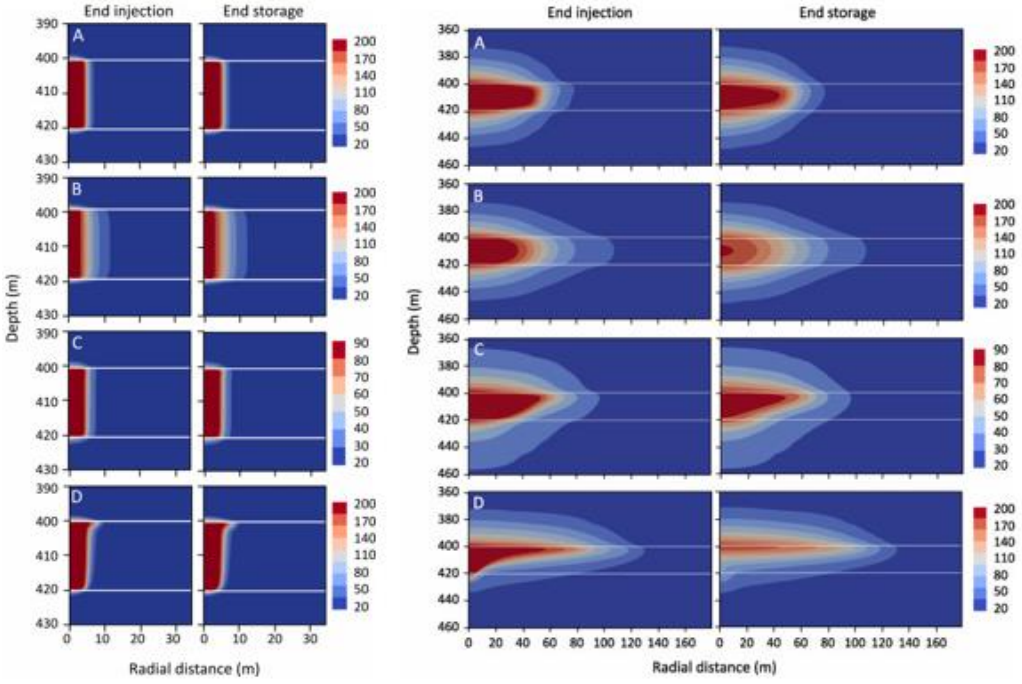

Figure 28. Temperature profile of different scenarios at the end of the injection and at the end of storage for the daily cycle [left], and the annual cycle [right] (Sheldon et al., 2021)**.**

2.7.5 Reservoir TES temperature

Temperature is a key factor that impacts the amount of energy stored in the reservoir and the thermal efficiency of the sedimentary energy storage system. The higher the temperature the higher is the utilization efficiency when the produced heat is converted into power (Beckers and McCabe, 2019) (**Figure 29**). Reservoir depth affects the TES temperature and thermal productivity. In reservoir from 500 to 1,000 m depth the differential temperature between the storage system and the

neighboring rocks decreases, which minimizes the thermal losses, increasing the efficiency (Homuth et al., 2013). Higher temperature storage allows a significant differential temperature between the extracted and infiltrated water, enhancing the energy supplied per unit of volume of pumped water. Consequently, compared to lower temperature TES, the water production rate needed to meet a given heat demand is much lower (Drijver et al., 2012). Deeper reservoirs offer higher pore pressures, providing the opportunity to store liquid water at higher temperatures (Green et al., 2021). In Karlsruhe, Germany, a high temperature TES is planned to reach 1,400 m TVD (true vertical depth), targeting to store water up to 150ºC (Karlsruhe Institute of Technology, 2020).

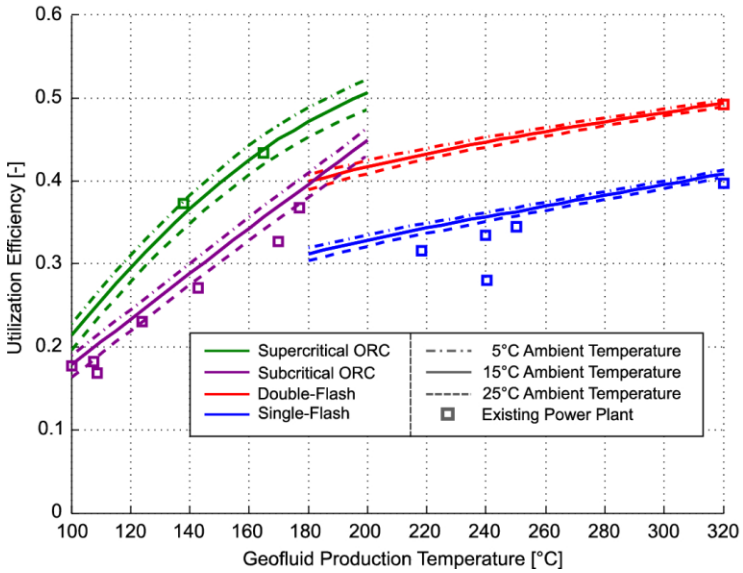

Figure 29. Utilization efficiency versus fluid production temperature (Beckers and McCabe, 2019)**.**

Initial reservoir temperature has an influence in the heat loss during production-injection cycles (Buscheck et al., 2017; Green et al., 2021; Wendt et al., 2019; Xu and Pruess, 2004). The process of pre-charging the reservoir before the cycling process contributes to the differential temperature generating during the injection-production stages (Green et al., 2021; Wendt et al., 2019). Wendt et al. (2019) analyzed the effect of pre-charging the reservoir using numerical

simulations. In the study, scenarios from no pre-charging, 30, 60, 90, and 180 days of pre-charge were evaluated. In the **Figure 30** it is observed how pre-charging the reservoir for 30 days made an apparent effect in the temperatures obtained in a daily cycle simulation. Above 60 days of pre-charging the improvement is less notorious. The concept of reservoir thermal pre-charging positively contributes to the overall TES efficiency (Wendt et al., 2019).

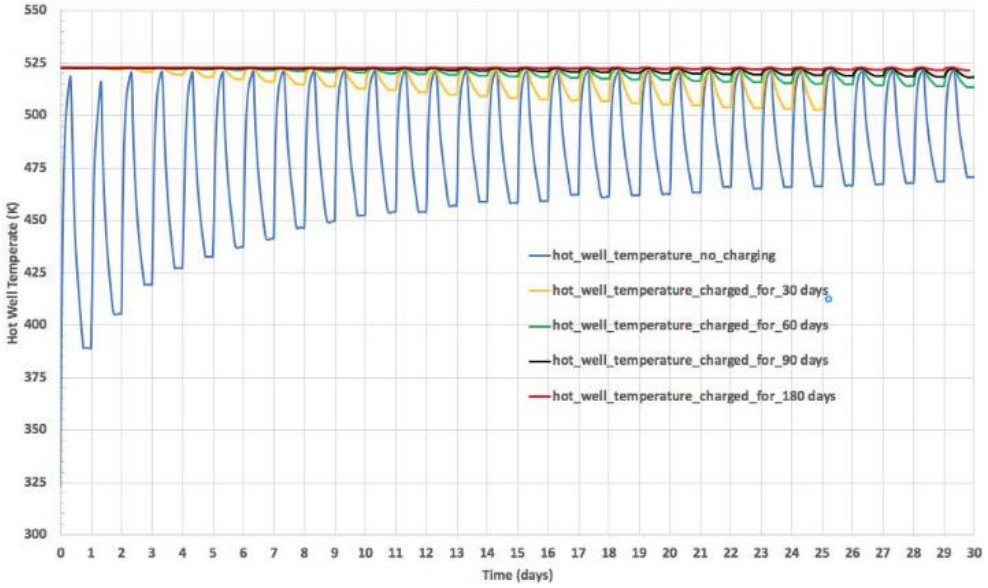

Figure 30. Effect of reservoir thermal pre-charging time in a simulated daily cycle over 30 days (Wendt et al., 2019)**.**

In the **Figure 30** it is observed in the scenario of no pre-charging that the temperature variation during cycles is reducing during time. This shows that the reservoir improves its thermal efficiency as it heats up with the thermal cycles. This effect is evidenced by Bakr et al. (2013) when they analyzed the real efficiency of 19 TES systems with time (**Figure 31**). In all TES systems, the thermal energy efficiency increased with time. This endorse that with cycles, the reservoir temperature increases, improving the TES efficiency.

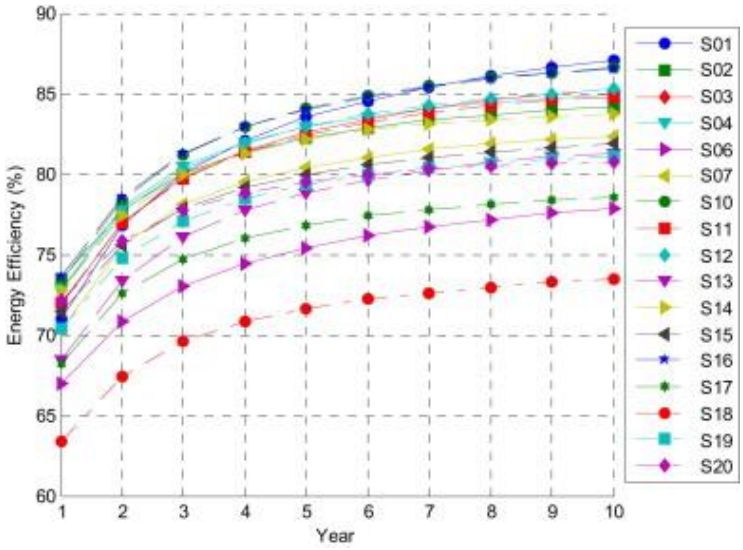

Figure 31. Energy efficiency of 19 TES systems during a period of 10 years in the region of The Hague, Netherlands (Bakr et al., 2013)**.**

2.8 Laboratory Experimental Studies of Thermal Energy Storage

Experimental studies of thermal energy storage in sedimentary rocks are limited. High-pressure / high-temperature (HPHT) environments are difficult and expensive to mimic. In the Chapter 3, it was presented different experimental studies related to thermal and petrophysical rock properties. This chapter will complement the previous experimental results presented, which aggregate insight into different phenomena that affect the performance or compromise the operability of thermal energy storage systems in sedimentary rocks.

2.8.1 Geochemical TES Research

Significant changes in rock geochemistry or mineral precipitation during the interaction of hot brines with the sedimentary reservoirs can be one of the potential causes of TES failures (Neupane et al., 2021, 2020). McLing et al. (2022) presented a comprehensive experimental study with more than 140 experiments using rock samples from Weber and Tuscaloosa formations. The experiments were conducted over periods of time from 1 to 84 days, with pressures ranging from 1 to 80 bars and temperatures of 140, 160, 200, and 250ºC. The authors generated 21 combinations of brines with different analytes (Ca++, Fe++, Mg++, Sr++, K+,

Na+, Cl-, and HCO3-) at different concentrations. The objective was to find which conditions and components contribute to the generation of scaling and potential techniques for mitigation. The researchers calculated the saturation index (SI) for different scale minerals. The saturation index indicates if a component is undersaturated (SI < 0), in equilibrium (SI = 0), or supersaturated (SI > 0). The authors analyzed the factors influencing carbonate scaling. Data show that below 200°C, for the Weber and Tuscaloosa samples, that there is not presence of calcite saturation or supersaturation, but in the Weber sandstone samples at 250°C there was a presence of calcite supersaturation (**Figure 32)**. Scanning electron microscopy (SEM), and energy dispersive X-ray spectroscopy (EDS) were used to identify the formation of scale and identify the composition. The authors wanted to evaluate the effect of CO_2 on calcite saturation index as carbonate scale inhibitor. **Figure 32** shows the results of 3 different CO_2 pressures (P_{CO2}), low (right), medium (center), and high (left) as function of calcite SI in terms of Q (ion activity coefficient) and K (temperature equilibrium constant). The authors conclude that there is not an apparent effect of CO_2 addition on the samples.

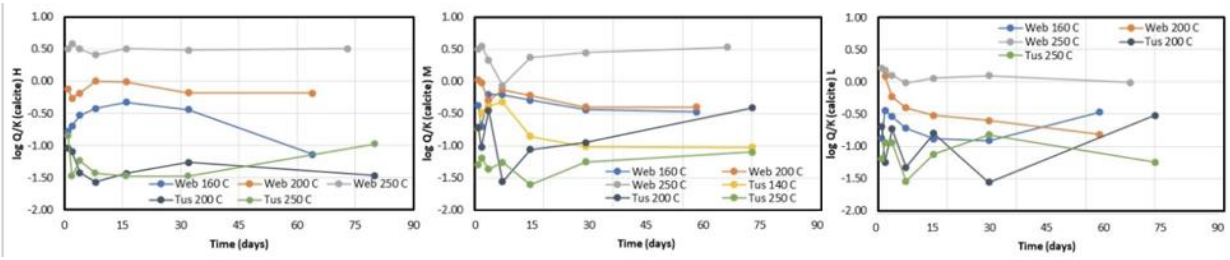

Figure 32. Influence of CO_2 pressure on the calcite saturation index (SI=log Q/K) as function of time at multiple temperatures (after McLing et al., 2022)**.**

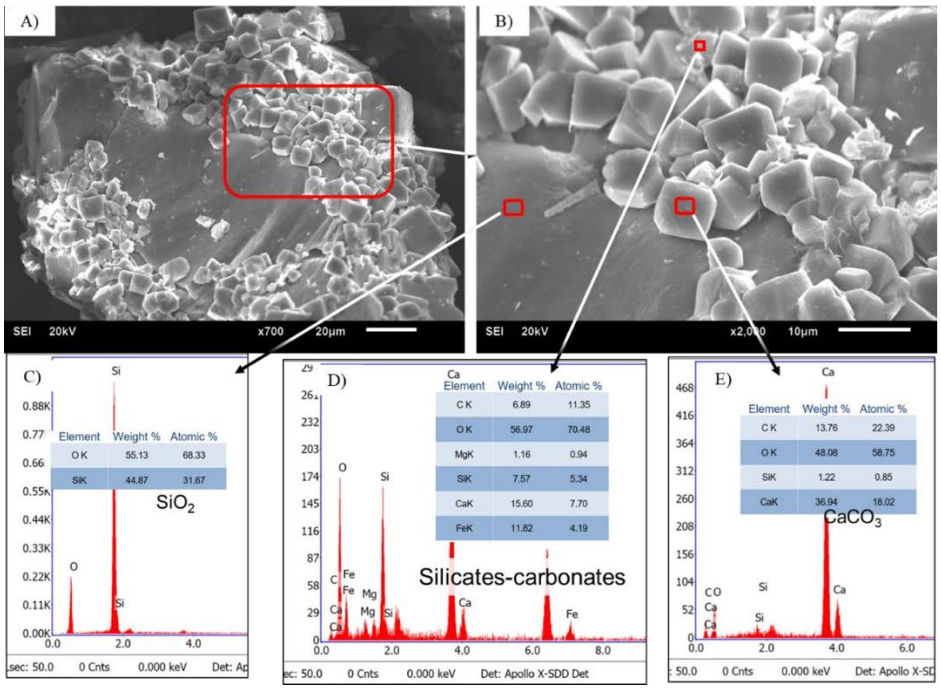

Figure 33. SEM image with secondary silica coating a grain of quartz, and composition of portions selected in the images (McLing et al., 2022; Neupane et al., 2021)**.**

As the referenced study (McLing et al., 2022) released the detailed input variables, experimental conditions, and the results of each experiment, the data was processed to analyze if additional information can be extracted. The authors divided the data in two groups. The first group included the input parameters and experimental conditions of each experiment, including duration, temperature, pressure, pH, dissolved inorganic carbon (DIC), CO_2 pressures (P_{CO2}), and the concentrations of analytes. The second group contains the calculated saturation indexes for the scale minerals per experiment. For the data, the time is in days, temperature in °C, pressure in bars, and analyte concentrations in M molar (mol/L). The groups of data were combined and analyzed to find correlations between the variables. **Figure 34** presents the correlation of 18 variables to the calcite saturation index. For testing conditions, the calcite SI (CAL) seems to be uncorrelated with time and cell pressure, and is slightly positively correlated with temperature. In contrast, pH seems to be highly positively correlated with calcite SI. Regarding the analytes, the increase in concentration of Na+, Mg++, Cl-, and Sr++ are negatively correlated to the calcite SI. Conversely, K+ is positively correlated with the calcite SI. Finally, it seems that

the addition of CO_2 can potentially reduce the carbonate scaling; when the values of P_{CO2} were above 40 bars, all calcite SI shows that calcite was undersaturated.

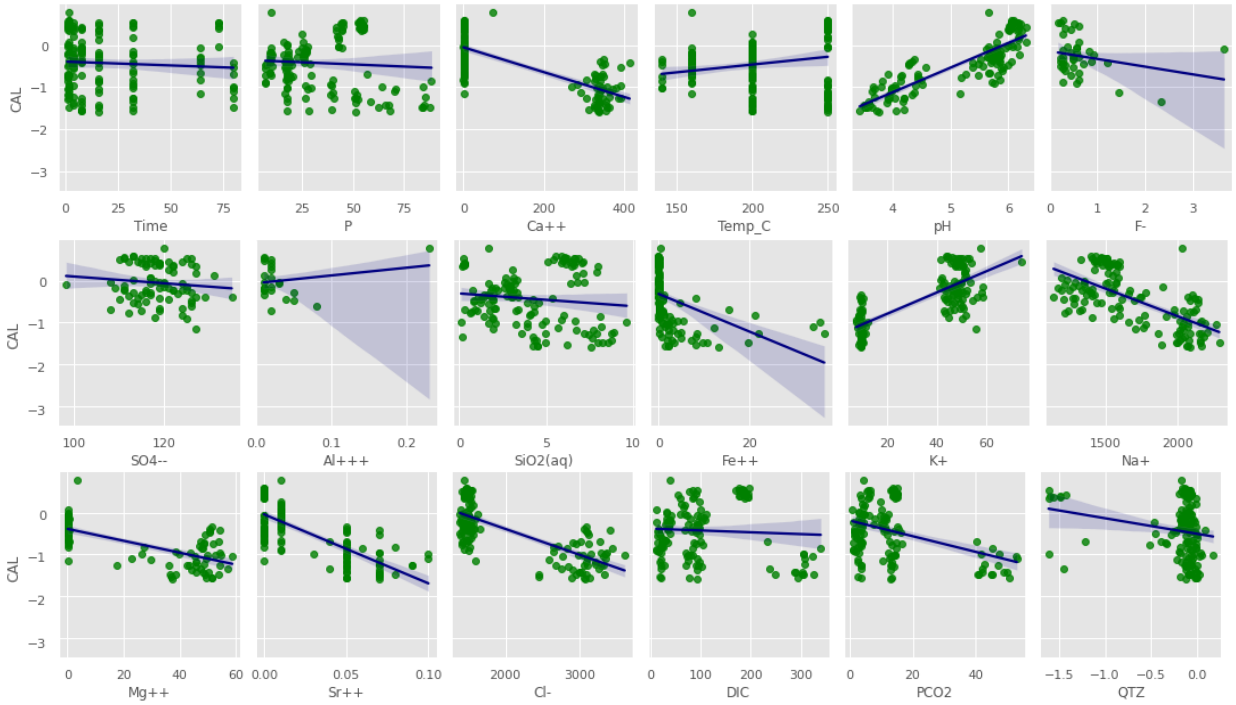

Figure 34. Scatterbox plot of variables correlated with calcite (CAL) saturation index.

The same analysis was performed to evaluate the silica scaling. **Figure 35** presents the correlation of 18 variables to the quartz saturation index (QTZ). For testing conditions, the quartz SI seems to be uncorrelated with time, cell pressure, and pH, and it was slightly negatively correlated with temperature. Quartz saturation index seems to be uncorrelated with the analytes evaluated. As expected, the addition of CO_2 show no influence in quartz SI. In general the variables evaluated in this data set show no conclusive correlation with quartz saturation index, showing that non of them are good candidates to control (or be contributors to) silica scaling.

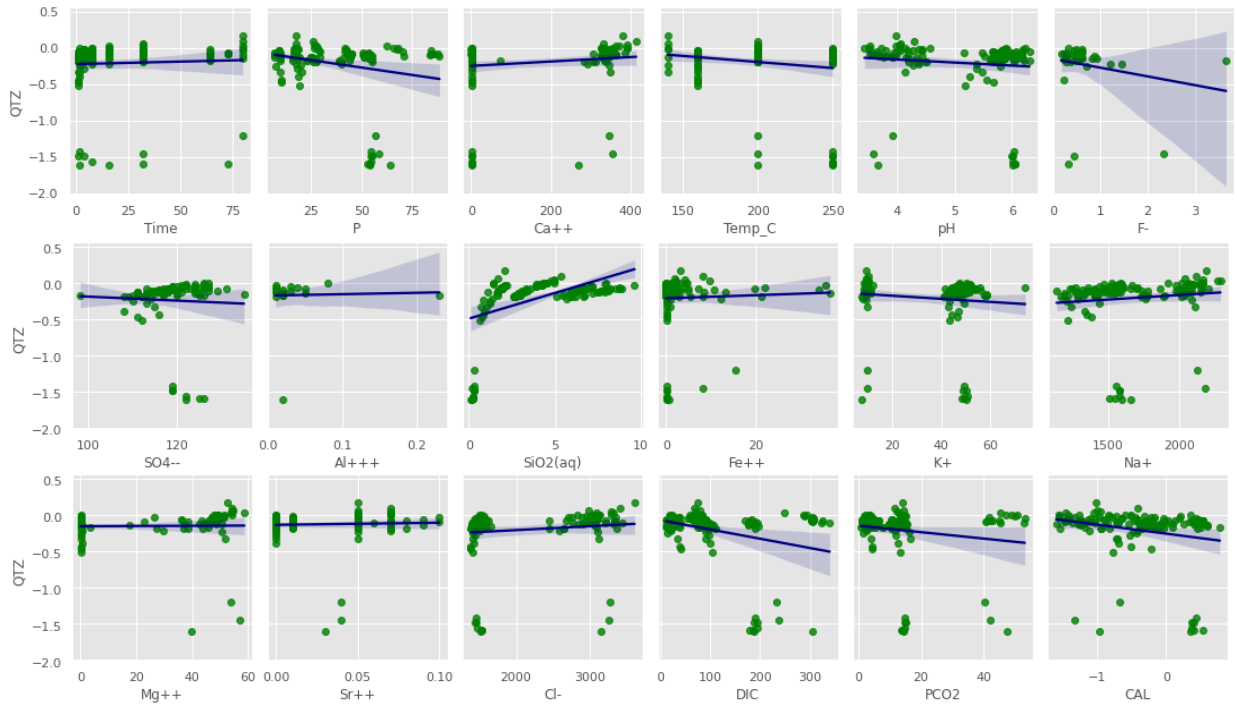

Figure 35. Scatterbox plot of variables correlated with quartz (QTZ) saturation index

Figure 36 presents how the different variables evaluated correlate with the quartz (QTZ) and calcite (CAL) saturation index. The Pearson correlation coefficient was the method used to calculate the level of correlation between variables. The results confirm the strong positive correlation between the pH (0.86) and the molar concentration of K+ (0.76) with the calcite saturation index. In this case the information suggest that mitigating low pH values and reducing the concentration of K+ can contribute for carbonate scaling control. Besides, the results justify the usage of CO_2 for controlling the calcite saturation index. For silica scaling control it is confirmed that none of the variables evaluated have special contribution to the increase of quartz saturation index.

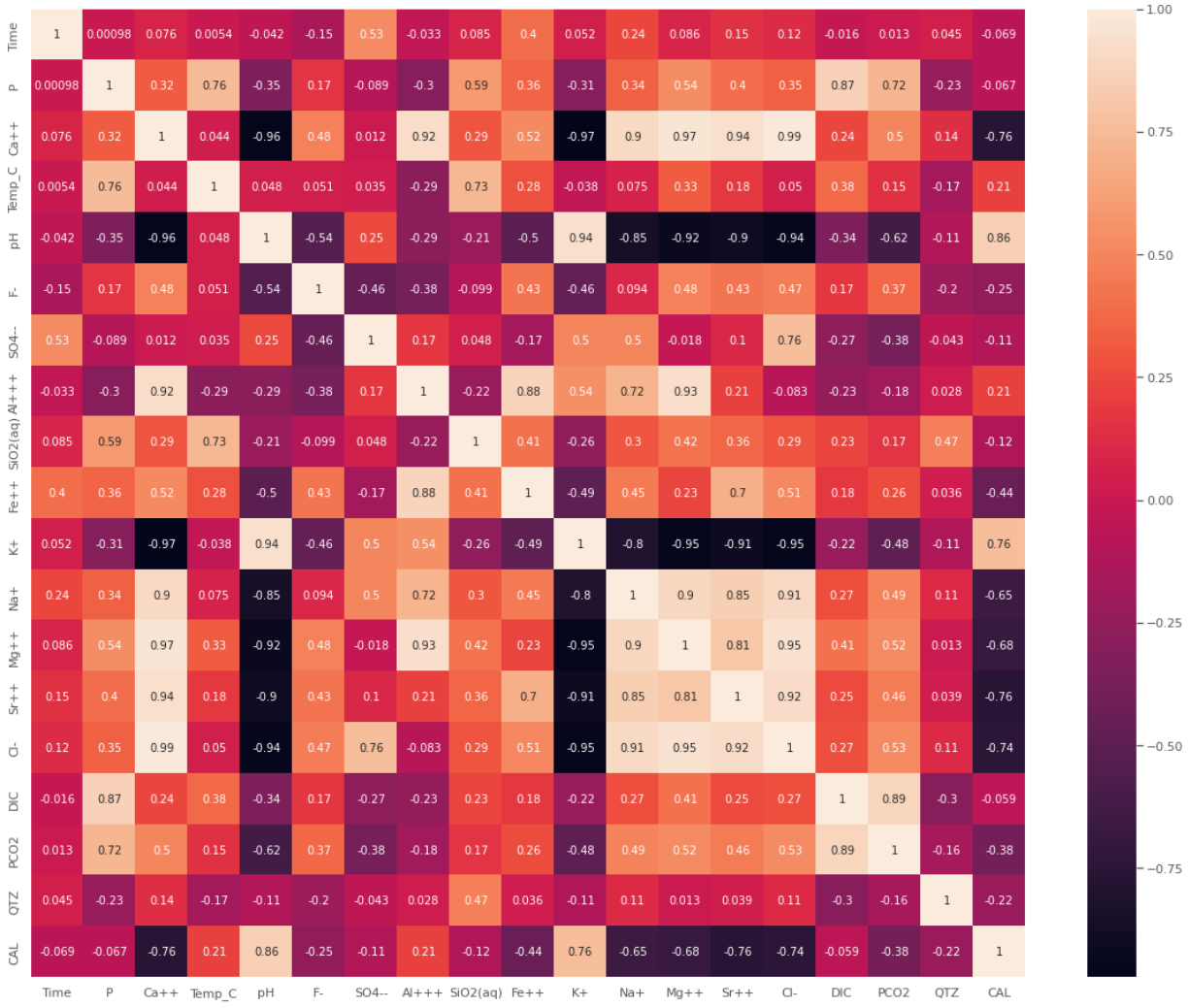

Figure 36. Heat map presenting the correlation between experimental input variables vs calcite (CAL) and quartz (QTZ) saturation index.

2.8.2 TES Laboratory Testing Apparatuses

Abbas et al (2020) build up a lab-scale bore holes in a vessel filed with sand. The novelty of this research is that addresses experimentally the cold storage. The setup consists of 9 pipes (boreholes) in a 3 x 3 layout, each one spaced by 0.1 m (**Figure 37**). The dimensions in the system are downscaled by a factor of 20. The depth of each pipe is 0.8 m (representing a 16 m depth), and the wells diameter is 0.002m (representing a well diameter of 0.04). The heat storage reservoir is a box is a 0.6 x 0.6 m insulated in the boundaries.

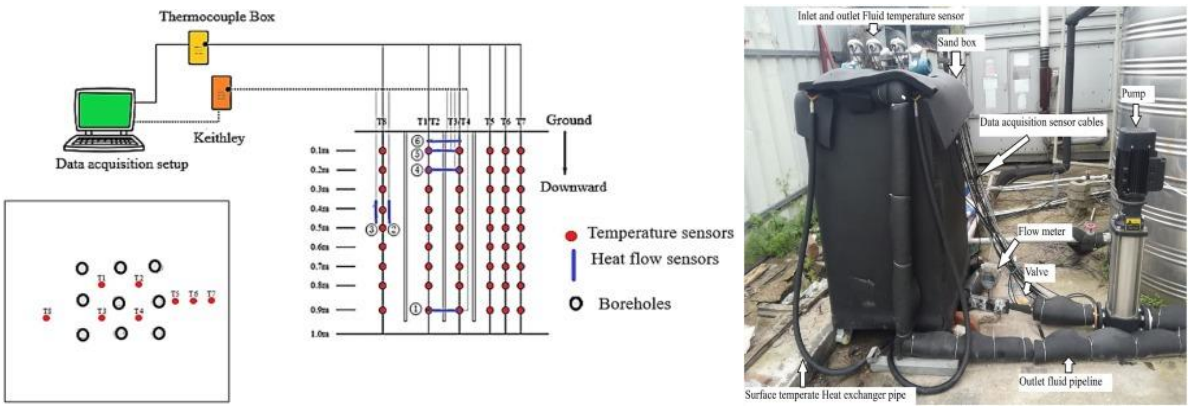

Figure 37. Lab-scale TES diagram with top layout of the 3 x 3 system (in the square), and location of temperature sensors (Abbas et al., 2020)**.**

The inlet temperatures mimic the weather conditions of Dunhuang, China. The heat transfer fluid is water mixed with glycol, to prevent water freezing. **Figure 38** shows the thermal evolution with time, showing that the temperature of the TES reservoir dropped 11°C. Besides, it is observed that the temperature change impacts the TES efficiency. The input energy in the TES was 46,620 kJ, and the extracted energy was 67,134 kJ, for a total efficiency of 69%.

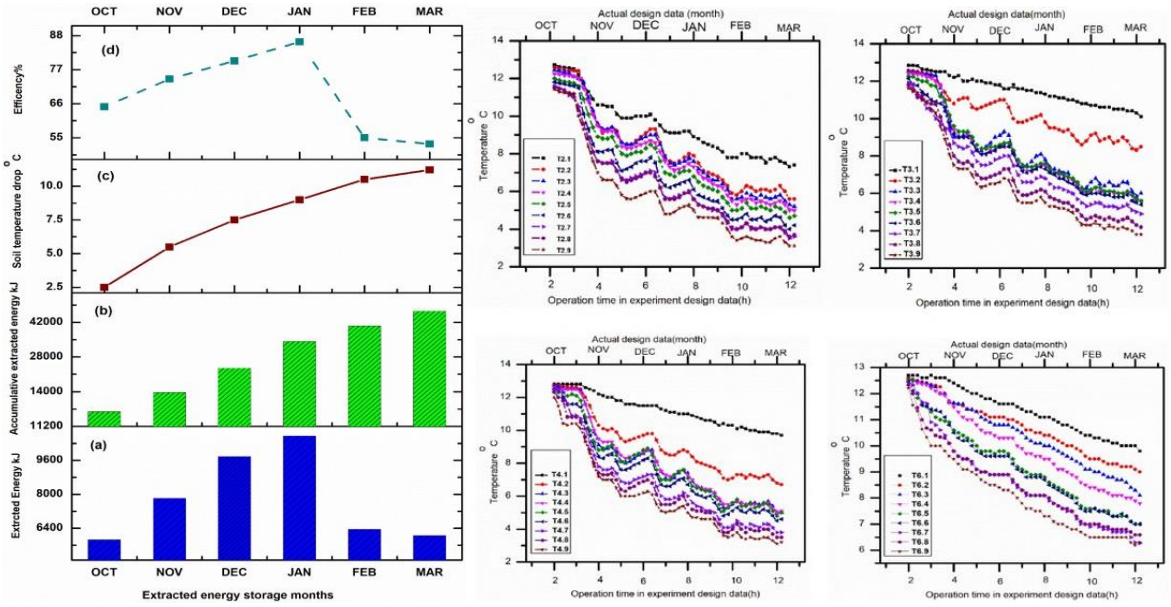

Figure 38. Sumary of energy extracted [left], and reservoir temperature evolution with time from different temperature sensors (Abbas et al., 2020)**.**

Moradi et al. (2015) built an apparatus to evaluate the heat transfer in 2D. The equipment consists in a 0.6096 m x 0.6096 m x 0.089 m box, filled with wet sand, that contains 22 dielectric and temperature sensors in the wide sides distributed in 3 rows as shown in **Figure 39**. In the narrow sides of the box there are aluminum heat plates that are heat sources. A u-tube connected the aluminum plates to circulate hot water, and 2 thermocouples were connected in the inlet and outlet tubes to measure the flow temperatures. As observed in **Figure 39** (right) the deeper sensors (bottom row), recorded the higher temperatures. Besides, the system captures how the temperature decreases with distance from the heat source.

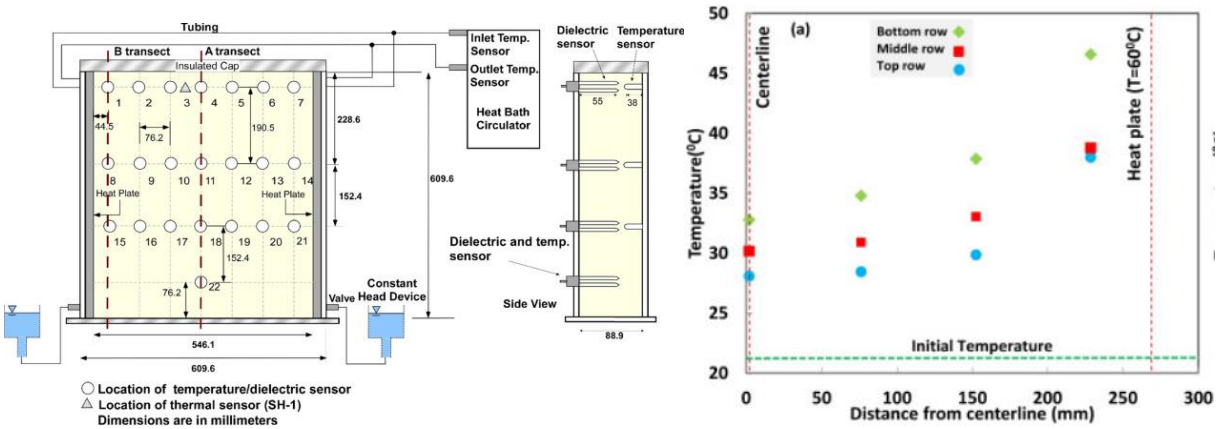

Figure 39. Squematic of the apparatus including sensor's placement [left], and reservoir temperature from different temperature sensors (Moradi et al., 2015)**.**

The data recorded was used by the authors to calibrate a numerical model. In **Figure 40** (right) it is observed a comparison of experimental and numerical simulation at 0 and 7 days. As observed in the images, the numerical model captures the heat flow trend. The data fitting ranges from R=0.66 to R=0.907. The authors of the study attributed the differences to sensors accuracy. With numerical model calibrated the authors evaluated the effect of conductive and convective heat flux (right-top [a] and right bottom [b] of **Figure 40** respectively), finding that the convective heat flow is significantly larger than the conductive heat flow.

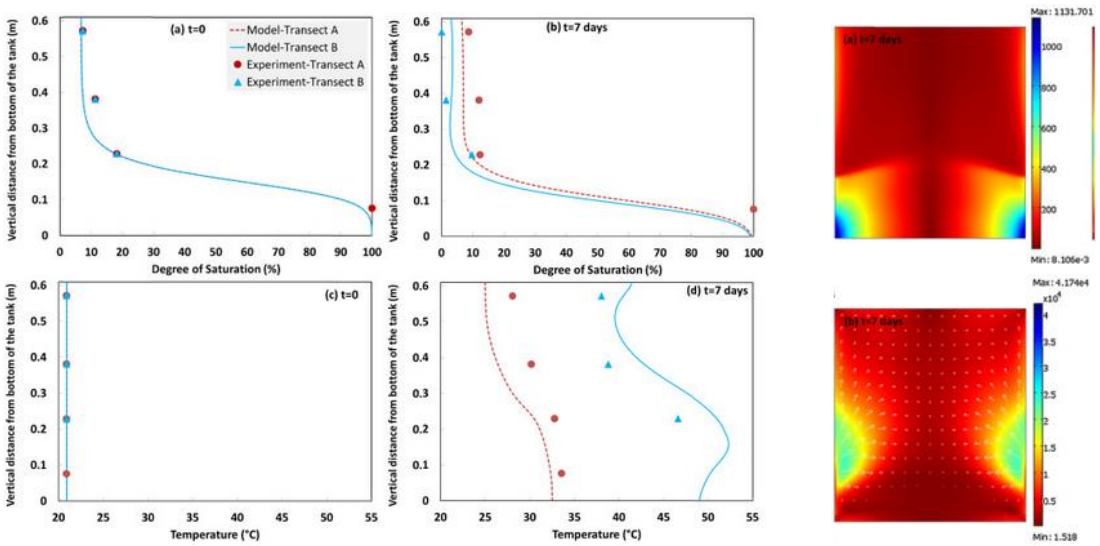

Figure 40. Schematic of the apparatus, including sensor's placement [left] and reservoir temperature from different temperature sensors (Moradi et al., 2015)**.**

2.9 Risks and Mitigation Plans for TES Developments

Developing a sedimentary reservoir aquifer thermal energy storage system is a long-term project that is not exempt of facing problems that can affect the projects technically and financially. In large-scale projects, high temperatures, thermal cycling, or high flow rates make long-term TES development challenging. Understanding the potential problems will guide us to face them. In this chapter, we will explore some of the most relevant issues documented in the literature and see what the potential actions that are also proposed in a risk assessment matrix will be proposed.

The fundamental reason for the low number of active high-temperature sedimentary thermal energy storage projects is that the elevated temperatures add complexities and risks that do not exist in low-temperature initiatives. Many technical issues arose in experimental and pilot high-temperature TES projects throughout the 1980s (Sanner and Knoblich, 1999). Mineral precipitation, pipelines, downhole equipment corrosion, and low recovery efficiency are critical issues for the practicality of HT-SRTES. Cold and low-temperature heat storage have far fewer technical issues than high-temperature heat storage (Snijders, 2000).

The risks that a high temperature TES can be categorized in technical, financial, organizational, political, legal, and social (Fleuchaus et al., 2020). Technical risks can be operational, geological, or geochemical **Figure 41**.

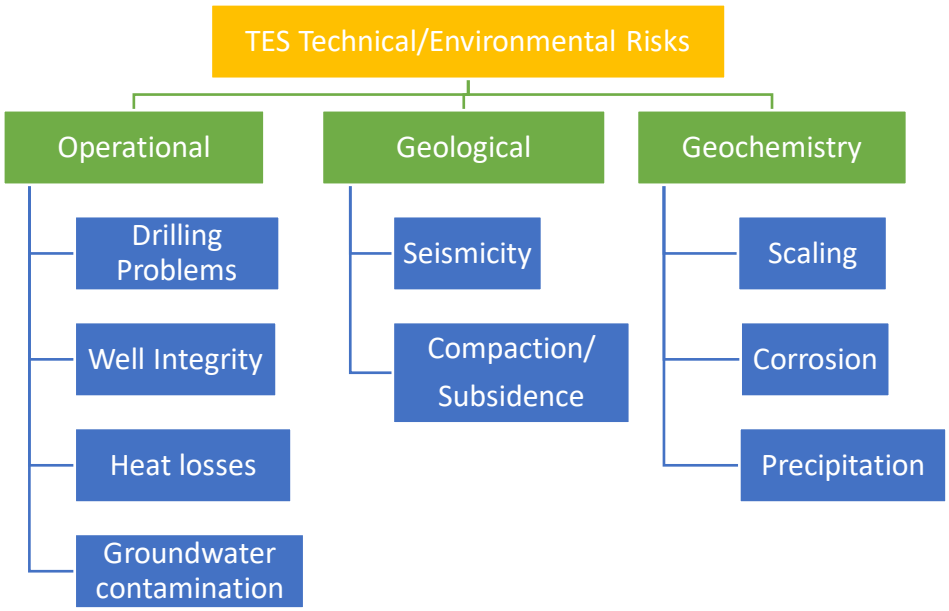

Figure 41. Operational, geological and geochemistry risks for a sedimentary reservoir thermal energy storage.

2.9.1 Operational Risks

Operational risks cover the risks associated to well construction and TES systems operations

Drilling Problems

Drilling thermal energy storage wells is an activity that is not exempt from challenges. The drilling depths are not especially deep, so the problems associated with hard rock drilling are not expected (vibrations, downhole tool failures, etc.). However, shallow mud losses and wellbore swelling can occur. One of the potential risks associated with addressing mud losses is related to formation damage. In Drilling, fluid additives, solids, and lost circulation materials can affect the permeability of the thermal energy storage reservoir (Kallesøe et al., 2019; Mercer et al., 1981). Drilling in deep

TES includes open hole collapse, failure in equipment, or sudden changes in the inflow-outflow balance of drilling fluid (Kallesøe et al., 2019).

Well Integrity

TES wells are expected to be operative in the long term, which can be up to 30 years or more. There are not official well integrity standards that covers TES or geothermal wells, however there are oil and gas well integrity norms that can be adapted to thermal energy storage or geothermal energy production (Khalifeh, 2021). The long time exposure of thermal cycling can affect the casing-cement system integrity (Vivas et al., 2020). If the temperature differential between the casing and the formation is substantial, irrespective of the direction of heat transfer, the probability of failure at the cement casing interface is significant (Wu et al., 2020).

Thermal losses

Thermal losses cause low thermal efficiency, which is a major cause of TES projects abandonment (Bakema and Drijver, 2019). There are multiple causes of heat losses. Rocks with low heat capacity are prone to heat loss (El Alami et al., 2020). High pore gradient can cause heat losses by convection (Bakr et al., 2013). The interaction of the TES with active ground water is a common cause of heat loss (Willemsen and Weiden, 1991). Sommer et al. (2012) documented a case in Netherlands where ground water flow reduced the efficiency of a TES by 50%. Hahne and Hornberger (1994) calculated that the thermal losses in the reservoir of an integrated solar and sedimentary TES project in Germany account for 20% of total project efficiency. Doughty et al., 1982) (demonstrate numerically that the heat loss is related to the ratio of reservoir surface to reservoir volume. High permeability can potentially cause heat loss due to buoyancy effect (Drijver et al., 2012). Kallesøe et al. (2019) concluded that when HT-SRTES systems are compounded by excessively coarse sand, thermal losses by density-driven groundwater flow will increase.

In addition to the losses in the hydrogeological system, there are heat losses due to flow friction, collector losses, heat pump losses and piping losses (Abbas et al., 2020; Bakema and Drijver, 2019; Kallesøe et al., 2019; Vangkilde-Pedersen and Kallesøe, 2019).

An insulating layer has been constructed on top of the SRTES heat exchanger field to prevent heat losses to the atmosphere in a thermal energy storage project in Netherlands. The heat is gathered using solar collectors and utilized to heat 100 homes (Wijsman, 1983).

Groundwater contamination

The risks associated to ground water contamination are not sufficiently understood (Bonte et al., 2011). There are interaction occurring underground that makes contamination difficult to be traceable. The loss of well integrity can have both economic and environmental effects, such as groundwater contamination and greenhouse gas emissions. Since the mitigation techniques are complex and costly, preventing integrity problems during well construction is crucial (Wu et al., 2021). Deep thermal well construction should be designed to reduce drilling risks while protecting intermediate aquifers from heat storage thermal cycling (Kallesøe et al., 2019).

Bonte et al. (2011) summarized the environmental risks that can affect the ground water, which are presented in **Table 6**.

Table 6. Summary of groundwater contamination risks (after Bonte et al., 2011)**.**

Risk	Probability	Consequence	Impact
Hydrological impacts			
Changing water levels and fluxes	Very high	Desiccation, water logging, settlements	Low
Changing other well's capture zone	Very high	Increasing vulnerability, pollution	High
Poorly sealed boreholes	High	Cross-aquifer flow	High
Thermal impacts			

Risk	Probability	Consequence	Impact
Changing water temperature	Very high	Temperature, reaction kinetics	Moderate
Chemical impacts			
Mixing processes and chemical reactions	Very high	Salinity, inorganic micro-pollutants, organic micro-pollutants	High
Reactivation of otherwise stable groundwater pollution plumes	Moderate	inorganic micro-pollutants, organic micro-pollutants	High
Oxidation of organic matter	Moderate	Nutrients, dissolved organic carbon, color	Moderate
Oxidation of iron sulfides	Moderate	Fe, SO4, As, Ni, Co, Zn	Moderate
Dissolution/precipitation of carbonates	Low	Ca, HCO3, Sr	Low
Dissolution/precipitation of silicates	Low	SiO2	Low
Leaching from installation materials	Moderate	Cd, Cu, Cr, Ni, Pb, VC	Moderate
Leaking anti-freeze fluids or additives	Moderate	Glycol, biocides, corrosion inhibitors	High
Microbiological impacts			
Introduction or mobilization of pathogens	Low	Pathogens	Low
Increasing biodegradation rate	Moderate	Nutrients, inorganic micro-pollutants, organic micro-pollutants	Moderate
Changing microbiological population	High	Unknown	Unknown

Geological Risks

In the operational phase of a sedimentary TES, the reservoir undergoes geofluid injection and production cycles. The reservoir rock is exposed to depletion in some areas and fluid injection in others for the enthalpy extraction. These cycles have the potential to cause alterations in the effective stress levels within the reservoir rocks and the surrounding formations, including the caprock, overburden, and underburden formations. These mechanical effects change the original stresses, with the potential to lead to rock deformations, that not only could affect the well integrity of the wells in the SRTES but have negative impacts at the surface in the form of surface deformation and seismicity events.

Compaction and reservoir subsidence

The extraction of reservoir fluids results in pore pressure reduction within the reservoir, leading to compaction and shrinkage. This deformation is not limited to just the reservoir itself, but also impacts the overlying caprock and surrounding rocks in response to stresses induced by the shrinking reservoir volume. As the reservoir depletes, the accompanying compaction can alter stresses and induce deformation in nearby formations. According to Zoback (2007), reservoir depletion specifically tends to trigger reverse faulting above and below the crest of the reservoir as the volume shrinks, while normal faulting occurs near the edges. Thus, compaction due to fluid depletion can potentially cause fault activation in rocks adjacent to the compacting reservoir.

Reservoir compaction and associated rock deformation can also threaten wellbore integrity. Dusseault et al. (2001), describe that shear distortion resulting from depletion is often concentrated along discrete planes rather than being uniformly distributed. Areas of concentrated stress may displace or shear well casing, particularly in brittle overburden rocks. The strongest shear stresses arise near the reservoir, with intensity declining with distance above and below it. Therefore, casing shear is most likely to happen in sections proximate to the reservoir interval as a result of compaction-induced shear distortion focused along high stress planes in the surrounding rocks.

Sedimentary reservoirs are typically characterized by much greater lateral extent compared to their thickness. Zoback (2007) explains that as such reservoirs undergo depletion, the horizontal stresses decrease relative to the vertical stresses. This results in an increase in the differential stress defined as the difference between the vertical and horizontal stresses. If sufficiently large, the growth in differential stress can surpass the fault reactivation threshold and trigger slip along existing faults around the reservoir.

Seismicity

For a sedimentary TES system of utility-scale, large volumes of water are expected to be injected and produced. These rates must be limited to prevent hydrofracturing, condition that can induce seismicity (Sheldon et al., 2021). Seismicity in geothermal projects is commonly associated with injection in deep reservoirs. Considering the seasonal storage/production operations planned, and although there are no records of seismicity associated to SRTES projects, it is an element of impact that has to be considered, modelled, and monitored (Guglielmetti et al., 2020).

2.9.2 Geochemistry

Injecting high temperature water in the thermal energy reservoir results in the alteration in the chemical composition of the groundwater. To avoid mineral precipitation that can lead to clogging the wells, pipelines or the heat exchanger of the system, a chemical treatment of the groundwater is required (Bakema and Drijver, 2019). Corrosion, scaling and precipitation generate negative impacts that can jeopardize a TES success.

Scaling

Scaling is one of the most documented issues in high temperature TES projects (Fleuchaus et al., 2018). Scaling is the process where a continuously growing "skin" is developed on metal surfaces, ultimately completely clogging narrow channels like those in pipes, plate heat exchangers, or well screens (Andersson, 1990). Scaling tends to increase with temperature (Molz et al., 1979). In most abandoned high-temperature SRTES projects, scaling was a significant risk factor (Banks et al., 2021). Scaling is a major issue, particularly in deep wells with temperatures above 120 °C, where the significant volumes of calcite scaling obstruct the subsurface pumps and clog the heat exchangers on surface (Wanner et al., 2017). Jenne et al. (1992) documented a carbonate scaling that caused extensive blockage in a TES in St. Paul, Minnesota. The scaling was attributed to the

carbonate minerals inverse solubility activated by temperature. As a result, the amount of carbonate predicted for precipitation was miscalculated, and the calcite scale plugged the system within a day due to the excessive precipitation. The scaling problem was fixed by building a Na ion exchange system, which returns the operation to normal. Willemsen and Weiden, (1991) analyzed the groundwater in SRTES in Utrecht, Netherlands, finding that the calcite saturation index increased from 0.47 to close to 1.0 by increasing the temperature from 15°C to 90°C. A water treatment including Ca-Na to reduce the SI, was successfully applied.

Multiple components can generate scaling, but the indisputable dominating ones are the diverse forms of carbonates. In SRTES applications, two leading causes will bring the water to a supersaturated condition for carbonates: the temperature increase and the hydraulic pressure reduction. Generally, high-temperature SRTES plants commonly are affected by carbonate scaling, commonly as a result of the temperature increase in the heat exchanger (Andersson, 1990).

Another common cause of scaling is by silica deposition. Experimental research and field observations have shown the aspects that influence the kinetics of silica deposition. Level of supersaturation, pH, temperature, flow rates, level of aeration, and interaction with different ions in solution are aspects that contribute to silica scaling formation (Brown, 2013). Thermodynamic equilibrium functions can be employed to evaluate the probable phases and extent of mineral scale development in TES surface infrastructure. Besides, precipitation, dissolution, and ion exchange reactions that might contribute to SRTES reservoir formation damage can be computed (Banks et al., 2021).

Corrosion

High temperatures exacerbate corrosion problems. Indeed, high-temperature thermal energy storage systems are prone to chemical and electrochemical corrosion. Chemical corrosion is frequently

revealed by the metal's progressive thinning due to the dissolution of the 'passive' layer that originally protects the surface of the metal (Bakema, 2001). CO2, O2, H2S, dissolved sulfide, chloride, and sulfate cause chemical corrosion. Significant corrosion has occurred at sites that have utilized HCl to eliminate or mitigate carbonate precipitation (Jenne et al., 1992). Chemical corrosion seems to be less common than electrochemical corrosion. Electrochemical corrosion is primarily induced by the interaction of metals with varying electrochemical potentials. Still, electrochemical corrosion arises on stressed monometallic parts, like welded seams, cut surfaces, or damaged coatings (Jenne et al., 1992). Snijders (2000) evaluated 100 thermal energy storage projects in the Netherlands, finding that one of the most significant problems is the corrosion of the downhole components.

Besides, aquifers with a low concentration of calcium, iron, and magnesium are advantageous to lower the risks of obstruction and corrosion of well casings (Bakr et al., 2013). Bakema (2001) summarized issues caused by corrosion in TES:

- Corrosion of the steel screens can cause the slotted holes to expand, allowing the gravel pack to be removed with the drained groundwater.
- The steel screen and steel casing corrosion can minimize the material's strength triggering a structural collapse of the wellbore.
- Corrosion in the surface casing allows water with different properties to the TES water to infiltrate the well. For example, the leaching of oxygen-rich water into a well that produces anoxic water can lead to an obstruction generated by iron precipitation.
- Iron particles generated during the corrosion process of steel-made components may clog pipelines and injection wells.

- Corrosion may cause damage to pumps, accessories, heat exchangers, and other components in addition to serious impairment to the well and pipelines.

Precipitation

Dissolution and mineral precipitation constitute some of the most significant issues in the operation of sedimentary reservoir thermal energy storage systems (Banks et al., 2021). There is a number of mechanisms that influence of precipitation occurrence. Temperature changes in thermal storage reservoir may cause chemical reactions including carbonate precipitation (Kallesøe et al., 2019). Changes is water chemistry can trigger the precipitation of iron and manganese oxides (Jenne et al., 1992). Microbial proliferation can trigger organic carbon oxidizing, which may affect the mineral equilibrium by raising the partial pressure of C02, expanding the possibility of carbonate precipitation (Andersson, 1990). When groundwater is produced, the pore pressure in the TES reservoir decrease, leading to CO2 release. Consequently, the pH level will increase, initiating calcium precipitation in the form of calcium carbonate (Bakema, 2001). Consequences of precipitation include the change in porosity and permeability, affecting the performance of the TES (Banks et al., 2021).

2.9.3 Non-technical / operational risks

The administrative risks in a SRTES project if not addressed can generate significantly negative impacts that can lead to the project failure. Fleuchaus et al. (2020) stated that the non-operational risks in a high temperature TES can be categorized in financial, organizational, political, legal, and social (**Figure 42**). Some of the non-operational risks have mutual interaction with the operational risks; seismicity events can negatively affect the public perception, or severe scaling and corrosion control increase the project costs (Fleuchaus et al., 2020).

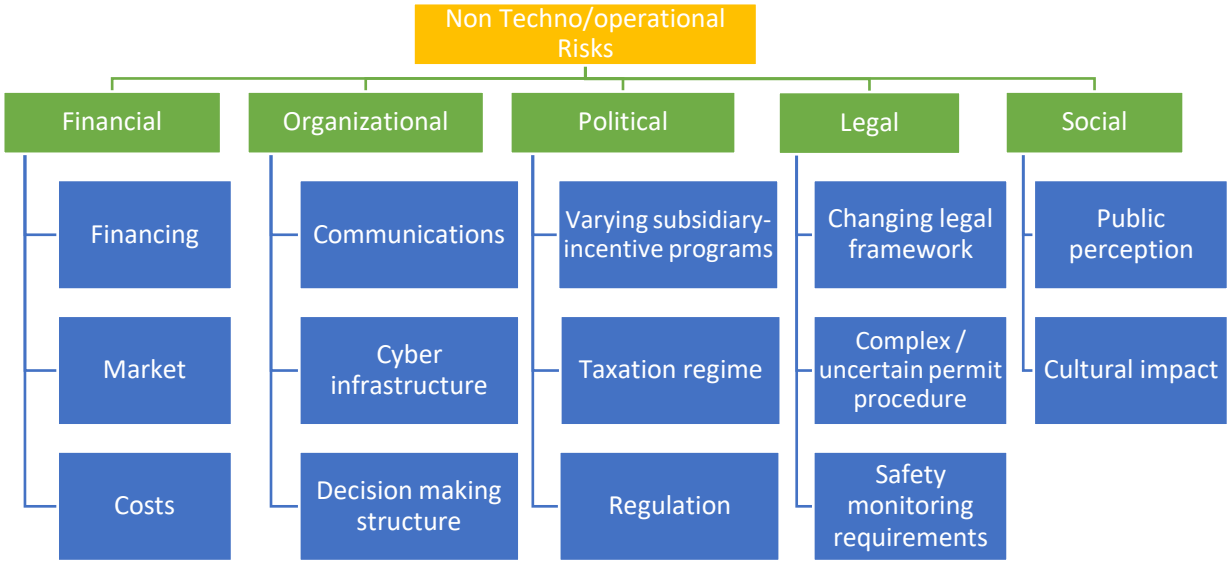

Figure 42. Financial, organizational, political, legal and social risks for sedimentary reservoir thermal energy storage (generated with information from Fleuchaus et al., 2020)**.**

(Kallesøe et al., 2019) collected the major concerns of a group of experts, operators, and researchers working in the high-temperature underground thermal energy storage industry, which are summarized below:

- The lack of standardized international policies for HT-SRTES.
- The lack of national guidelines for HT-SRTES projects.
- The lack of regulatory framework for HT-SRTES.
- Lack of district heating networks in a considerable number of regions/countries
- Lack of proven successful business cases
- Poor system integration leads to inaccurate business cases.
- In some regions, Subsidies for Sustainable Energy Transition and Climate Transition on HT-SRTES are not available.
- Many regions/places with the proper conditions to assemble an HT-SRTES project are underpopulated.

- Disputes with groundwater usage - public authorities

2.9.4 Controlling and mitigation of risks

In **Table 7** it is presented multiple issues and their solutions documented in the literature. The information presented offered a brief explanation of the issue and the mitigation measure. For more detailed information, the reference is provided.

Table 7. Operational, geologycal and geochemical risks and solutions.

Kind Of Risk	Issue	Cause	Mitigation Measure	Reference
Operational	Drilling problems	Collapsing wellbores	Casing while drilling in soft-ultra-soft formations	(Kallesøe et al., 2021)
	Drilling problems	Mud losses while drilling the HT-SRTES	Addition of shape memory polymers and micronized cellulose as lost circulation materials at high temperatures	(Vivas et al., 2020)
	Well integrity	Cement retrogression at high temperatures	Use alkali-silicate activated slag cement as an alternative to Portland cement	(Bernal et al., 2015)
	Well integrity	Cement failure by carbonation and sulfidation	Chemical treatment to remove H_2S and CO_2	(Ahmed et al., 2020)
	Well integrity	Casing corrosion in HT high H_2S environment	high-strength copper-nickel alloys	(Klapper and Stevens, 2013)
	Well integrity	casing-cement failure in high-temperature thermal cycling	cemented throughout the whole length of the non-productive interval of the well	(Vivas et al., 2020)
	Well construction / Downhole equipment	Cavitation and vibrations in downhole pumps	Lower flow rate and softer starts	(Andersson, 2007)
Heat Losses	Heat Losses	Thermal breakthrough between warm and cold wells	Warm water disposed into the sewage system to balance the storage	(Bakema, 2001)

Kind Of Risk	Issue	Cause	Mitigation Measure	Reference
	Heat Losses	Reservoir TES start-up losses and heating losses	It is suggested to utilize the heat storage as the baseload of the heating system. This permits the heat storage to run nearly constantly.	(Drijver et al., 2019)
	Heat Losses	Loss of efficiency	Identify the efficient temperature cut-off. For instance, to use a cut-off temperature during the unloading phases and cease producing warm water when its temperature falls below 80ºC	(Collignon et al., 2020)
	Heat losses	90°C SRTES systems inefficiencies	Lowest storage volume between 250,000 and 500,000 m^3/season.	(Drijver et al., 2019)
	Heat losses	50°C SRTES systems inefficiencies	Lowest storage volume between 35,000 and 180,000 m^3/season.	(Drijver et al., 2019)
	Heat losses	Buoyancy-driven heat losses	Increase the salinity of the injected hot water to compensate the density differential	(van Lopik et al., 2016)
	Heat losses / Environmental	Losses through casing-cement system. Risk of heat transfer to shallow aquifers.	The heat losses can be controlled by applying insulation in the well's casing, preventing heating up shallow groundwaters	(Kallesøe et al., 2019)
Geological	Heterogeneity / Heat losses	Heterogeneity affects the distribution of the stored heat in the subsurface.	Increase the separation between the injection and production wells.	(Sommer et al., 2012)
	Seismicity	Hydrofracturing	Use the Theis solution to estimate the injection/production limits	(Sheldon et al., 2021)
	Seismicity / Compaction	Environmental impact	Evaluate the seasonal TES cycling of loading and unloading. Monitoring techniques should be implemented (i.e. GPS leveling, INSar, Micro earthquake monitoring network)	Guglielmetti et al., 2020

Kind Of Risk	Issue	Cause	Mitigation Measure	Reference
Geochemistry	Scaling	Calcite Scaling	Regulating the well pressure with a downhole pump. This allows restraining the calcite scale and permits control over the scaling deposition depth	(Pereira, 2014)
	Scaling	Calcite Scaling	Chemical Inhibition strategy by applying phosphate molybdenum treatment.	(Zotzmann et al., 2018)
	Scaling	Silica Scaling	Silica gel has compatibility to attach with dissolved silica in groundwater, reducing the probability of silica forming scaling on the pipelines..	(Setiawan et al., 2019)
	Scaling	Silica Scaling	Controlling temperature and separation pressure	(Reyes et al., 2003)
	Scaling	Silica Scaling	Increasing pH, removing silicas adding CaO, Inhibit the colloid formation using hydrochloric acid	(Brown, 2013)
	Precipitation	Iron precipitation	HCl treatment and pumping away of reduced water	(Bakema, 2001)
	Precipitation	Carbonate Precipitation	Carbonates precipitation can be controlled by an ion exchange CO2 treatment, and the iron and manganese precipitation can be prevented by the usage of a high-pressure airtight system	(Snijders, 2000)
	Precipitation	Carbonate Precipitation	Water acidification Removal of carbonate by precipitation pre-treatment. Before heating the water for storage, decrease its calcium and magnesium saturation by cation exchange.	(Jenne, 1990)

Kind Of Risk	Issue	Cause	Mitigation Measure	Reference
	Precipitation	biochemical precipitations	Flushing of the wells at regular intervals (at least once a year) to remove sediments and biochemical precipitations.	(Bakema, 2001)
	Precipitation	Clogging with iron in injection wells	Wells abandoned and replaced by infiltration ponds	(Schüppler et al., 2019)
	Precipitation	Clogging with iron in wells and system	Chemical treatment and pumping	(Bakema, 2001)
	Corrosion	Corrosion of pump in dug well	Changed to a corrosion-resistant pump and airtight well construction	(Bakema, 2001)
	Corrosion	Corrosion in heat exchangers	Material changed to titanium	(Bakema, 2001)
	Corrosion	Corrosion on pumps and casing	Casing relined with PEM tubing New corrosion-resistant pumps	(Bakema, 2001)
	Corrosion	Clogging with iron in wells and system	DTH packer to avoid the mixture of water in wells	(Bakema, 2001)
	Corrosion	Carbonate clogging of one well	Replaced by a new well	(Bakema, 2001)

2.10 Environmental and Economic Feasibility Analysis for The Application of Thermal Storage on Large-Scale Projects.

The development of HT-SRTES started about 50 years ago, but there are constraints that have undermined the expansion of this technology. In previous chapters it was explored some of the technical challenges faced by HT-SRTES. Considering that an important quantity of HT-SRTES have been abandoned or cancelled (Bakema and Drijver, 2019; Fleuchaus et al., 2020; Kallesøe et

al., 2021; Sanner and Nordell, 1998; Vangkilde-Pedersen and Kallesøe, 2019), it is beneficial to explore economic and environmental aspects, and how they have been analyzed in SRTES projects.

Few SRTES economic feasibility analyses are documented, and most are superficial and lack detailed information about actual costs. Furthermore, the utilized economic evaluation methodologies are little specified and inadequately explored for reconstruction (Schüppler et al., 2019). Another limitation of the previous SRTES economic analysis is that the effect of the pandemic is not captured. This effect has implications for lifestyle habits (for instance, the increase in home office, which increments residential energy consumption and reduces commercial consumption), the cost of equipment and services, and electricity prices. Still, thermal energy storage is a technological alternative that represents one third of the cost of chemical battery systems for commercial and industrial sectors (DOE, 2021) (**Figure 43**).

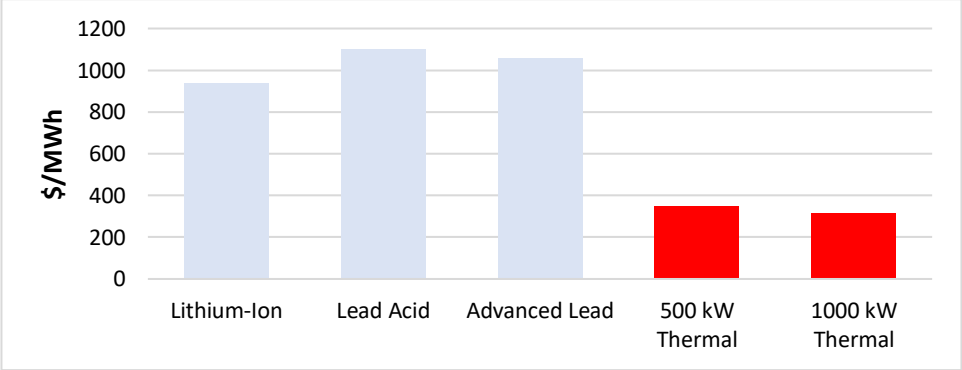

Figure 43. Levelized Technology Costs for BTM (behind the meter) applications (After DOE, 2021)**.**

Schüppler et al. (2019) evaluated multiple economic evaluations of TES in Europe and North America (**Figure 44**). The authors compare the specific capital costs (cost per kW), the total capacity of the TES, the payback time, and the capital costs of TES systems that are currently operational. It would be naturally expected that TES with higher power capacity would have a more efficient cost per kW; however, the information presented in **Figure 44** shows that the specific capital costs seem

uncorrelated to the system capacity. The authors attribute that some projects were built 30 to 40 years ago and that there are projects related to research projects where the cost efficiencies are affected by the research matters. The older and the research projects analyzed have payback times above 8 years, supporting the author's conclusion.

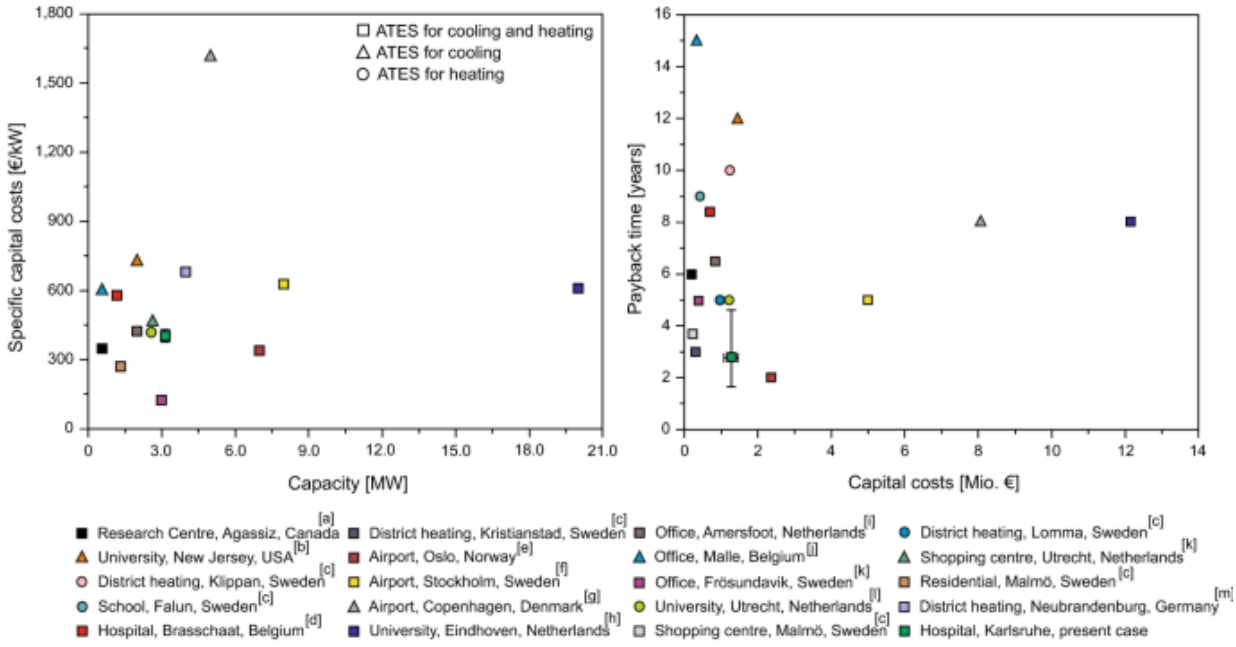

Figure 44. Comparative economic analysis of several TES projects that are currently operational (Schüppler et al., 2019)**.**

There is an undisputable variability of economical efficiencies between projects, that can be attributed a number of factors, including the source of heat efficiency, the distance from the projects to the end users, surface irregularities, access to roads, electric grid, the deep of the TES reservoir, regulatory framework, and some others. Well construction is the major contributor of SRTES capital costs accounting for approximately the 50% costs of a TES (Kallesøe et al., 2021; Welsch et al., 2018). Schüppler et al. (2019) ranked the initial capital costs for multiple TES projects, where the costs associated to well construction have the highest correlation to the total capital costs (**Figure 45**).

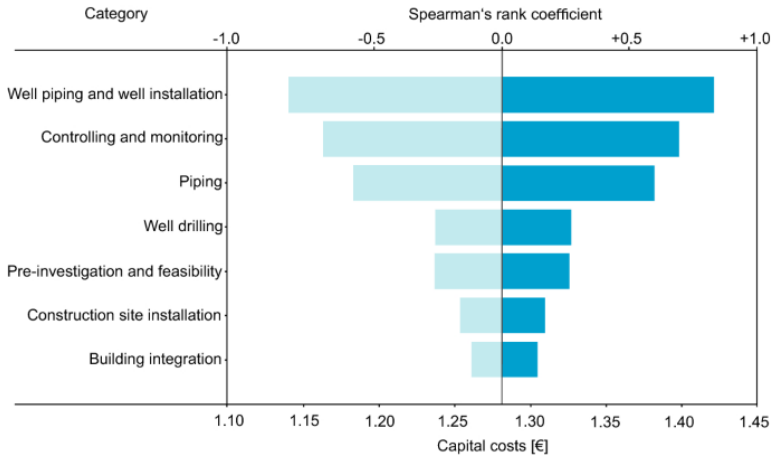

Figure 45. Spearman's ranking of initial capital costs of a multiple TES evaluations (Schüppler et al., 2019)**.**

Drijver et al. (2012), analyzed the integration of thermal energy storage with geothermal energy, by deepening the wells 500 m in a Netherlands project, which increases the downhole temperature from 75ºC to 93ºC, and lowers the capital costs per GJ produced from 30% to 50%. Vivas and Salehi (2022) studied the concept of a SRTES naturally recharged with geothermal energy. The solution implied the drilling of a deep well targeting the geothermal reservoir, and then use the heat to charge a shallower sedimentary reservoir to produce 3 MW. The main costs are associated with the deep well cost and the Organic Rankine Cycle (ORC) surface equipment. **Figure 46** presents the deep well costs. In total, the well cost, including drilling and well completions, is 6.4 MUSD. The ORC equipment is the equipment that is selected to convert the heat into power. The heat from the SRTES produced water warms up a refrigerant fluid in the ORC equipment. Then, the refrigerant changes from liquid to vapor. That vapor generates the mechanical movement of a turbine generating electricity. **Figure 47** shows the main costs associated with the ORC equipment.

AFE - Drilling & Completion

Operator:	WCTC Exploration, LP	Prepared By:	CSR	Tax Rate	
Well Name:	WCTC-Chicago #1p	Field:	Expl	Depth:	6750
Legal:		Parish/County:	Chicago	Days:	66 7
Contractor:	Nabors ???	State:	Illinois	Spud Date:	TBA

Well Program

Casing	Hole Size	Casing Size Weight, & Grade	Depth	Drilling Fluid	Formation Evaluation
Conductor	26	26" Wall Welded	80	Bentonite+Wate	None
Surface	20	16" 84 ppf J-55	450	Spud	None
Intermediate	14 3/4	10 3/4" 51 ppf J-55 HC	4850	LSND	Triple Combo
1st Production	9 3/4	7" 26 ppf N-80	6000		Triple Combo
2nd Production	9 3/4	7" 28 ppf Cr13-80	11000		Triple Combo

Costs

Code	Item	Item Cost	Days/Units	Drilling Cost	Days/No.	Completion	Total Cost
Capitalized Intangible Drilling & Completion Costs							
100	**Site Preparation & Maintenance**			**135,000**		**0**	**135,000**
	Permits & Surveys	7,500	1	7,500		0	7,500
	Location, Roads, Pits	75,000	1	75,000		0	75,000
	Water/Water Well/Plugging	7,500	1	7,500		0	7,500
	Conductor/Mousehole Installation	25,000	1	25,000		0	25,000
	Site Restoration & Land Use	20,000	1	20,000		0	20,000
	Wellsite Security			0		0	0
	Roustabouts & Labor			0		0	0
110	**Title Opinion**			0		0	0
120	**Drilling/Completion Rig**			**1,371,000**		**129,500**	**1,371,000**
	Mob/Demob	150,000	1	150,000		0	150,000
	Rig Rental	18,500	66	1,221,000	7	129,500	407,000
	Top Drive & Mousehole			0		0	407,000
	Additional Crew/Oil Base pay			0		0	407,000
130	**Engineering & Supervision**			**234,300**		**15,000**	**259,150**
	Wellsite Supervision	3,000	66	198,000	7	21,000	219,000
	Engineering & Geology			0		0	0
	Rig Supervisor Camp	400	66	26,400	7	2,800	29,200
	Communications	150	66	9,900	7	1,050	10,950
	Field/Office Supplies			0		0	0
140	**Fuel**	4,500	66	**297,000**	7		**297,000**
150	**Well Evaluation**			**164,700**		**7,500**	**204,700**
	Open Hole Logging	102,000	1	102,000		0	102,000
	Cased Hole Logging	7,500		0	1	40,000	40,000
	Mud Logging	950	66	62,700		0	62,700
	Core Analysis			0		0	0
	Drill Stem Testing			0		0	0
	Fluid Analysis			0		0	0
	Production Testing			0		0	0
160	**Casing Services**			**100,000**		**10,000**	**110,000**
	Casing Crews & Rental Tools	10,000	10	100,000	1	10,000	110,000
	Roustabouts & Cleaning			0		0	0
	Thread Specialist			0		0	0
170	**Cementing Services**			**570,000**		**35,000**	**605,000**
	Primary Cementing	35,000	2	70,000	1	35,000	105,000
	Remedial Cementing			0		0	0
	Loss Circulation	500,000	1	500,000		0	500,000
	Squeeze Packers & Cementers			0		0	0
	Kick-Off Plugs			0		0	0
180	**Drilling Tools**			**212,902**		**0**	**212,902**
	Drill Bits	203,902	1	203,902		0	203,902
	Core Bits			0		0	0
	Stabilizers/Reamers	1,500	5	7,500		0	7,500
	Performance Motors	15,000		0	0	0	0
	Turbines			0		0	0
	Shock Subs	500	3	1,500		0	1,500
190	**Drilling/Completion Fluids & Services**			**306,900**		**0**	**306,900**
	Fluids & Servcies	4,500	66	297,000		0	297,000
	Shaker Screens	150	66	9,900		0	9,900
200	**Equipment Rentals**			**55,110**		**19,000**	**74,110**
	Shale Shaker			0		0	0
	Mud Cleaner			0		0	0
	Centrifuge	350	66	23,100		0	23,100
	Transfer Pumps			0		0	0
	Steam Cleaners			0		0	0
	Wear Bushing	35	66	2,310		0	2,310
	Rentals - Surface			0		0	0
	Rentals - Subsurface			0		0	0
	PVT/Flo-Show	350	66	23,100		0	23,100
	BOP Rental			0		0	0
	Forklift	100	66	6,600		0	6,600
	Hydraulic Choke	4,000		0	4	16,000	16,000
	Tankage (Frac Tanks)	15		0	200	3,000	3,000

210	**Drill String**			**180,000**		**0**	**180,000**
	Drill Pipe	2,500	66	165,000		0	165,000
	Drill Collars			0		0	0
	Drill Pipe Protectors	100		0		0	0
	Inspections & Repair	7,500	2	15,000		0	15,000
	Corrosion Control			0		0	0
220	**Environmental**			**13,200**		**35,000**	**48,200**
	Solid Waste Disposal	200	66	13,200		0	13,200
	Brine & Water Disposal	750		0	20	15,000	15,000
	Cuttings Haul-off & Disposal			0		0	0
	Closed Loop Services			0		0	0
	Reserve & Flare Pit Closure	20000		0	1	20,000	20,000
	Spill Cleanup			0		0	0
230	**Miscellaneous**	250	66	**16,500**	10	**2,500**	**19,000**
240	**Specialty Tools & Services**			**576,500**		**4,500**	**581,000**
	Directional & MWD Services	10,000	56	560,000		0	560,000
	Well Surveying (SS,EMS,Gyro)	7,500	1	7,500		0	7,500
	Fishing Tools and Services			0		0	0
	Sidetrack: Whipstock,Mills,Service			0		0	0
	Coring Services			0		0	0
	Safety (H2S)			0		0	0
	Control Of Well			0		0	0
	BOP NU & Testing Services	3,000	2	6,000	1	3,000	9,000
	Wellhead Technician	1,500	2	3,000	1	1,500	4,500
250	**Trucking & Transportation**	650	66	**42,900**	10	**6,500**	**49,400**
260	**Welding**	1,000	2	**2,000**	1	**1,000**	**3,000**
270	**Production Services**			**0**		**975,000**	**975,000**
	Stimulation	200,000		0	4	800,000	800,000
	Perforating	150,000		0	1	150,000	150,000
	Wireline Services -BP,cement, lubricators, cranes			0		0	0
	Slickline Services			0		0	0
	Coil Tubing & Nitrogen Services	60,000		0		0	0
	Misc. Rental Equipment			0		0	0
	Pressure Testing Services			0		0	0
	Facilities Construction	25,000		0	1	25,000	25,000
300	**Contract Labor**			0		0	
310	**Plug and Abandonment**			0		0	
400	**OEE Insurance**	4	13,150	**52,600**		0	**52,600**
500	**Overhead Allocation**	1,000	66	66,000	5	5,000	71,000
Total Intangible Cost				**4,396,612**		**1,245,500**	**5,554,962**
Tangible Drilling & Completion Costs							
100	**Casing**			**143,600**		**587,000**	**329,600**
	Conductor Casing	40	80	3,200		0	3,200
	Surface Casing	21	450	9,450		0	9,450
	Intermediate Casing	27	4850	130,950		0	130,950
	1st Production Casing	27		0	6,000	162,000	6,000
	2nd Production Casing	50		0	5000	250,000	5,000
	Slim Sleeves and Packers	175,000		0	1	175,000	175,000
110	**Production Tubing**			**0**		**48,000**	**48,000**
	Tubing	6		0	8000	48,000	48,000
	Pups and cross-overs			0		0	0
120	**Subsurface Equipment**			**10,000**		**320,000**	**330,000**
	Liner Hanger & Packer			0		0	0
	Production Packer, Anchor, Seals, Pump	20,000		0	1	20,000	20,000
	Cementing Equipment	10,000	1	10,000		0	10,000
	Gas Lift Mandrels & Valves			0		0	0
	ESP Pump	300,000		0	1	300,000	300,000
	Bridge Plugs			0		0	0
130	**Wellhead Equipment**	15,000	1	**15,000**	3	**45,000**	**60,000**
140	**Production Equipment**			**0**	1	**47,000**	**47,000**
	Tank Battery	9,000		0	3	27,000	27,000
	Compressors			0		0	0
	Pump Unit	0		0	1	0	0
	Fluid Meters & run			0		0	0
	Production Skid - separator, heater treater, de-hy	20,000		0	1	20,000	20,000
	Treatment Units			0		0	0
150	**Miscellaneous Equipment**			**0**		**31,500**	**31,500**
	Surface Lines/Gathering System	7,500		0	1	7,500	7,500
	Line Pipe			0		0	0
	Sucker Rods	3		0	8000	24,000	24,000
Total Tangible Cost				**168,600**		**1,078,500**	**646,100**
				Drilling		**Completion**	
			Total Costs	**4,565,212**		**2,324,000**	**6,401,062**

Figure 46. Detail of the deep well costs

Technology	Plant Factor	CAPEX USD/kW	OPEX USD/MWh
Solar (Thermal)	28%	3,800	12
Solar (Photovoltaic)	28%	3,700	0.5
Eolic	29%	2,200	7.7
Nat Gas	85%	900	86
Biomass	85%	2,400	60
Coal	85%	2,300	44
Nuclear	90%	4,000	20
ORC	85%	3,550	6

Figure 47. ORC equipment (image courtesy of Mitsubishi Heavy Industries) [left]. Table of capital and operational expenditures per technology (Modified from Garcia, 2017)**.**

For the economic evaluation of the project, the Levelized Cost of Electricity (LCOE) was used. LCOE indicates the power generation cost for a specific energy source throughout a particular lifetime (Beckers and McCabe, 2019). The LCOE obtained were compared with other power generation LCOEs and results are presented in **Figure 48**. The project, there were built 2 scenarios: one for the discount rate of 3% and the other with 11%. The resultant LCOEs were 109 $/MWh and 116 $/MWh respectively. The results were not competitive compared with other power generation methods. However, if compared with the other battery storage (**Figure 43**) the increase in production makes the SRTES more competitive.

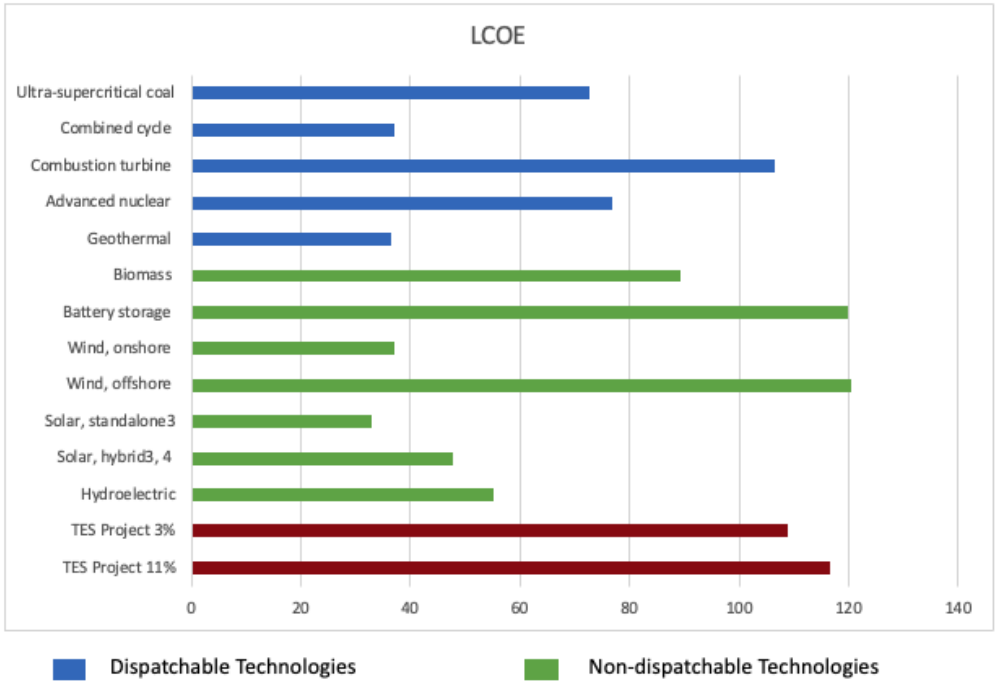

Figure 48. LCOE values for different power generation projects in $/MWh (Source EIA, 2022)

The life cycle assessment (LCA) evaluates the amount of pollution a project generates during its life cycle (Thomas et al., 2020). LCA is based on the international standards ISO 14040 (ISO, 2006a) and ISO 14044 (ISO, 2006b). There is a limited number of studies related to the environmental impact of sedimentary TES. However, several studies using LCA analysis to evaluate

thermal energy storage projects have recently been published (Ghaebi et al., 2017; Schüppler et al., 2019; Thomas et al., 2020; Tulus et al., 2016; Welsch et al., 2018). Stemmle et al. (2021) evaluated the environmental impact of TES implementation. The study compared the greenhouse gas (GHG) emissions in gCO_{2eq} per kWh for the most common heat sources and some reservoir TES systems (**Figure 49**). The authors compared the emissions of a heating TES project in Germany (83 gCO_{2eq} per kWh), finding that it is significantly lower than heating using oil or natural gas and, in 2050, is projected to be a fraction of the current emissions. The explanation of lower values of pellets and firewood is related to the fact that the CO_2 liberated by burning wood products is CO_2 that was naturally sequestered by the trees, but it is not generating additional emissions. Karasu and Dincer (2020), compared the emissions of residential heating in Drake Landing, Canada, using conventional natural gas, and a combined solar + TES, finding a reduction in 70% of global warning potential emissions in kg CO_{2eq}.

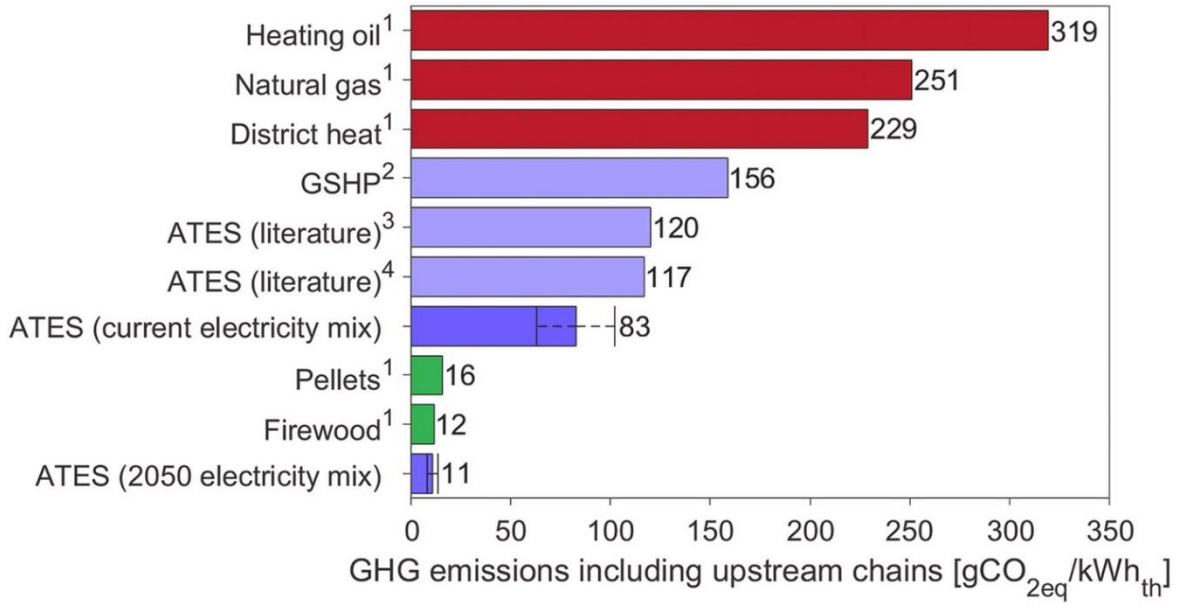

Figure 49. Green house gas emmissions per kWh for multiple heating systems (Stemmle et al., 2021)**.**

The LCA in a deep HT-SRTES project the environmental impact associated to the well construction is divided into 4 stages representing the life cycle of the well life: material production, material transportation and construction, using the system, and end-of-life. The deep well drilling and completion environmental impacts include producing raw and manufactured/engineered materials required for the well construction process, such as the casing and cement manufacturing. The material transportation and construction stage consists of the impact of the materials mobilization from their manufacturing place to the drilling rig and the amount of combustible used in the drilling rig and service equipment mobilization. Considering the long project period (30 years or more), it is expected that the most significant environmental impact of the project will be generated during the energy production stage. However, this effect can be neutralized by using the energy produced by the TES to power an artificial lift equipment or by the maintenance of the reservoir pressure due to the constant water cycling. In this case, the environmental impact of the production operation stage is significantly reduced. Finally, the end-of-life stage considers the environmental impact caused by the decommissioning process and well abandonment. **Figure 50** presents the different amounts of pollutants generated during the different stages of the well cycle using the well geometry described in **Figure 46**. As it is observed, the primary pollutant generated is CO2, with around 40 million kg. The fossil fuel depletion environmental cost is defined by MJ Surplus (Thomas et al., 2020). This represents the future environmental cost of materials production. This represents the second-largest environmental impact of the project, with 26 million kg equivalent. It is associated with the impact of the production of steel, cement, and diesel in the project.

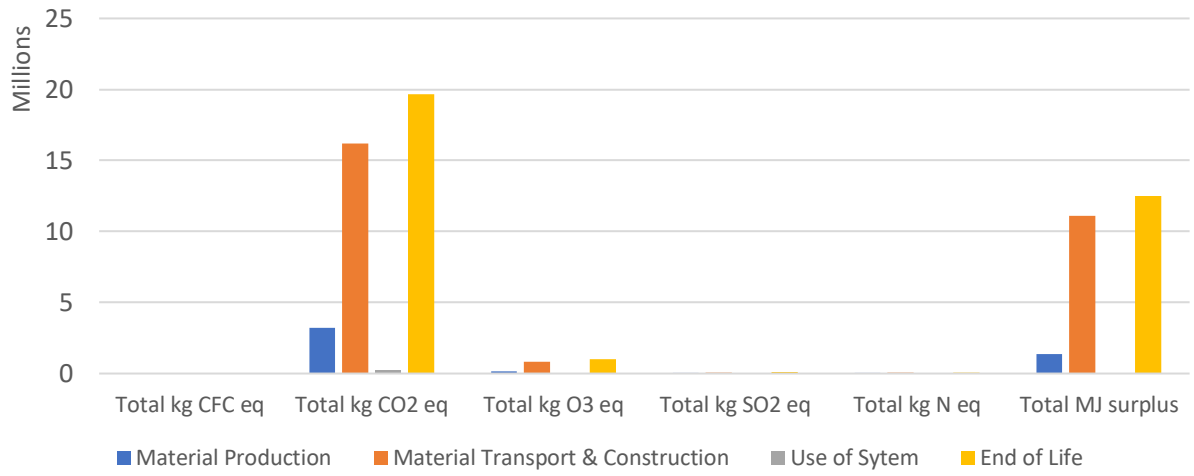

Figure 50. Life cycle assessment of the SRTES project

3. Experimental Study of Rock Properties

Mineralogy can have a significant influence on the thermal properties of sandstones. Thermal properties refer to how a material conducts, stores, and transfers heat. The most critical mineralogical properties that affect the thermal properties of sandstones are density, mineralogy, and texture. In this section of the study the relationship between mineralogy, petrophysical, and thermal properties of sandstone rocks is investigated. 30 core samples were examined using laboratory equipment, including Fourier-transform infrared spectroscopy analyzer (FTIR), porometer-permeameter equipment, and laser flash apparatus (LFA). The experimental research focuses on four main mineral groups: quartz, clay minerals, carbonates, and feldspars. Quartz, the most abundant mineral in sandstones, positively correlates with both thermal and petrophysical properties. Clay minerals have a high heat capacity but low thermal conductivity. Carbonates negatively correlate with thermal properties due to their low thermal conductivity. Feldspars have a somewhat negative correlation with thermal properties and show no correlation with petrophysical properties. These findings are essential in predicting the behavior of sedimentary rocks in various applications, including geothermal energy systems, oil and gas reservoirs, and underground thermal storage systems.

3.1 Materials and Methods

For utility-scale applications, sensible heat storage is generally considered the best thermal energy storage type for sedimentary reservoir thermal energy storage (Sarbu and Sebarchievici, 2018). Sensible heat storage involves storing thermal energy in the form of sensible heat. This can be done by heating or cooling a heat transfer fluid, such as water or air, and then storing it in a geological

formation, such as a sandstone reservoir. Sedimentary rocks have a high thermal conductivity, which allows for efficient heat transfer between the heat transfer fluid and the rock formation. This makes them well-suited for sensible heat storage systems, which require a large volume of storage to be effective.

In addition, sensible heat storage is a cost-effective and environmentally friendly option for thermal energy storage. It involves the use of low-cost materials, such as water or other low-cost fluids, and does not require the use of toxic or harmful materials (Alva et al., 2018). Sensible heat storage systems are also relatively easy to operate and maintain, making them an attractive option for utility-scale thermal energy storage projects.

30 rock samples of different sandstones were obtained from Berea Sandstone, Boise Sandstone, and Kentucky Sandstone formations. Error! Reference source not found. depicts the w orkflow and the equipment used for measuring the petrophysical properties, thermal properties, and mineralogy of the samples.

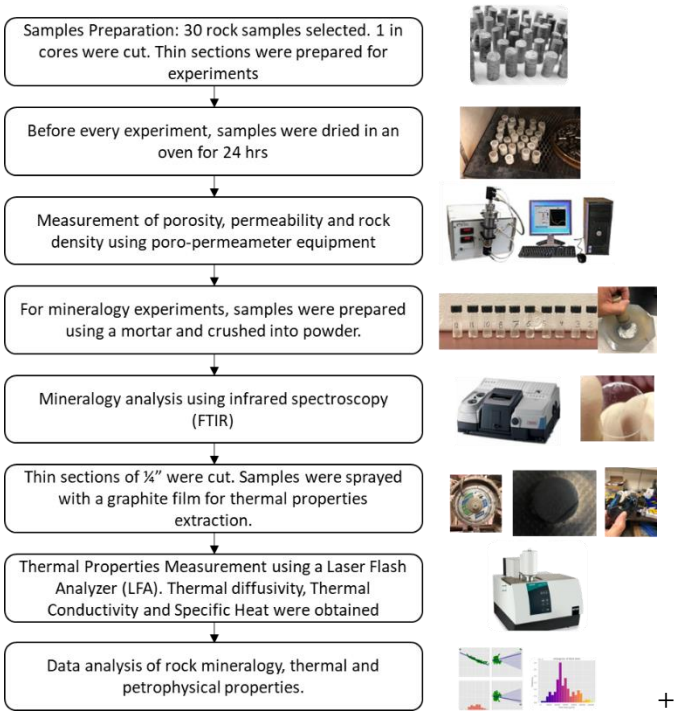

Figure 51. Experimental workflow of this study

3.1.1 Samples preparation

Before performing every experiment, the samples were stored in an oven at 65°C for 24 hours. The objective of this was to have the samples completely dry, prevent moisture affecting the measurements, and have comparable results. For the petrophysical and thermal properties experiments, cores of 2.54 mm in diameter were cored using a core drilling setup. For mineralogy experiments, samples were prepared using a mortar, where the sandstones were crushed into a powder by hitting and rubbing them with a pestle. Then the powder samples were placed in the oven as described earlier before every experiment. For the scanning electron microscope images, the samples were fractured to have a fresh face, unaffected by the saw cutting.

3.2 Experimental equipment and experiment description

For measuring the petrophysical properties of core samples, the AP-608 porometer-permeameter is a device that uses Boyle's law to determine porosity and the Klinkenberg effect to determine

permeability. Helium gas, safe and non-destructive to core samples, was utilized as pore fluid due to its ability to diffuse quickly, allowing for accurate porosity and permeability measurements.

The mineralogy was measured using the Nicolet 6700 Fourier-transform infrared (FTIR) spectroscopy equipment. FTIR spectroscopy is a type of analytical technique that uses infrared light to identify and characterize chemical compounds based on their unique molecular vibrations. In this technique, the samples were exposed to a beam of infrared light, and the absorption and transmission of this light by the sample were measured. By analyzing the resulting infrared spectrum overall molecular structure of the sample was obtained.

The thermal properties were measured using the LFA (light flash apparatus) Netzsch LFA 467. The equipment uses a short pulse of energy light to heat up the front surface of a flat sample, which is parallel to a plane. An infrared detector measures the temperature change of the back surface caused by the heat pulse. This measurement allows for the determination of thermal diffusivity and specific heat. When combined with the density of the sample, these thermophysical properties can be used to calculate thermal conductivity.

The variation of equation 3 is used to calculate the thermal conductivity:

$$\lambda = \kappa * \rho * c \qquad (5)$$

3.3 Experimental results

3.3.1 Porosity and Permeability

The petrophysical rock properties were measured in the 30 samples, and the results are summarized in **Table 8**:

Table 8. Porosity and Permeability of different rock samples at 5,000 psi

Sample	Length [cm]	Diam [cm]	V Bulk [cm³]	V Pore [cm³]	Porosity [%]	K_Air [mD]	K_Klink [mD]
S01	2.99	2.54	15.151	2.133	14.078	31.932	30.465
S02	2.77	2.54	14.036	1.300	9.261	0.062	0.036
S03	2.81	2.47	13.464	2.763	20.518	548.438	542.012
S04	3.07	2.50	15.070	3.077	20.417	440.129	434.267
S05	2.93	2.54	14.847	2.510	16.910	164.929	161.935
S06	3.01	2.45	14.19	2.679	19.004	41.916	40.366
S07	2.95	2.54	14.948	2.869	19.195	426.206	420.584
S08	2.85	2.55	14.555	2.524	17.339	101.233	98.645
S09	2.71	2.50	13.303	2.560	19.242	45.112	43.407
S10	2.92	2.54	14.796	2.598	17.561	155.758	152.62
S11	2.56	2.51	12.667	2.585	20.408	11.42	10.644
S12	3.04	2.50	14.923	2.643	17.710	119.385	116.381
S13	2.69	2.51	13.310	2.730	20.510	15.833	14.906
S14	3.18	2.49	15.485	3.080	19.891	12.495	11.679
S15	2.635	2.54	13.352	2.038	15.263	1.946	1.679
S16	3.025	2.50	14.849	3.161	21.287	498.588	492.229
S17	2.96	2.535	14.940	2.858	19.133	183.947	180.21
S18	3.03	2.535	15.293	3.302	21.593	391.713	386.12
S19	3.02	2.53	15.182	2.646	17.430	11.291	10.530
S20	3.01	2.44	14.075	3.136	22.281	501.235	494.851
S21	4.05	2.475	19.485	3.619	18.576	86.128	83.690
S22	3.005	2.535	15.167	2.682	17.683	3.405	3.031
S23	2.93	2.525	14.672	3.098	21.117	433.583	427.704
S24	2.91	2.46	13.831	3.108	22.469	485.119	478.935
S25	2.94	2.505	14.489	2.938	20.274	309.14	304.146
S26	2.595	2.525	12.994	2.401	18.475	3.437	3.059
S27	2.31	2.53	11.613	2.163	18.625	3.471	3.093
S28	2.545	2.47	12.195	2.302	18.880	106.020	103.266
S29	2.74	2.475	13.182	2.570	19.498	98.381	95.722
S30	4	2.48	19.322	3.548	18.364	158.222	154.768

In **Figure 52** it is presented the cross-plots between variables to understand potential relationships, identify outliers, and the need for data cleaning. The porosity ranges from 9.2 to 22.5 %, and the permeabilities cover from 0.06 to 500mD, which allows us to cover a range of different common reservoir rocks. The level of correlation between parameters is presented in **Figure 53**. The correlation method used is the Pearson correlation coefficient, which measures the linear correlation

between two variables (Kirch, 2008). The values closer to 1 have strong positive information; values closer to negative 1 have a strong negative correlation. In contrast, the uncorrelated variables have correlation values close to zero; the closer to zero, the less correlated are the variables.

The cores were intended to have the same diameter, 2.54 cm with slight variations happening during core cutting. This is required by the instrument used to measure porosity and permeability. In contrast, different core lengths were used. This helps us to understand if the core length has an influence on the results, especially if this data is compared with external data, where the cores do not have the same length. In the Pearson correlation heat map, it is observed that the length of the cores is uncorrelated with the porosity and permeability values. For this dataset the values of porosity and permeability have a positive correlation of 0.63, showing that are directly correlated.

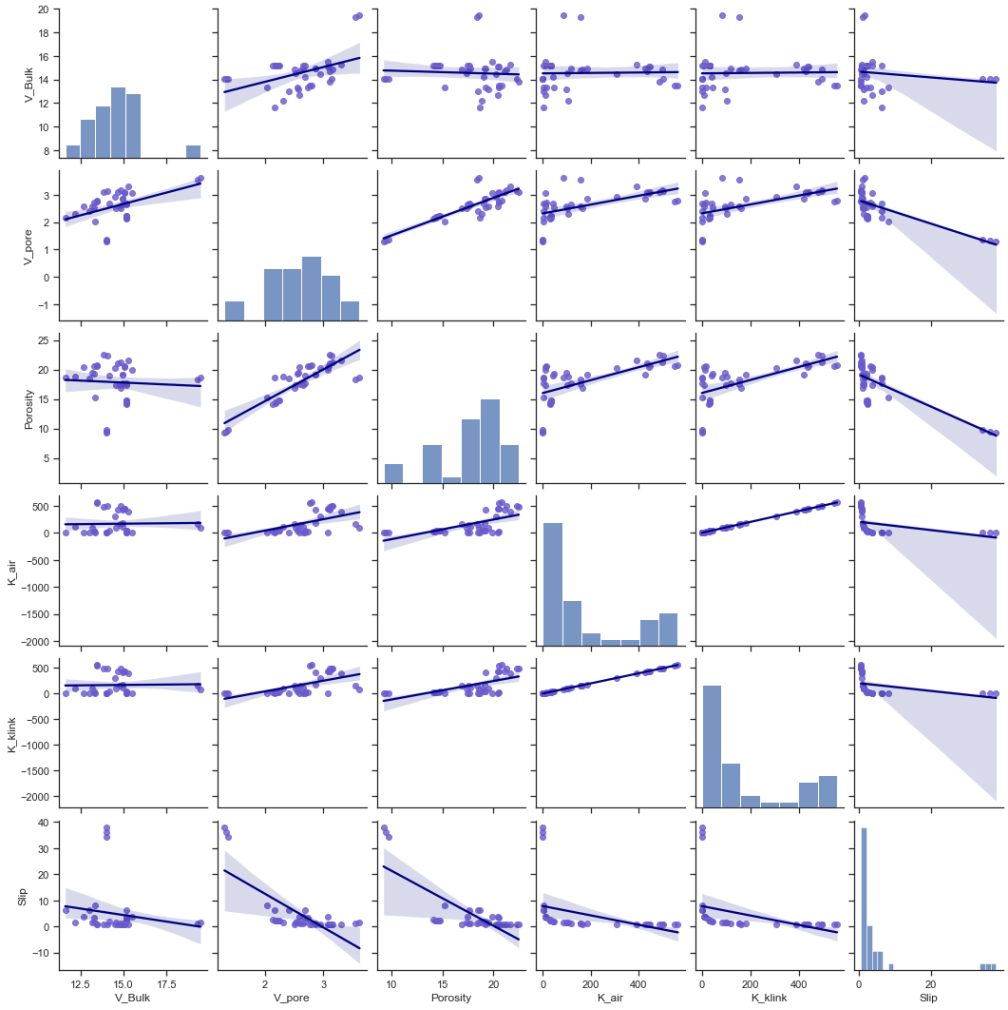

Figure 52. Cross-plot of petrophysical parameters

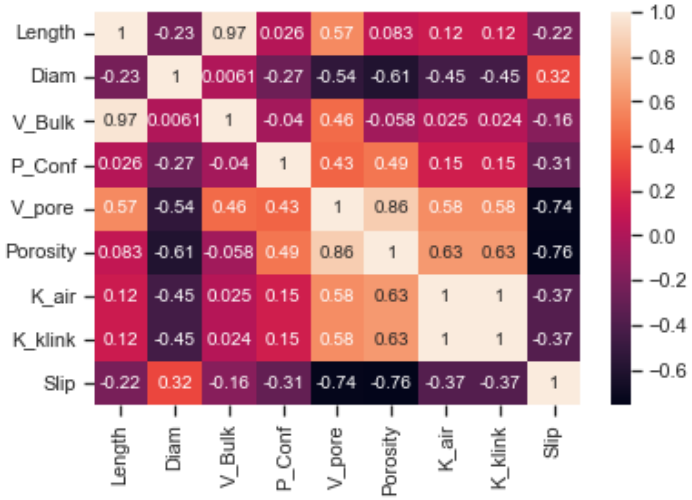

Figure 53. Correlation between petrophysical parameters.

3.3.2 Mineralogy

FTIR equipment was used to analyze the mineralogy of the core samples by measuring the absorption or transmission of infrared radiation per sample. The information obtained provided the presence of minerals such as quartz, feldspar, clay minerals, calcite, dolomite, and can distinguish between different types of clay minerals. In **Figure 54**, it is presented the spectrum of sample 1, sample 2, sample 21 and sample 24.

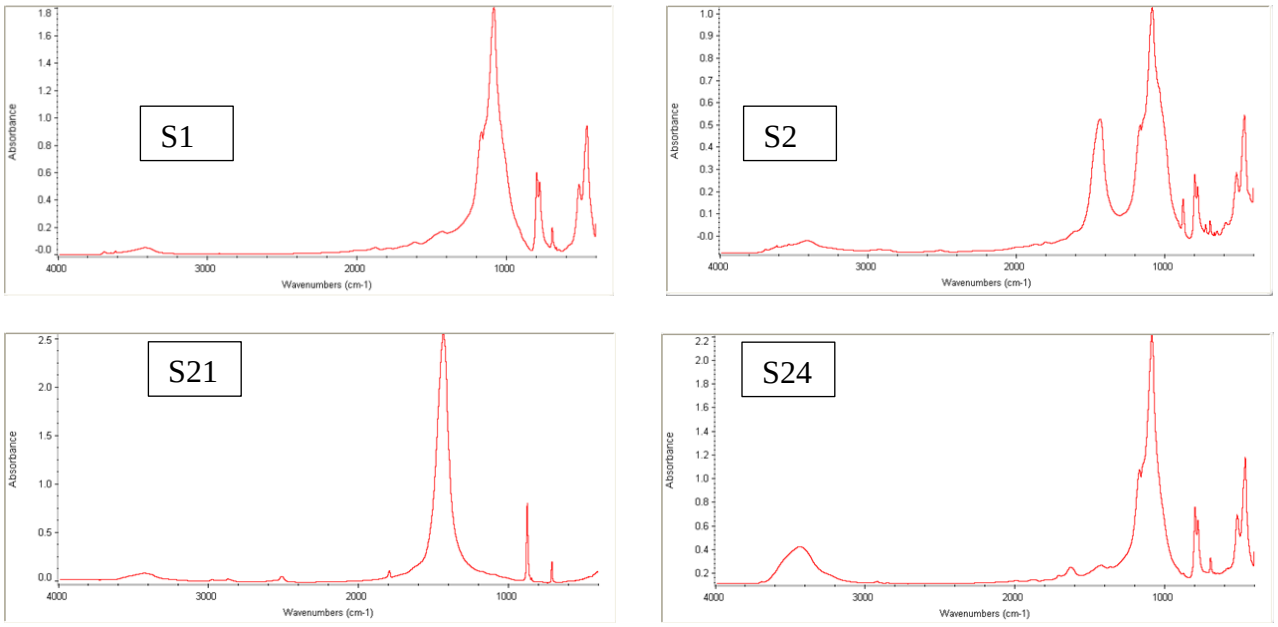

Figure 54. FTIR spectrums of samples

In the **Table 9**, there is presented the fraction of the following minerals per sample: quartz, calcite, albite, siderite, mixed clays, and others (dolomite, illite, smectite, kaolinite, chlorite, pyrite, orthoclase feldspar, oglioclase feldspar, anhydrite, apatite, and aragonite).

Table 9. Mineralogy composition of core samples

Sample	Quartz	Calcite	Albite	Siderite	Mix_Clays	Others
S01	0.77	0.00	0.02	0.02	0.08	0.11
S02	0.43	0.02	0.18	0.14	0.07	0.15
S03	0.79	0.00	0.03	0.02	0.00	0.16
S04	0.71	0.00	0.09	0.01	0.00	0.20

S05	0.59	0.00	0.04	0.07	0.00	0.30
S06	0.58	0.00	0.21	0.05	0.00	0.16
S07	0.51	0.00	0.01	0.06	0.17	0.25
S08	0.57	0.00	0.06	0.06	0.14	0.17
S09	0.74	0.00	0.18	0.03	0.01	0.04
S10	0.68	0.00	0.11	0.05	0.00	0.15
S11	0.60	0.00	0.26	0.07	0.05	0.01
S12	0.66	0.00	0.08	0.00	0.04	0.23
S13	0.65	0.00	0.18	0.06	0.02	0.09
S14	0.56	0.00	0.22	0.04	0.00	0.17
S15	0.45	0.02	0.17	0.17	0.07	0.12
S16	0.78	0.00	0.05	0.03	0.00	0.14
S17	0.74	0.00	0.04	0.08	0.00	0.14
S18	0.88	0.00	0.03	0.03	0.04	0.02
S19	0.59	0.00	0.22	0.08	0.04	0.06
S20	0.73	0.00	0.06	0.03	0.00	0.18
S21	0.00	0.95	0.00	0.00	0.00	0.05
S22	0.00	0.93	0.00	0.02	0.00	0.04
S23	0.71	0.00	0.04	0.06	0.12	0.07
S24	0.79	0.00	0.06	0.05	0.06	0.04
S25	0.65	0.00	0.07	0.06	0.14	0.09
S26	0.82	0.00	0.04	0.02	0.06	0.06
S27	0.00	0.78	0.00	0.08	0.00	0.14
S28	0.59	0.00	0.07	0.08	0.13	0.14
S29	0.65	0.00	0.09	0.07	0.06	0.13
S30	0.59	0.09	0.09	0.05	0.05	0.13

On average, the most abundant mineral in the samples is quartz, with an average composition of 59%. There are 3 samples that do not contain quartz, samples 21, 22 and 27. Those samples are carbonates, with a calcite content of 95 and 93%. **Figure 55** presents the various relationships among the most abundant minerals. The figure illustrates that there is no significant correlation between the presence of one mineral and the presence of another.

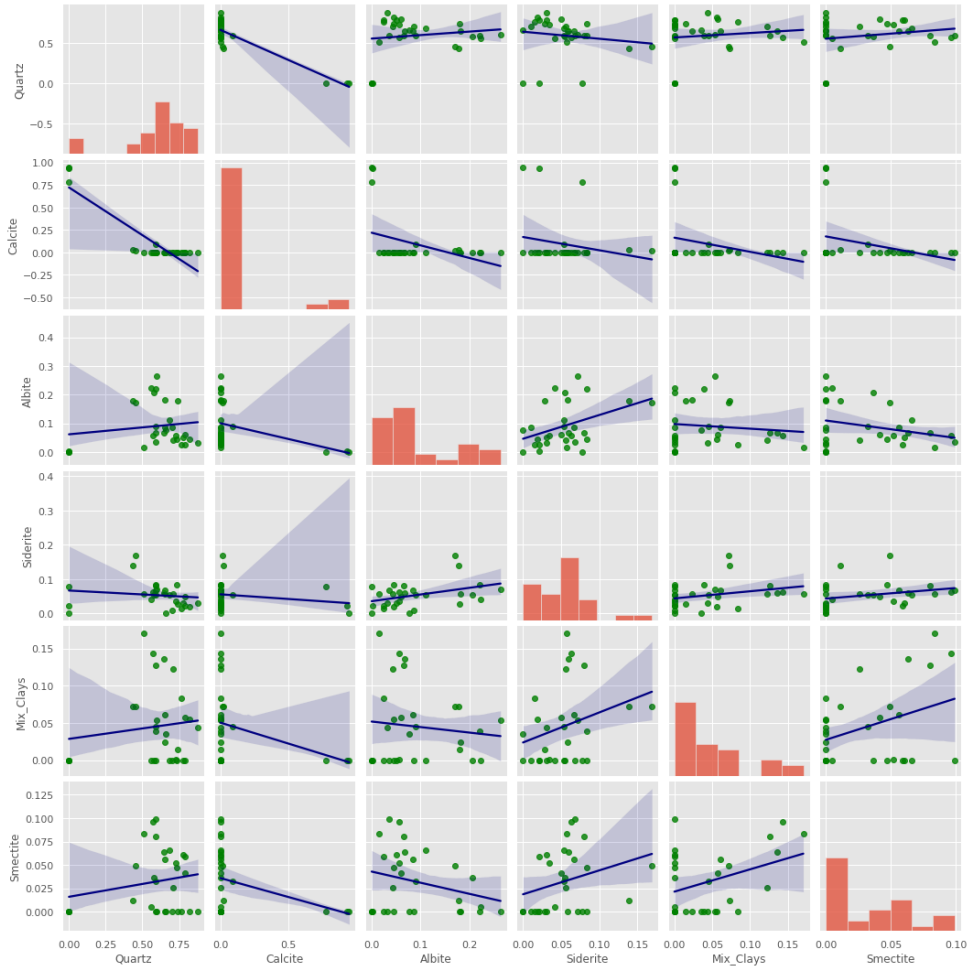

Figure 55. Scatterbox plot of most frequent minerals in the core samples

3.3.3 Thermal properties

LFA was used to determine thermal properties of the core samples. The LFA analyzer generates a heat source on the surface of the material using a short-pulsed laser, and the temperature rise is measured using a detector located at a fixed distance away from the source. The temperature rise curve is analyzed using a mathematical model to extract the thermal properties of the sample, and the calculated values can be used to interpret the thermal behavior of the material. The accuracy and precision of the measurements depend on several factors, such as sample preparation,

calibration, and data analysis, and attention to these factors is crucial for obtaining accurate results.

In **Table 10** it is presented the results of the LFA tests on the 30 samples.

Table 10. Thermal properties of core samples

Sample	Density [kg/m^3]	Specific Heat [J/kg*K]	Thermal Diffusivity [m^2/s]	Thermal Conductivity [W/m*K]
S01	2556.47	843.81	1.8650E-06	4.023
S02	2807.64	824.47	1.3193E-06	3.054
S03	2536.28	839.24	1.6283E-06	3.466
S04	2539.58	826.20	1.4577E-06	3.058
S05	2593.52	793.01	1.6127E-06	3.317
S06	2581.43	814.28	1.2193E-06	2.563
S07	2569.66	812.38	1.5753E-06	3.289
S08	2557.46	830.72	1.6067E-06	3.413
S09	2573.23	840.21	1.1927E-06	2.579
S10	2586.93	824.02	1.7497E-06	3.730
S11	2662.36	827.81	9.7300E-07	2.144
S12	2633.30	799.04	1.6007E-06	3.368
S13	2653.74	830.85	1.0873E-06	2.397
S14	2643.76	827.61	1.0870E-06	2.378
S15	2735.20	823.61	1.3123E-06	2.956
S16	2607.88	838.58	1.6053E-06	3.511
S17	2639.34	824.77	1.6090E-06	3.503
S18	2637.43	865.63	1.5197E-06	3.469
S19	2739.91	828.97	1.4697E-06	3.338
S20	2652.01	820.84	1.5250E-06	3.320
S21	2639.76	811.84	1.5383E-06	3.297
S22	2688.39	810.76	9.3533E-07	2.039
S23	2641.89	849.87	1.7637E-06	3.960
S24	2622.33	859.11	1.5563E-06	3.506
S25	2650.91	847.12	1.7140E-06	3.849
S26	2695.21	853.85	1.8233E-06	4.196
S27	2701.88	805.57	1.0020E-06	2.181
S28	2662.19	830.50	1.6250E-06	3.593
S29	2673.66	829.07	1.6373E-06	3.629
S30	2572.64	828.75	1.7417E-06	3.713

4. Data Analysis and Integration of Petrophysical, Mineralogy and Thermal Properties Results

The data generated allows us to analyze the rock properties and mineralogy together with thermal properties. In this section we are going to analyze the results per mineral and per core sample and examine the individual patterns between properties. The benefit of analyzing the thermal properties of rocks by individual minerals is that each mineral has different thermal properties. Thermal properties such as thermal conductivity, heat capacity, and thermal diffusivity can vary widely depending on the mineral composition of the rock. By analyzing the thermal properties of individual minerals, we can gain a better understanding of the thermal behavior of the rock as a whole.

4.1 Quartz

Quartz is typically the most abundant mineral in sandstones and the most abundant mineral among the samples analyzed. The presence of quartz per sample variates from less than 0.01% to 87.8%, with a mean value of 59.4%. Quartz is a common mineral in sandstones because it is resistant to weathering, so it can survive transport and deposition processes that break down other minerals. In the present data set, the quartz content has a positive correlation with thermal properties, as depicted in **Figure 56**. Quartz is a crystalline mineral that is made up of silicon and oxygen atoms arranged in a three-dimensional network. The arrangement of atoms in this network allows heat to be conducted through the mineral more efficiently than in other minerals that do not have this type of crystal structure. Besides quartz has a relatively low thermal resistance compared to other minerals, meaning that it is easier for heat to pass through it. This is because quartz has a low number of defects and impurities that can hinder the flow of heat.

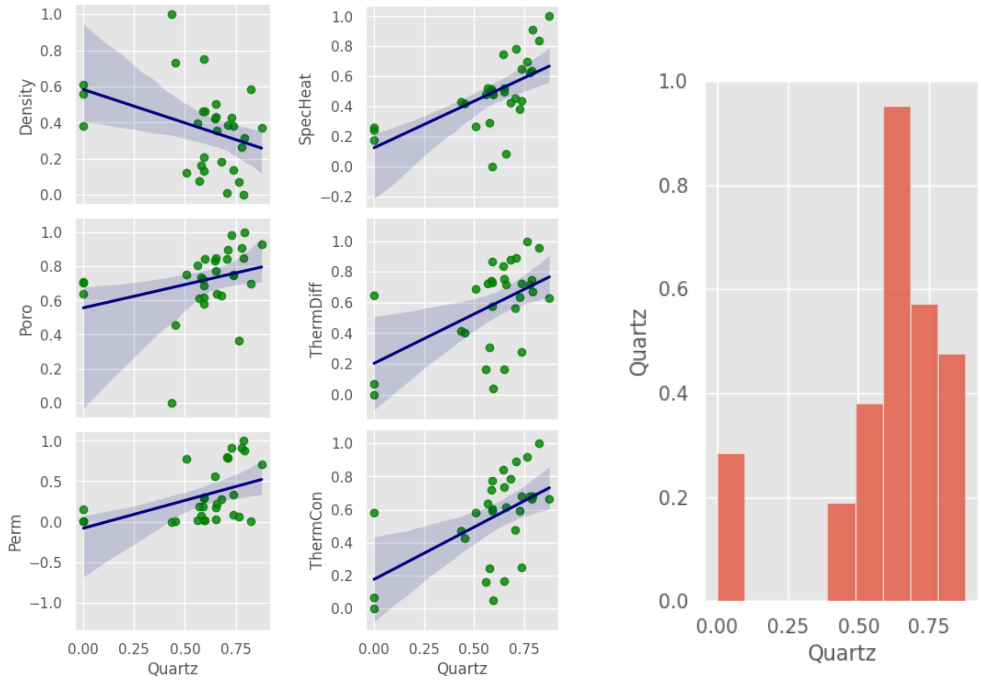

Figure 56. Scatterbox plot of quartz vs. porosity, permeability and thermal properties.

In this data set the quartz content also has a positive correlation with petrophysical properties. The quartz content is typically uncorrelated with porosity and permeability. As an example, a sample of shale and sandstone can have the same quartz content, but porosity and especially permeability, can vary in order of magnitude.

4.2 Clay minerals

In the samples analyzed, clay minerals are compounded by Illite, Smectite, Siderite, Kaolinite, Chlorite, and other clays. The presence of clay minerals per sample variates from 1.4% to 25.4%, with a mean value of 10.0%. In the present data set, the clay minerals content is uncorrelated with thermal properties and the petrophysical properties analyzed, as depicted in **Figure 57**. The thermal conductivity of clay minerals is relatively low compared to other materials. This is explained by the clay minerals' unique structural characteristics. The structure of clay minerals is composed of layers of silicate tetrahedrons and octahedrons held together by weak

interlayer forces. These layers are arranged in a repeating pattern, with water molecules and other ions located in the interlayer spaces between them. The layers in clay minerals are very thin, typically only a few nanometers thick, and the interlayer spaces are also very small. These factors limit the movement of heat through the material, as the heat energy cannot easily propagate through the narrow channels between the layers. In addition, the weak interlayer forces make it difficult for heat to be conducted from one layer to the next.

The heat capacity of clay minerals is relatively high, which means they can store a large amount of thermal energy; however, as the percentage of clays in the samples measured is low, 10% on average, the influence in the total specific heat of the samples is low.

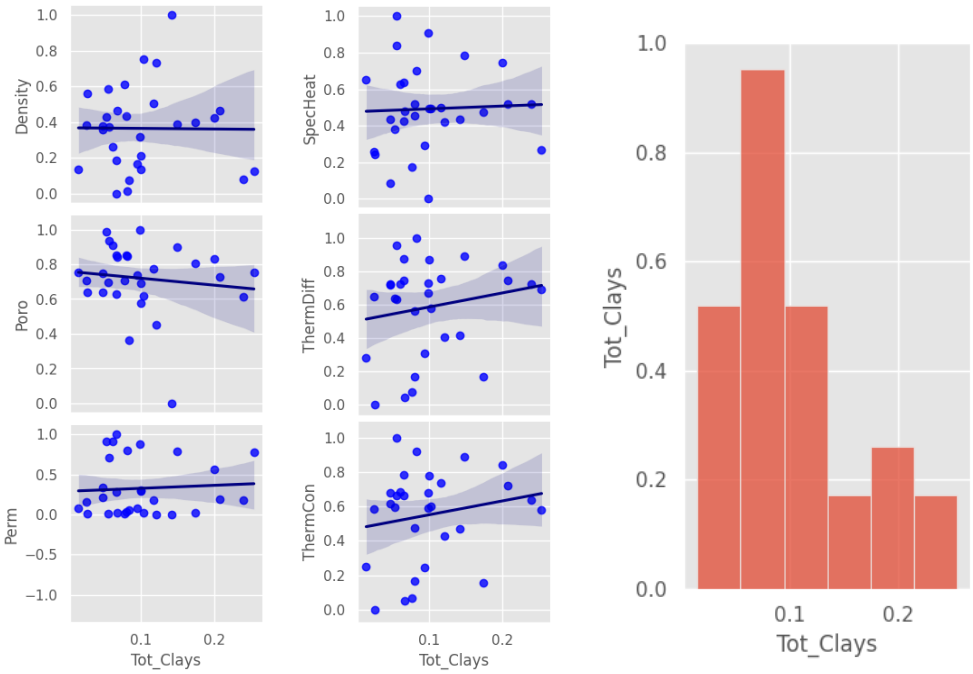

Figure 57. Scatterbox plot of clay minerals vs. porosity, permeability and thermal properties.

4.3 Carbonates

In the samples analyzed, carbonate minerals are compounded by Calcite, Dolomite, Siderite, and Aragonite. The presence of carbonate minerals per sample variates from 1% to 95.3%, with a

mean value of 15.4%. In the present data set, the carbonates content has a negative correlation with thermal properties, as depicted in **Figure 58**. A possible explanation is that carbonate minerals, have a lower thermal conductivity than many other minerals commonly found in sedimentary rocks, including quartz. This means that sedimentary rocks with a high proportion of carbonate minerals will generally have lower thermal conductivity than those with a high proportion of other minerals. Carbonate minerals, such as calcite and dolomite, are made up of carbonate ions (CO3)2- combined with metal ions, such as calcium, magnesium, or iron. The crystal structure of carbonate minerals is relatively open and contains many void spaces, which makes them less efficient at conducting heat compared to minerals with a more tightly packed crystal structure, such as quartz. In addition, the carbonate ion itself has a low thermal conductivity compared to other ions. This is because the carbonate ion has a polarized bond with a positive and negative end, which reduces the transfer of heat between adjacent ions.

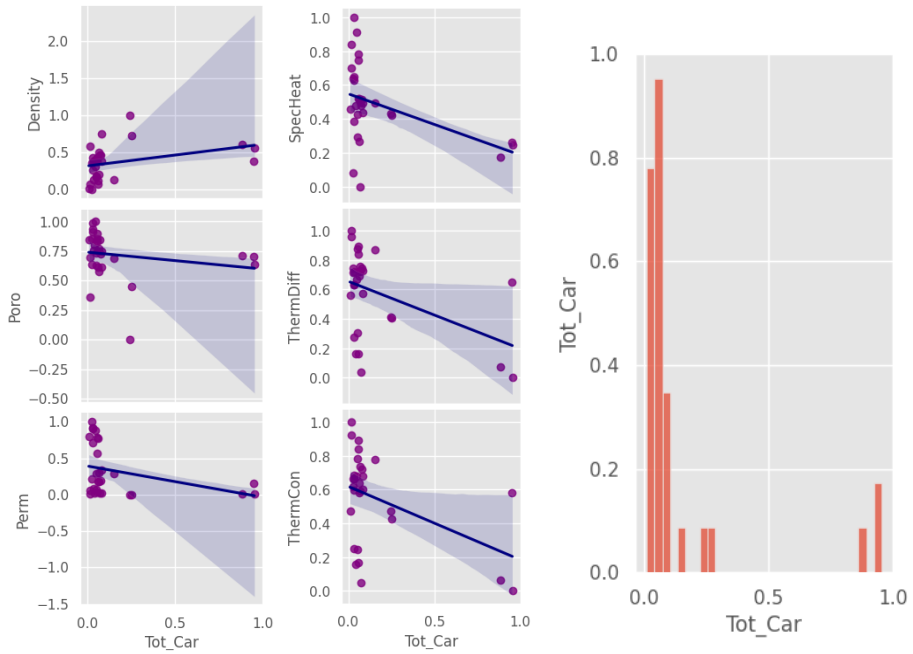

Figure 58. Scatterbox plot of carbonate minerals vs. porosity, permeability and thermal properties.

4.4 Feldspars

In the samples analyzed, feldspars are compounded by Orthoclase Feldspar, Oglioclase Feldspar, and Albites. The presence of clay minerals per sample variates from less than 0.1% to 26.4%, with a mean value of 12.4%. In the present data set, the clay minerals content is somewhat negatively correlated with thermal properties and uncorrelated to the petrophysical properties analyzed, as depicted in **Figure 59**. Feldspar minerals typically comprise a three-dimensional framework of tetrahedra (SiO4) and aluminum-oxygen octahedra (AlO4). These tetrahedra and octahedra are linked together through oxygen ions, forming a complex network of interconnected channels and voids. The nature of this framework means that there are few continuous pathways for heat to travel through the material, which leads to low thermal conductivity.

Additionally, feldspars have relatively weak bonding between the layers of the crystal structure, which also contributes to their low thermal conductivity. These weak interlayer bonds make it difficult for heat to be conducted between adjacent layers of the crystal structure, resulting in limited thermal conductivity.

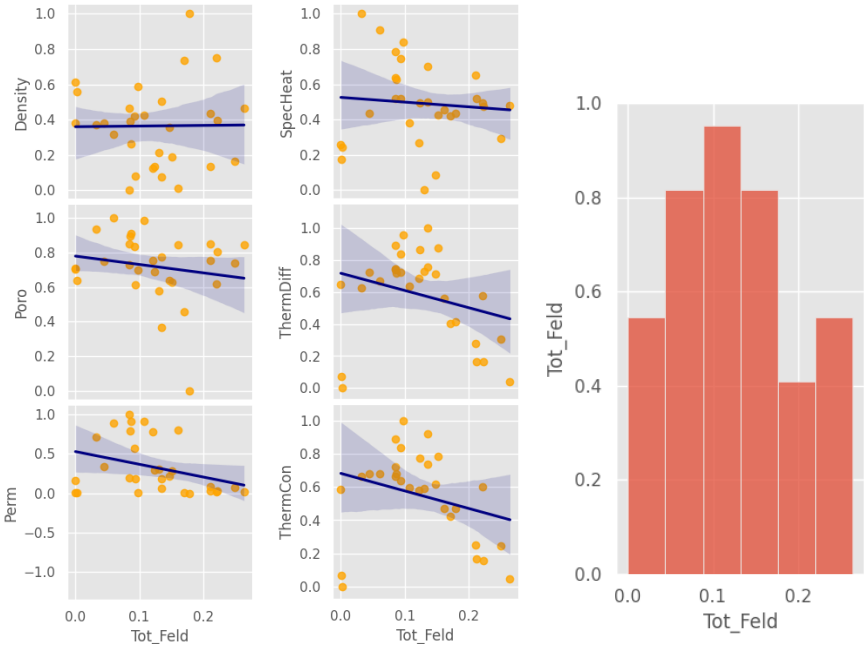

Figure 59. Scatterbox plot of feldspars vs porosity, permeability, and thermal properties.

4.5 Correlation between minerals and thermal properties

An analysis of the results provided some insight and helped to understand the implication found in the mineral composition of sandstone samples. The study aimed to investigate the relationship between the mineral content and the thermal and petrophysical properties of the samples. The paragraphs describe the findings for four main mineral groups: quartz, clay minerals, carbonates, and feldspars.

The study found that quartz is the most abundant mineral among the samples, with a mean value of 59.4%, and its content has a positive correlation with thermal properties. Quartz is resistant to weathering and has a crystalline structure that allows heat to pass through it efficiently. The study also found that the quartz content is uncorrelated with porosity and permeability.

Carbonates, on the other hand, are the second most abundant mineral group in the samples, with a mean value of 15.4%, and their content has a negative correlation with thermal properties. Carbonate minerals have a lower thermal conductivity than many other minerals commonly found in sedimentary rocks, including quartz. The crystal structure of carbonate minerals is relatively open, containing many void spaces, which makes them less efficient at conducting heat compared to minerals with a more tightly packed crystal structure, such as quartz.

Clay minerals are present in the samples with a mean value of 10.0%, and their content is uncorrelated with thermal and petrophysical properties. The layered structure of clay minerals limits the movement of heat through the material, and the weak interlayer forces make it difficult for heat to be conducted from one layer to the next.

Feldspars are present in the samples with a mean value of 12.4%, their content is somewhat negatively correlated with thermal properties and uncorrelated to petrophysical properties. Feldspar minerals typically comprise a three-dimensional framework of interconnected channels and voids, which leads to low thermal conductivity. The weak interlayer bonds also make it difficult for heat to be conducted between adjacent layers of the crystal structure.

Figure 60 displays the correlation between the thermal properties and mineral composition of the analyzed samples. Among the minerals studied, Quartz has the most significant positive impact on the thermal properties of the core samples; 0.53 for thermal conductivity, 0.52 for thermal diffusivity, and 0.61 for specific heat. In contrast, carbonates have a predominantly negative effect on the samples analyzed; -0.43 for thermal conductivity, -0.43 for thermal diffusivity, and -0.42 for specific heat. It is worth noting that this negative effect is noteworthy, despite the relatively low percentage. It is crucial to consider that the distribution of carbonates is not evenly spread, which means that a few exceptionally low values can significantly influence the overall trend.

Figure 60. Heat map with the Pearson correlation between thermal properties and mineral content

The experimental results analysis provides an understanding of the relationship between the mineral composition of sandstone samples and their thermal and petrophysical properties. This knowledge can be useful in predicting the performance of sandstone reservoirs for thermal energy storage, such as geothermal energy production, where the thermal properties of the rock are essential for efficient energy transfer.

From the experiments it is observed that quartz, the most abundant mineral among the samples, has a positive correlation with thermal properties. This information can help in the selection of sandstone reservoirs with a high quartz content for thermal energy storage projects.

Additionally, the study found that carbonates, the second most abundant mineral group in the samples, have a negative impact on thermal properties. This finding suggests that sandstone reservoirs with a high carbonate content may not be suitable for thermal energy storage.

The study confirms that clay minerals are good heat insulators. This information may help to identify and ideal thermal energy storage system, where the main reservoir is a sandstone with high content of quartz, bounded by shales or claystones that provide seal to store the hot water, and as well provide insulation that improves the performance of the thermal energy storage system.

5. Texture-Dependent Thermal Properties of Sandstone Rocks Examined by SEM

Sedimentary rocks are widely used as geological reservoirs and as host rocks for geothermal energy systems. The thermal properties of sedimentary rocks, such as thermal conductivity, thermal diffusivity, and volumetric specific heat, play a critical role in their suitability for these applications. This study examined the thermal properties of 30 different sandstone rock samples using scanning electron microscopy (SEM) analysis. The SEM images of rock samples with different thermal properties were compared to analyze how textural properties influence thermal properties. Our results suggest that the thermal properties of sedimentary rocks are highly dependent on their texture. Specifically, we found that rocks with a higher degree of roughness tend to exhibit lower thermal conductivity and thermal diffusivity. The presence of pores and cracks impacted the thermal properties of the sandstone rocks examined. The average surface roughness extracted from images showed a strong negative correlation with thermal conductivity and diffusivity (-0.59 and -0.6, respectively) obtained experimentally, while pore, cracks, and voids area have a less apparent negative correlation (-0.18 and -0.17) likely due to their complex effect on heat transfer. The size, shape, and distribution of voids affect heat transfer, with interconnected voids providing networks for heat flow, and smaller voids trapping heat more effectively. The texture of sedimentary rocks plays a critical role in determining their thermal properties. This knowledge can be used to optimize the understanding of the potential of sandstone reservoirs in applications, such as geothermal energy or thermal energy storage.

5.1 Rock texture properties

The surface roughness of sandstones is affected by several factors, including the size distribution of sand grains, their shape, and the amount of pore space in the rock. Well-sorted, fine-grained sandstones tend to have smoother surfaces compared to coarser-grained or poorly sorted types (Steel

and Thompson, 1983). This is because rounded, spherical sand grains pack together more smoothly than angular ones, which create rougher textures (Bowman et al., 2001). Another factor to consider is the pore space. Surface roughness increases with the amount of pore space in the rock. Higher porosity from interconnected pores and voids creates more surface irregularities (Sahimi, 1993). The mineral composition also plays a role in surface roughness, with quartz-rich sandstones being more resistant to weathering processes that roughen surfaces over time. The surface roughness of sandstones, which is primarily a reflection of the size, shape, and arrangement of the individual grains within the rock, can also be influenced by the quartz content. Quartz grains tend to be rounded and typically exhibit a smooth surface texture. Therefore, sandstones that are composed almost entirely of quartz (i.e., quartz arenites) often have a relatively smooth surface compared to sandstones that contain a significant proportion of other minerals, such as feldspar or clay minerals, which can contribute to a rougher surface texture (Pettijohn et al., 1987).

5.2 Use of SEM to analyze rock properties.

Scanning electron microscopy (SEM) can be used to analyze the thermal properties of rock samples by examining the mineralogical and textural features of the rock at high magnification. SEM can provide detailed images of the rock surface, allowing for the identification and measurement of mineral grain size and shape, porosity, and connectivity. Therefore, using SEM analysis to evaluate the thermal properties of rocks can provide more accurate and reliable results than relying on visual inspection with the naked eye. SEM images can provide insights into the microstructure and composition of the rocks, which can indirectly influence their thermal properties (El Alami et al., 2020).

SEM enables the identification of different minerals present in sedimentary rocks. Certain minerals have specific thermal properties, such as thermal conductivity or thermal expansion

coefficient (Knobloch et al., 2022). The thermal properties of rocks are influenced by the contact between individual grains. SEM analysis can reveal the nature and quality of grain-to-grain contacts, including the presence of cementing materials or pore-filling minerals (Baiyegunhi et al., 2017). The effectiveness of heat transfer within the rock matrix is affected by these contacts.

Sedimentary rocks contain pore spaces that can significantly impact their thermal properties (Fuchs et al., 2013). SEM analysis allows for the characterization of pore structure, including pore size distribution, connectivity, and shape (Nole et al., 2016). The presence of open or closed pores, as well as the type of pore-filling materials, can influence the rock's thermal conductivity, heat capacity, and thermal diffusivity (Heap et al., 2020). A number of researchers have used SEM as complementary tool, to analyze thermal properties of sedimentary rocks (Korte et al., 2017; Labus and Labus, 2018b). SEM can indirectly contribute to understanding the thermal properties of sedimentary rocks by providing valuable information about their microstructure, mineral composition, pore characteristics, and thermal alteration effects. SEM data, combined with other rock properties data, can be extrapolated to field scale using machine learning and data analytics solutions (Sharma et al., 2023; Sletcha et al., 2020; Vivas and Salehi, 2021a, 2021b).

The objective of the study is to establish a relationship between the thermal properties of 30 identified core samples and the corresponding characteristics observed in SEM images. The core samples analyzed exhibit a range of thermal properties. Advanced image processing and analysis methods were utilized to identify and measure microstructural attributes like grain size, pore size, and connectivity. The objective is to compare the identified thermal properties of the core samples to the observed image characteristics in order to identify connections between the core microstructures to the thermal properties of the samples.

5.3 Materials and Methods

The methodology involves the analysis of 30 core samples with diverse known thermal properties, preparing them for SEM analysis, and capturing high-resolution SEM images. Image processing and analysis techniques are employed to identify and quantify microstructural features such as grain size, pore size, and connectivity. The known thermal properties of the core samples are then compared with the observed image characteristics to determine any significant correlations.

The rock samples of different sandstones were obtained from Berea Sandstone, Boise Sandstone, and Kentucky Sandstone formations. **Figure 61** depicts the workflow and the equipment used for measuring the petrophysical properties, thermal properties, and mineralogy of the samples.

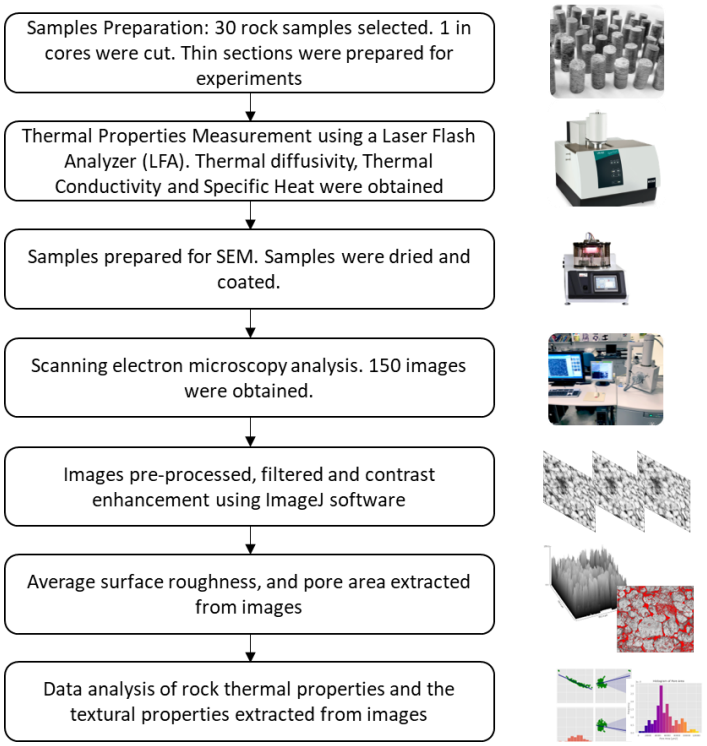

Figure 61. Experimental workflow of this study

5.3.1 Samples Thermal Properties

The thermal properties of the 30 sandstone samples were obtained experimentally. The thermal properties were measured using the LFA (light flash apparatus) Netzsch LFA 467. The equipment uses a short pulse of energy light to heat up the front surface of a flat sample, which is parallel to a plane. An infrared detector measures the temperature change of the back surface caused by the heat pulse. This measurement allows for the determination of thermal diffusivity and specific heat. When combined with the density of the sample, these thermophysical properties can be used to calculate thermal conductivity.

The variation of equation 3 is used to calculate the thermal conductivity:

$$\lambda = \kappa * \rho * C_P \qquad (6)$$

Where λ represents thermal conductivity, κ represents thermal diffusivity, C_P represents specific heat capacity, and ρ represents the density of the samples collected in the laboratory.

5.3.2 Samples preparation

The 1-inch core samples were cut to expose the surfaces that are going to be analyzed by SEM. This is done to obtain more insight about sample texture. Once the samples were cut to the appropriate size, they were coated with a conductive metal layer to improve conductivity. For this study a carbon coating was applied, to prevent the buildup of electrical charges during SEM analysis. Before performing every experiment, the samples were stored in an oven at 65°C for 24 hours. The objective of this was to have the samples completely dry, prevent moisture from affecting the measurements, and have comparable results.

5.3.3 SEM Experimental equipment and experiment description

To quantitatively assess the morphological features of the rocks, the samples were prepared and examined using an FEI Quanta 200 Scanning Electron Microscope. A total of 150 SEM images were captured and the magnification considered was 300 times. Micrographs with magnifications of 500, 1000, and 2000, were evaluated, however, the mentioned sizes were discarded since they did not allow to capture textural details that are lost for the higher resolution.

The SEM instrument was then used to scan the surface of the cut section, producing high-resolution images of the rock's texture and structure. To extract the information required to understand how textural features affect the thermal properties of the rocks, the images were analyzed with the Fiji version of the software ImageJ. ImageJ is a widely used open-source image processing software that provides a range of tools and plugins for analyzing and quantifying various properties from SEM images. Image J has been used to analyze SEM rock images for analyzing morphological features, particle size evaluation, or porosity (Bai et al., 2013; Kelly et al., 2016; Nole et al., 2016; Tao et al., 2020; Voutilainen et al., 2019). In this study, the surface roughness and porosity were analyzed.

5.3.4 Image preparation

Once the SEM images were obtained, a pre-processing process helped to enhance the image features extraction process. Firstly, the images were filtered using the "Median" filter in ImageJ software. This is a type of spatial filter used to reduce noise in digital images. It works by replacing each pixel in the image with the median value of the neighboring pixels within a given radius. For this study, the radius of 2 pixels was sufficient to enhance the images. After the filter, the enhance contrast option in ImageJ software was used to automatically adjust the brightness and contrast of SEM

images to improve their visibility. Initially, the color scale of the image is normalized, which scales the pixel values in the image so that the minimum value becomes 0 and the maximum value becomes 255. This ensures that the full range of values is used in the image. Then, the pixels of the images were saturated, which refers to the percentage of pixels in the image that should be saturated (set to either 0 or 255). For this study, this was set to 0.5%, which means that the brightest and darkest 0.5% of pixels in the image were set to 255 and 0, respectively. An example of SEM preparation result is presented in **Figure 62**.

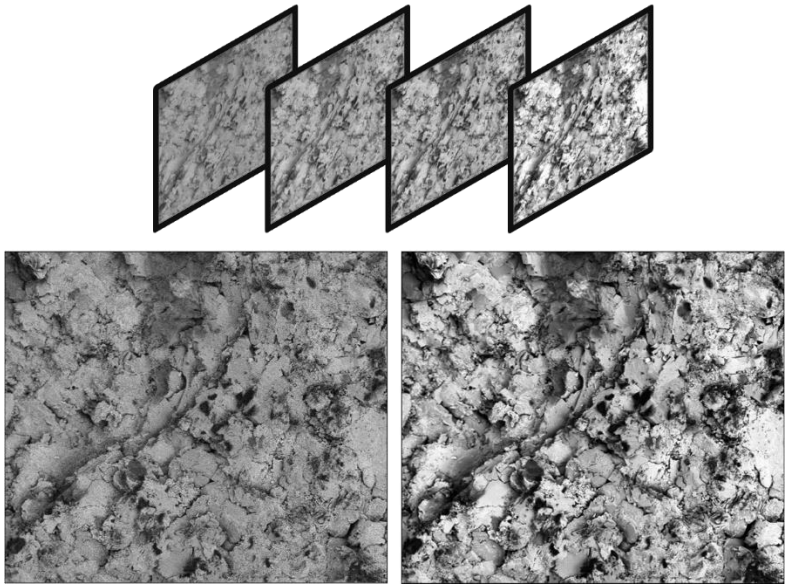

Figure 62. SEM Images, before [left], and after [rigth] pre-processing enhancement.

5.3.5 Pore Area Correction

To accurately analyze SEM micrographs, a statistical correction must be used since the two-dimensional images of the voids may cross-section at random points relative to the center, rather than precisely through the middle. (Zhao et al., 2020) presented a geometric correction for porous materials:

$$d_{corr} = 4 \cdot \frac{d_{SEM}}{\pi} \qquad (11)$$

Where d_{SEM} represents the average pore diameter directly extracted from the SEM images, and d_{corr} represented the corrected pore diameter.

5.4 SEM Rock Images Analysis

SEM images were examined to evaluate the feasibility of using them to assess their thermal properties based on textural features. **Figure 63** shows SEM images of 3 rock samples; they represent samples that have, from left to right, low, medium, and high values of thermal properties from the analyzed dataset.

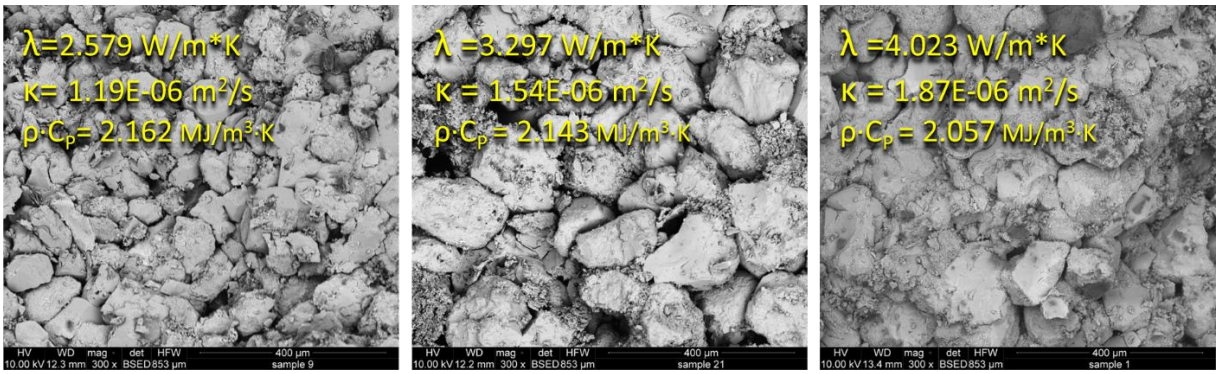

Figure 63. SEM images magnified 300X for samples with high [left] and low [right] thermal properties in the present dataset.

The SEM images showed how different grain sizes, pores and voids, and grains separation affect the rocks' thermal properties. More spaces between grains allow air pockets to form, trapping air that acts as a thermal insulator. The samples with higher porosity, and thus more air pockets, show higher thermal resistance as represented by their higher thermal properties. The software ImageJ was used to extract the morphological characteristics of the rocks.

5.4.1 Surface Roughness

Surface roughness analysis involves quantifying and characterizing roughness features of a surface profile using various variables obtained from SEM images. These variables play a crucial role in understanding the topographic characteristics of the surface.

In **Figure 64** it is depicted the analysis performed in all images. The average surface roughness is a measure of the height variations in the surface of a material. It is calculated by averaging the absolute values of the deviations of the surface from its mean plane. The average surface roughness is calculated by first subtracting the mean plane from the surface height data. This produces a residual height map that represents the surface roughness.

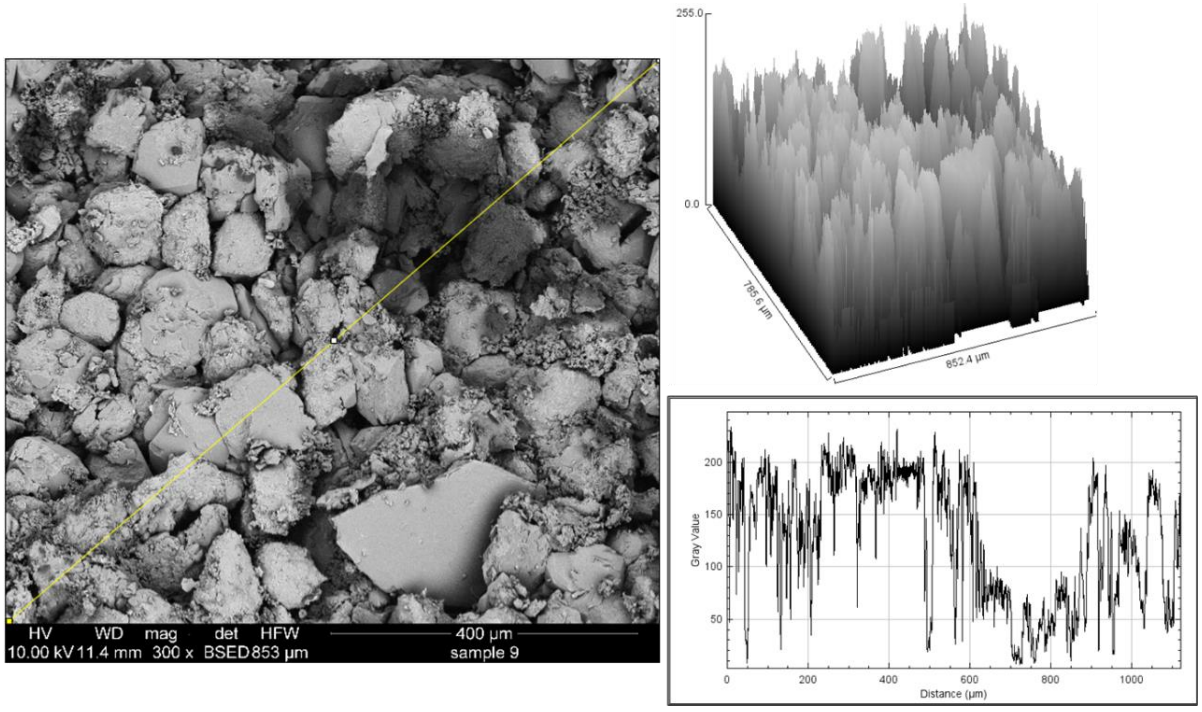

Figure 64. Surface roughness analysis of SEM rock images.

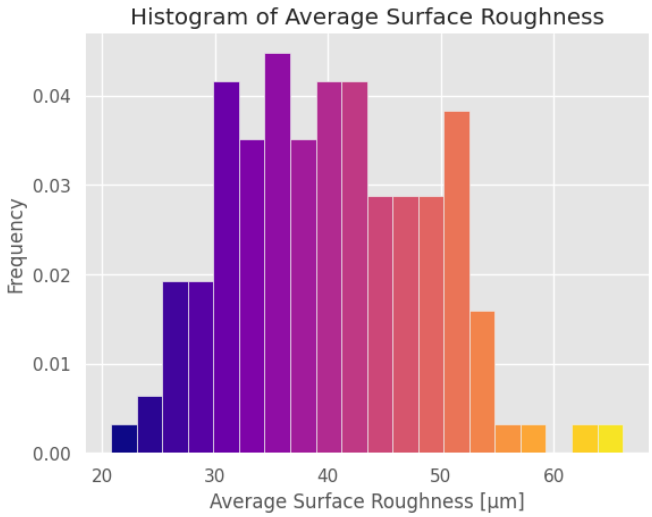

Figure 65. Histogram of the average surface roughness [Ra] values obtained.

5.4.2 Pore, Voids, and Cracks Area

SEM images of rocks contain complex textures and structures that make it difficult to identify and measure the areas of interest manually. By using the threshold function in ImageJ, the pores and voids in every image were identified and segmented **Figure 66**. The threshold function in ImageJ was the tool that was used to segment the SEM image into foreground and background based on pixel intensity values. The tool was useful for separating the pores, voids, and cracks of the rock SEM images from the background. The threshold function applies the threshold to the image and generates a binary mask that separates the foreground and background pixels. The mask can then be used for measuring the area of objects in the image that represents the pores, voids, and cracks. **Figure 67** shows the histogram of the calculated pore in μm^2.

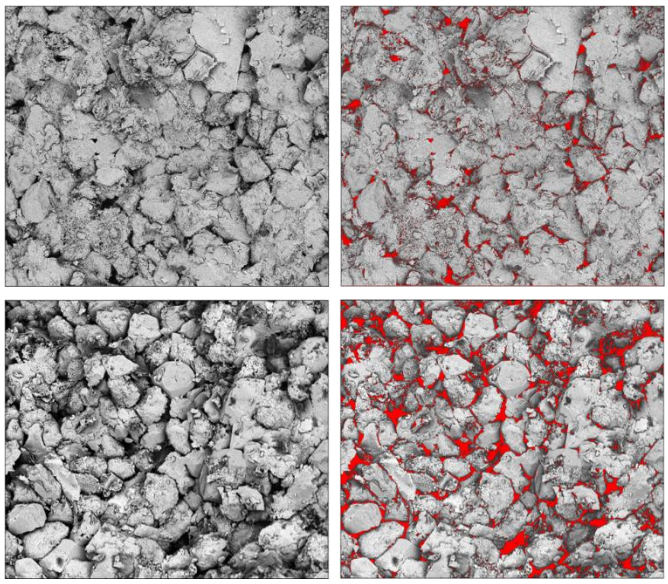

Figure 66. Pore, cracks and voids area analysis of SEM rock images.

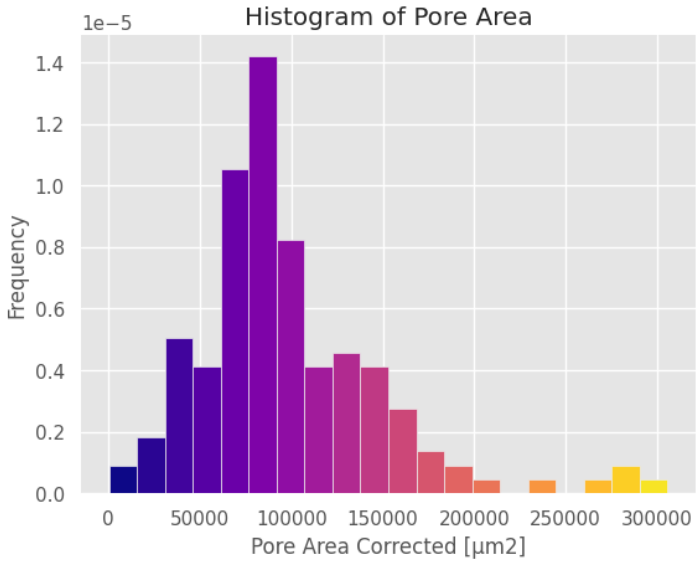

Figure 67. Histogram of pores, cracks, and voids surface area obtained.

5.5 Results Analysis

The analysis of textural properties in SEM images helps to understand the relationship between the morphologic characteristics of rock samples and the rock's thermal properties. In this section, the average surface roughness and the pores, cracks, and voids surface area extracted from the SEM images are compared with the thermal properties of the rock samples obtained experimentally.

5.5.1 Surface Roughness Analysis

Figure 68 presents the relationship between surface roughness (Ra) and thermal properties, specifically thermal diffusivity, thermal conductivity, and volumetric heat capacity for the 150 images. The plot of thermal diffusivity against Ra exposed a trend, indicating that as the Ra values increased, the thermal diffusivity consistently decreased. This suggests that higher surface roughness impedes the efficient conduction of heat, resulting in reduced thermal diffusivity. Similarly, in the plot of thermal conductivity against Ra, as the Ra values increased, indicating greater surface roughness, the thermal conductivity showed a corresponding decrease. When examining the relationship between volumetric heat capacity and Ra, no clear correlation was observed. The plot of volumetric heat capacity against Ra displayed scattered data points, indicating that volumetric heat capacity and Ra are uncorrelated.

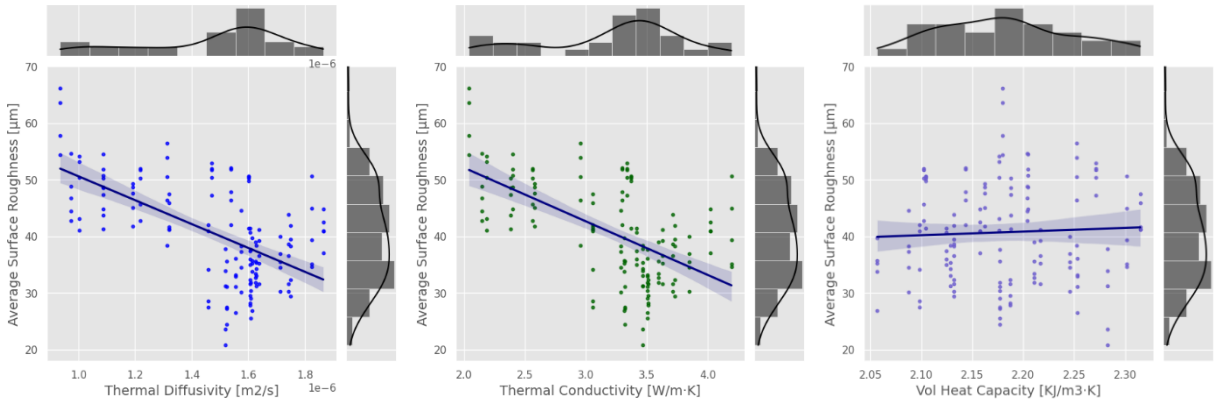

Figure 68. Arithmetic average roughness influence in thermal diffusivity [left], thermal conductivity [middle], and volumetric heat capacity [right].

The surface roughness of the rock is influenced by the grain size and distribution. A smoother surface is indicative of smaller grains that are well-sorted, possessing similar grain shapes. Smaller grains can pack tightly together, while similar grain shapes fit more harmoniously. Consequently, the result is a smoother surface. On the other hand, a rough and irregular surface indicates larger

grains that are poorly sorted, with varying grain shapes. The larger grains cannot pack as tightly, and the differing shapes do not align perfectly, leading to a rough and uneven surface.

Additionally, the scale or wavelength of roughness features can provide clues about the grain size. Larger grains produce roughness features on a larger scale, while smaller grains result in smaller-scale roughness. The presence of isotropic or uniform roughness in all directions indicates well-sorted grains with similar sizes and shapes. Conversely, anisotropic roughness, where smoother and rougher areas align in different directions, signifies poorly-sorted grains with variable sizes and shapes. Lastly, the texture of roughness features, ranging from smooth to jagged, can offer insights into the interlocking of grains. Jagged and angular features indicate grains that are not well-interlocked, while smoother undulations suggest grains that are more interfit, demonstrating their interlocking nature. These observations enable a deeper understanding of the geological properties and composition of rocks based on their surface roughness characteristics.

These findings highlight the impact of surface roughness on thermal properties. Higher Ra values lead to decreased thermal diffusivity and thermal conductivity, indicating a hindered ability to conduct and transfer heat. In contrast, the volumetric heat capacity does not exhibit a significant dependence on surface roughness, as indicated by the lack of correlation between volumetric heat capacity and Ra. These findings contribute to our understanding of the intricate relationship between surface roughness and thermal properties, aiding in the design and optimization of materials for efficient heat transfer applications.

5.5.2 Pore Area Analysis

Figure 69 shows the relationships between the pore area and the thermal diffusivity, thermal conductivity, and volumetric heat capacity. The plot of pore area versus thermal diffusivity indicates

an inverse relationship between the two variables. This means that as the pore area increases, the thermal diffusivity of rocks decreases. Thermal diffusivity is a measure of how quickly heat is conducted through a material, and a lower thermal diffusivity means that heat takes longer to travel through the material. This relationship makes intuitive sense since pores and cracks in rocks are essentially empty spaces that do not conduct heat as well as the solid material. Therefore, as the pore area increases, the proportion of non-conductive material in the rock increases, leading to a decrease in thermal diffusivity.

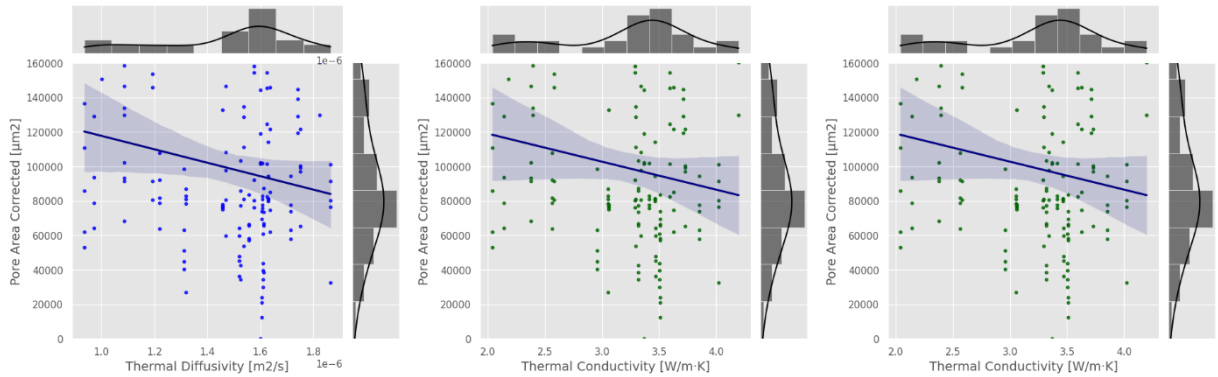

Figure 69. Pores, voids, and cracks area influence in the thermal diffusivity [left], thermal conductivity [middle], and volumetric heat capacity [right].

Similarly, the plot of pore area versus thermal conductivity also shows an inverse relationship between the two variables. This means that as the pore area increases, the thermal conductivity of rocks decreases. Thermal conductivity is a measure of how well a material conducts heat and a lower thermal conductivity means that the material is a poorer conductor of heat. This relationship is also understandable since pores and cracks in rocks act as thermal insulators, reducing the overall thermal conductivity of the rock.

The plot of pore area versus volumetric heat capacity, however, indicates that there is no correlation between the two variables. Volumetric heat capacity is a measure of how much heat a material can absorb before its temperature increases, and in this case, it seems that the presence of

pores and cracks in rocks does not have a significant effect on their volumetric heat capacity. This may be because the amount of solid material in the rock is still the primary determinant of its volumetric heat capacity.

5.6 SEM Results Discussion

The experimental study surface roughness of rocks can be correlated with their thermal properties. Rocks with rougher surfaces generally exhibit larger, more poorly-sorted grain sizes. This leads to a reduced number of grain boundaries per unit volume and inefficient packing, ultimately decreasing the connectivity of the grain network. As a result, heat transfer through the rock becomes more challenging, resulting in lower thermal conductivity and diffusivity.

In contrast, rocks with smoother surfaces tend to have smaller, well-sorted grain sizes. The smaller grain size increases the number of grain boundaries per unit volume, and efficient sorting enables effective packing. This results in a well-connected grain network that facilitates heat transfer. Consequently, rocks with smoother surfaces exhibit higher thermal conductivity and diffusivity.

The presence of grain boundaries can scatter or impede heat transfer. Rocks with smaller, well-sorted grains have a higher density of grain boundaries, providing more opportunities for heat transfer between grains. On the other hand, rocks with fewer, larger grains possess fewer grain boundary sites, limiting heat transfer. Additionally, better packing and grain sorting in rocks minimize the presence of air spaces or pores. This reduces scattering or impedance of heat transfer since air does not conduct heat as efficiently as mineral grains. In contrast, poorer sorting and packing results in more air spaces, creating barriers to heat flow. Smooth grain shapes allow for increased surface contact between grains, enhancing heat transfer. In contrast, angular and irregular

grain shapes lack sufficient surface contact, impeding the flow of heat. These insights highlight the significant influence of surface roughness and grain characteristics on the thermal properties of rocks, shedding light on their heat transfer behavior and conductivity.

Figure 70 displays the correlation between the textural features analyzed, average surface roughness, and the pore, cracks, and voids area extracted from the SEM images, with experimentally obtained thermal properties. Average surface roughness has a strong negative correlation, -0.59 and -0.6 with thermal conductivity and thermal diffusivity respectively. In contrast, the volumetric heat capacity and the average surface roughness are uncorrelated, confirming the results presented in the previous section. The pore, cracks, and void surface area have a less apparent negative correlation, -0.18 and -0.17, related to thermal conductivity and thermal diffusivity. The reason that the pore, cracks, and voids area values have a less apparent negative correlation with thermal conductivity and thermal diffusivity compared to the average surface roughness could be that these properties affect heat transfer differently. The negative correlation between average surface roughness and thermal conductivity/diffusivity is stronger, as the surface roughness directly affects the connectivity of the grain network and packing efficiency, which are important factors in determining thermal conductivity and diffusivity. On the other hand, the effect of voids on heat transfer is dependent on various factors, and the correlation between pore, cracks, and voids area and thermal conductivity and diffusivity may be weaker due to the complexity of the effect of voids on heat transfer. Factors such as the size, shape, and distribution of the voids affect heat transfer. If the voids are interconnected, they can provide networks for heat to flow through, which can increase the thermal conductivity and thermal diffusivity of the sandstone. Additionally, the size and shape of the voids can affect the rate at which heat is transferred. Smaller voids, for example, can trap heat more effectively than larger voids.

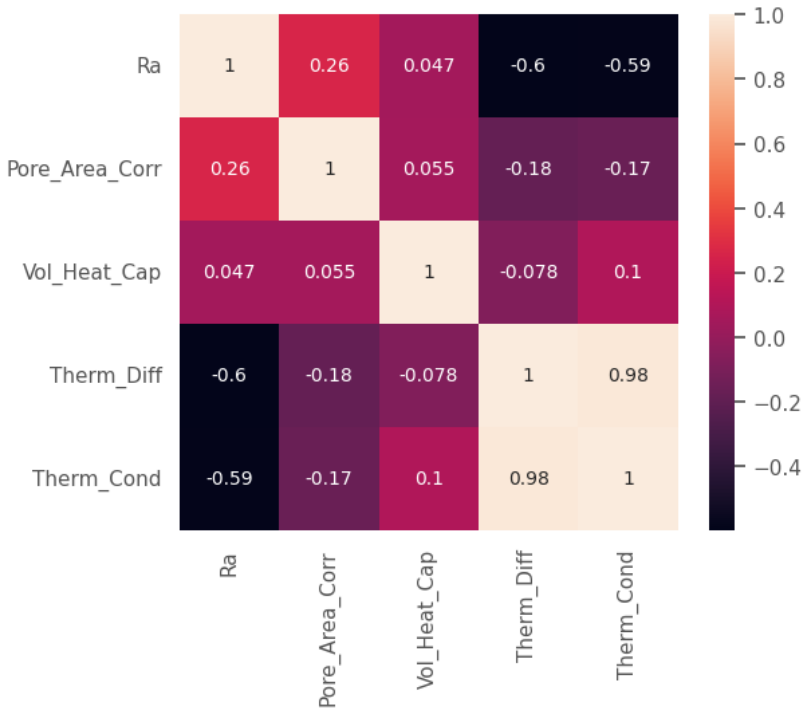

Figure 70. Heat map with the Pearson correlation between thermal properties and textural features where 'Ra' refers to average surface roughness [µm^2], 'Pore_Area_Corr' refers to the corrected pore area [µm^2], 'Vol_Heat_Cap' refers to volumetric heat capacity [KJ/m^3·K], 'Therm_Diff' refers to thermal diffusivity [m^2/s], and 'Therm_Cond' refers to thermal conductivity [W/m·K].

The thermal properties of rocks are influenced by several factors, including their texture, mineralogy, and porosity. These characteristics can be difficult to discern through visual inspection alone, especially when looking at a two-dimensional image. SEM provides high-resolution, detailed images of the rock's surface, allowing for a more accurate analysis of its texture and other characteristics that can impact its thermal properties.

6. Modeling Study to Expand the Rock Thermal Properties

To optimize the design and performance of SRTES systems, accurate modeling and simulation of the underlying processes are essential. In particular, the characterization of the subsurface thermal reservoir plays a critical role in accurately predicting system behavior. Heterogeneous porous media, with varying porosity, permeability, thermal conductivity, and volumetric heat capacity, are commonly encountered in subsurface environments. Understanding and incorporating these spatial variations into the modeling framework allows for obtaining reliable predictions. Few authors have analyzed the effect of heterogeneity in thermal storage reservoir performance. Sommer et al. (2013) generated a Montecarlo simulation to represent stochastically the heterogeneity of hydraulic conductivity, by using multiple homogeneous models created with longitudinal dispersivity. One of the main conclusions was that the increase of heterogeneity affects negatively the thermal energy storage reservoir performance. However, there were not found models built with actual rock properties values in deterministic models.

In this chapter, we focus on the construction of a three-dimensional (3D) model that capture the heterogeneity of porous media for SRTES applications. The properties required for model construction, including porosity, permeability, thermal conductivity, and volumetric heat capacity, are obtained through laboratory experiments conducted on the set of 30 sandstone rock samples. These samples represent a wide range of sandstones and exhibit distinct physical properties as presented in the previous chapters of the present study.

The laboratory-derived properties serve as the foundation for creating realistic and representative 3D model. The model was built by using advanced reservoir simulation software, CMG-STARS (Steam, Thermal and Advanced processes Reservoir Simulator), which allows for the integration of the acquired data and the generation of accurate representations of the subsurface

medium. By incorporating the heterogeneity of the rock types, the resulting models can capture the spatial variations in the physical properties and provide a more realistic representation of the actual system.

6.1 Model Development and Assumptions

To simulate the thermal behavior of the SRTES system, CMG-STARS, a widely used reservoir simulator, is employed. The software provides robust capabilities for modeling fluid flow and heat transfer in porous media, making it suitable for simulating the charge and discharge processes of the SRTES system. The laboratory measurements of the rock properties were incorporated into the numerical model to ensure accurate representation of the heterogeneity in the rock properties. The generated rock types were then used to simulate seasonal thermal energy storage reservoir performance under different conditions. The methodology of the study is drafted in **Figure 71**.

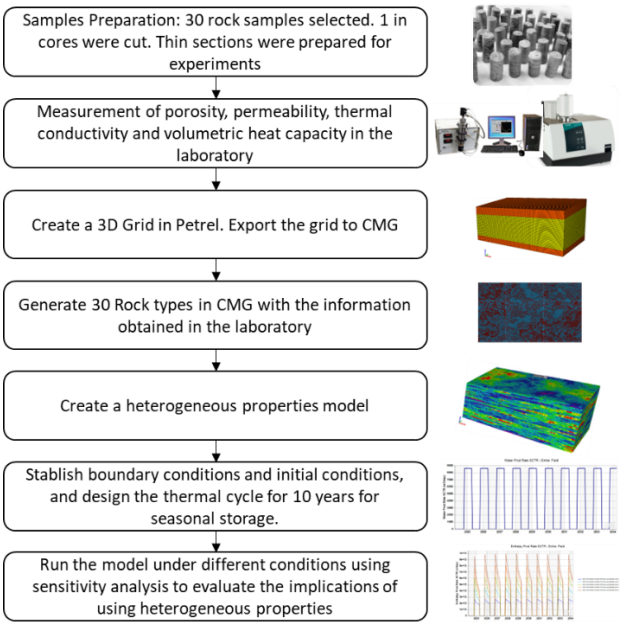

Figure 71. Workflow of the simulation study.

The thermal behavior of the storage medium is represented using a thermal 3D model that considers the heat transfer mechanisms occurring within the porous structure. The model incorporates the porosity, permeability, thermal conductivity, and volumetric heat capacity of the heterogeneous material obtained through laboratory testing, as described in chapters 3 and 4.

During the charge stage, thermal energy is injected into the storage medium. The injection process involves the injection well, where heated fluid is introduced into the reservoir. The injected fluid transfers its thermal energy to the surrounding medium, resulting in an increase in the temperature of the storage medium. The heat transfer within the reservoir is modeled using the appropriate thermal equations in CMG-STARS, accounting for conduction, convection, and radiation processes.

During the discharge stage, the same well used for injection is now utilized for production. The production well extracts the thermal energy from the storage medium, and the heated fluid is produced from the reservoir. The heat transfer mechanisms during the discharge stage are modeled in a similar manner to the charge stage, taking into account the temperature gradient and flow dynamics within the reservoir.

In order to simplify the modeling process and focus on the core aspects of the SRTES system, several assumptions are made. These assumptions are based on practical considerations and aim to provide a reasonable approximation of the system behavior:

- Constant Water Production and Injection Rates: It is assumed that the water production and injection rates remain constant at 100 l/s (8,640 m^3/day) throughout the charge and discharge stages. This assumption allows for simplified calculations and facilitates the analysis of the thermal behavior of the storage medium.

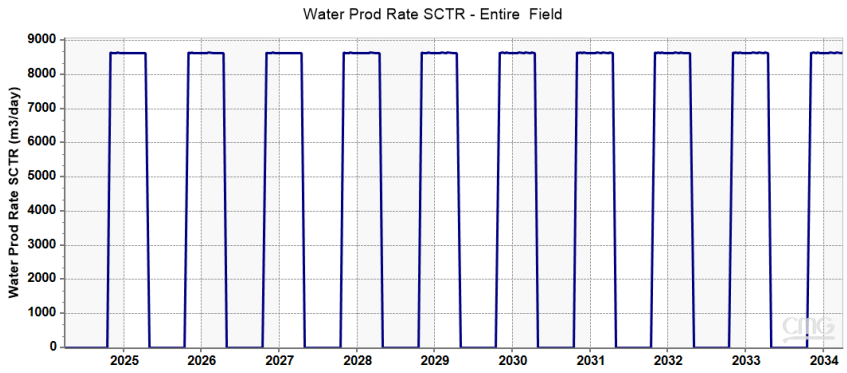

Figure 72. Seasonal discharging cycle schedule for the 10 years simulations.

- Constant Injection Temperature: The injection temperature remains constant during the charge stage. This assumption ensures a consistent and controlled thermal input into the storage medium, enabling accurate evaluation of the system's performance.
- Same Well for Injection and Production: The same well is used for both the injection (charge) and production (discharge) stages. This assumption ensures that the simulated charge and discharge processes occur in a consistent manner, enabling a comprehensive analysis of the thermal behavior of the SRTES system.

6.2 Model Grid and Initial Conditions

The model is constructed using a three-dimensional grid to represent the storage medium for the SRTES system. The model represents a sandstone reservoir bounded by 2 shale rocks. The grid has 168 cells in the i-direction, 96 cells in the j-direction and 42 cells in the k-direction, for a total of 677,376 cells. The grid covers a surface area of 3,745,850.5 m2 (3.746 km2), representing the region where the STES system is implemented. The grid cells are uniformly distributed throughout the area, providing a spatial representation of the storage medium.

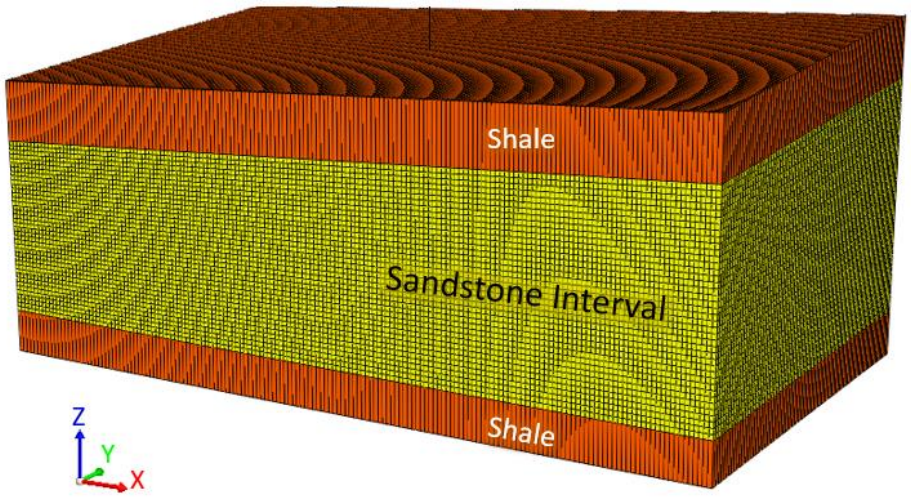

Figure 73. Model grid used in this study.

6.2.1 Initial Conditions

- ***Rock Properties and Heterogeneity***: The rock properties used in the model are generated based on 30 rock types obtained from laboratory testing. These types of rock exhibit heterogeneity in porosity, permeability, thermal conductivity, and volumetric heat capacity. The distribution of these properties within the model grid is representative of the natural geological formations. To evaluate the impact of heterogeneity in thermal properties, two separate models are constructed:
    - Model with Heterogeneous Rock Properties: This model incorporates the heterogeneity of thermal conductivity and volumetric heat capacity, as well as heterogeneous porosity and permeability. The distribution of these properties is based on the 30 rock types generated in the laboratory.
    - Model with Homogeneous Thermal Properties: In this model, the thermal conductivity, volumetric heat capacity, porosity and permeability are considered homogeneous (constant values), with their values set to the average value obtained from the heterogeneous model.

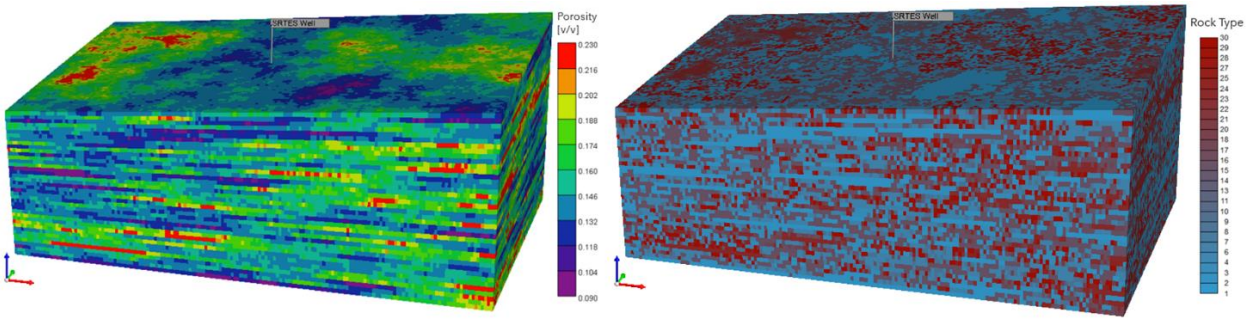

Figure 74. Rock properties distribuition in the heterogeneous 3D model.

- ***Saturation and Well Placement:*** The model assumes that the storage medium is 100% saturated with water. This assumption ensures that water is present throughout the porous structure, allowing for efficient heat transfer and storage. The thermal energy storage system consists of one well, located approximately at the center of the model grid. The well is positioned in cell i=80 and j=46, ensuring a central placement within the SRTES system. This placement facilitates uniform distribution of thermal energy and enables consistent charging and discharging processes.
- ***Charging and Discharge Timeframes***: The TES charging period is set from April 15 to October 15, representing the months of increased thermal energy supply. The discharge process starts from October 15 and continues until April 15, representing the months of higher thermal energy demand. The seasonal cycle is repeated 10 times, representing a simulation duration of 10 years. This extended timeframe allows for the evaluation of the long-term performance and effectiveness of the STES system under different conditions.
- ***Injection Conditions***: During the charging time, water is injected into the storage medium at a constant temperature and flow rate. The injection rate is set to a constant value of 100 liters per second, ensuring a consistent thermal input into the system. To assess the sensitivity of the system to water temperature, a sensitivity analysis is performed by varying the water

injection temperature. The analysis includes injection temperatures of 100°C, 150°C, 200°C, 250°C, and 300°C, allowing for a comprehensive evaluation of the system's response to different thermal inputs. Surface temperature was stablished as 21°C, average temperature in Oklahoma.

6.3 Simulation Results

Numerical simulation allows sensitivity analysis to evaluate the impact rock properties heterogeneity, temperature and cycling on the SRTES efficiency.

6.3.1 Effect of Heterogeneity

To understand the potential implication in the SRTES efficiency reflecting the natural heterogeneity of sandstone rocks, the enthalpy extraction was modeled at different temperatures during 10 years, and results are presented in **Figure 75**. The initial observation is that at all temperatures, the homogeneous model has better enthalpy production compared with the heterogenous model. Besides, it is observed that at 100°C the difference between the homogeneous and heterogeneous model is low. However, as the temperature increases, the deviation between the homogeneous and heterogeneous curves at the same temperature increases exponentially (Error! Reference source not f ound.). At 300°C the homogeneous model has additional 2.12 Terajoules, representing 16.95% of additional enthalpy produced after 10 years. The impact of heterogeneity on the efficiency of the SRTES appears to be influenced by temperature.

Table 11. Enthalpy production differential (homogeneous – heterogeneous) after 10 years of production.

Simulation	Enthalpy Difference [Terajoules]	% Of Difference
100°C	0.0323	0.79%
150°C	0.1323	2.06%
200°C	0.4347	5.05%

250°C	1.0229	9.54%
300°C	2.1026	16.95%

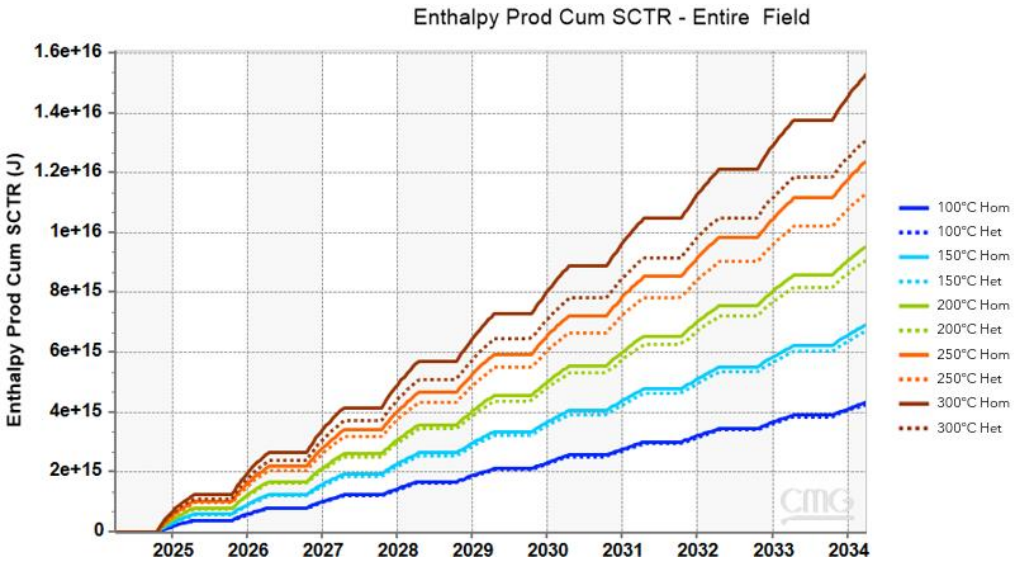

Figure 75. Cumulative enthalpy production at different temperatures for the homogeneous and heterogeneous models.

6.3.2 Effect of Temperature in the Production Rate

The seasonal charging of the SRTES was simulated at different temperatures, and the enthalpy production is presented in **Figure 76**. The temperature increase affects the production rate; the higher the temperature the enthalpy declination in each seasonal cycle is higher. **Figure 77** shows the bottom hole temperature of the SRTES reservoir during the seasonal charge and discharge, showing that the temperature declination increases with the temperature increase, with affects the enthalpy production. Also, as other researchers have found, the temperature declination is reduced with through time. The initial cycles help to charge the reservoir, increasing the enthalpy production cycle after cycle.

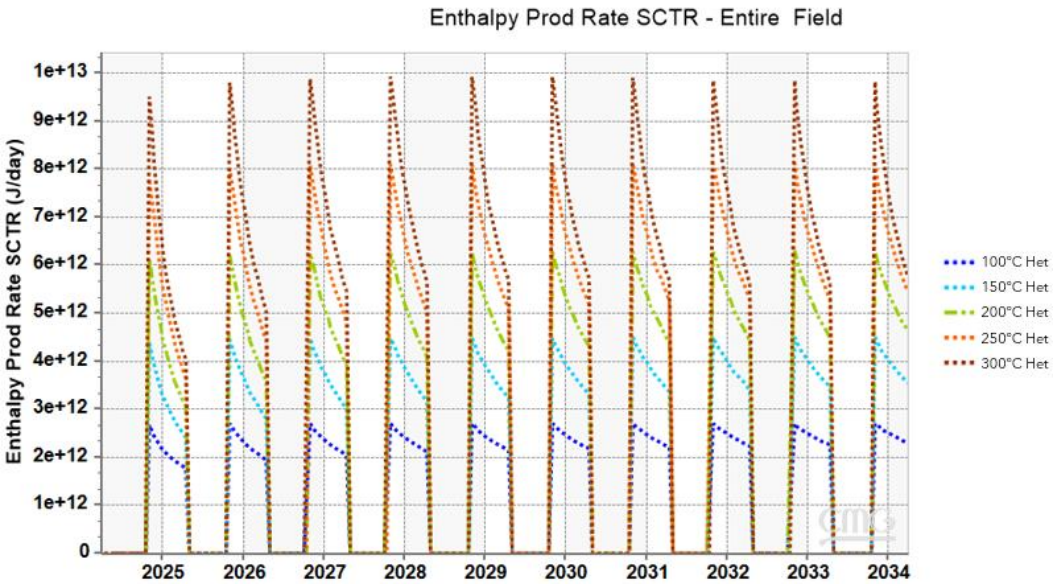

Figure 76. Cumulative enthalpy production at different temperatures for the homogeneous and heterogeneous models.

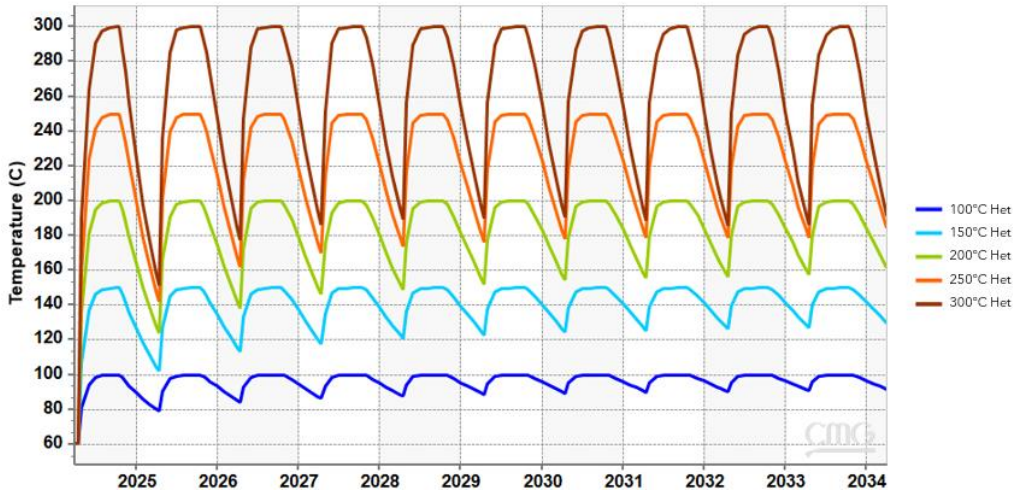

Figure 77. Bottom hole temperature during seasonal thermal cycling at different temperatures.

6.3.3 Effect of Temperature in the SRTES Efficiency

Figure 78 presents the SRTES efficiency at 100°C, 150°C, 200°C, 250°C, and 300°C during the 10 years seasonal cycling. At 100°C, 150°C, and 200°C the SRTES efficiency increases with time and becomes steady near year 10. For the 250°C, and 300°C simulations, in the initial cycles the

efficiency of the SRTES increases, but that increase is not sustained during time and there is a loss of efficiency. The effect is very noticeable, especially in the 300°C simulation after the 7th cycle.

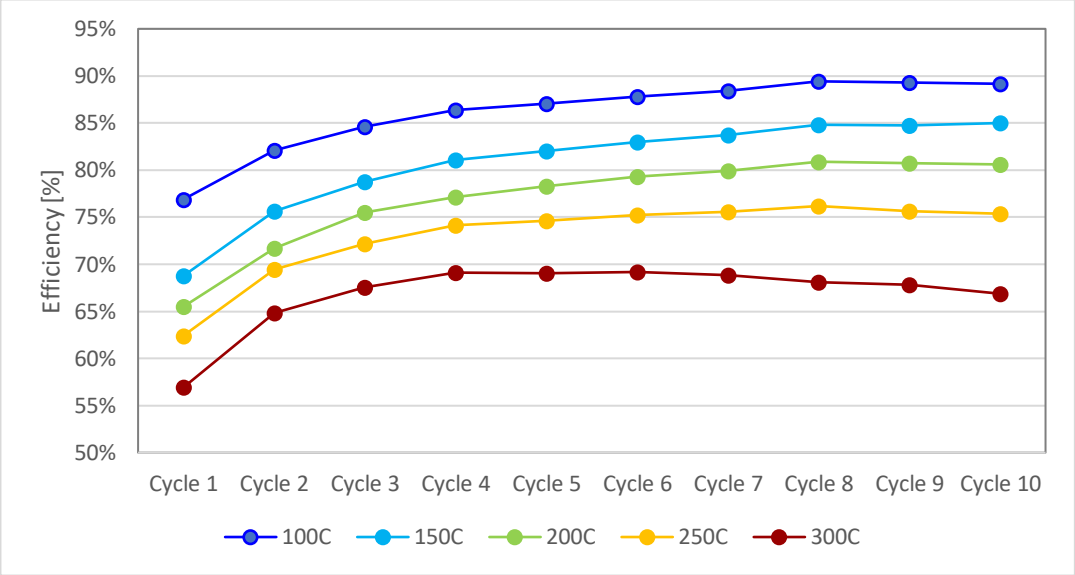

Figure 78. Bottom hole temperature during seasonal thermal cycling at different temperatures.

6.4 Model Results Discussion

The simulation results revealed several key findings. Firstly, the effect of heterogeneity on the efficiency of the SRTES system was observed to be influenced by temperature. The homogeneous model consistently exhibited better enthalpy production compared to the heterogeneous model at all temperatures. In the heterogeneous model, the presence of heterogeneities in rock properties, including thermal conductivity and volumetric heat capacity, can create variations in the ability of the storage medium to conduct and store thermal energy. These variations result in uneven distribution and movement of heat within the medium. Higher temperatures increase the rate of heat transfer, causing thermal energy to move more rapidly. However, the presence of heterogeneities in thermal properties introduces barriers to efficient heat transfer.

The variations in thermal conductivity affect the ability of the storage medium to conduct heat. Regions with lower thermal conductivity act as insulators, impeding the transfer of heat from the injection well to the surrounding rock matrix. Consequently, thermal energy may accumulate in the regions with higher thermal conductivity, reducing the overall enthalpy production in the heterogeneous model. Similarly, variations in volumetric heat capacity influence the storage capacity of the medium. Regions with lower volumetric heat capacity have a reduced ability to store thermal energy, leading to a lower overall enthalpy production in the heterogeneous model compared to the homogeneous model.

In addition to thermal properties, the heterogeneity of porosity and permeability can further impact the efficiency of heat transfer. Variations in porosity and permeability can create preferential flow paths or regions with restricted fluid movement. In the heterogeneous model, regions with higher porosity and permeability may allow for more efficient fluid flow and heat transfer. Conversely, regions with lower porosity and permeability act as barriers, impeding fluid movement and reducing heat transfer efficiency. This results in reduced enthalpy production compared to the homogeneous model, where fluid flow and heat transfer are more uniform. The combined effect of variations in thermal conductivity, volumetric heat capacity, porosity, and permeability in the heterogeneous model leads to an uneven distribution of thermal energy and reduced efficiency in enthalpy production compared to the homogeneous model. As the temperature increases, the impact of these heterogeneities becomes more pronounced, exacerbating the barriers to heat transfer. This is reflected in the exponential increase in deviation between the homogeneous and heterogeneous models with temperature.

The temperature had a significant effect on the production rate of the SRTES system. Higher temperatures resulted in a higher decline in enthalpy during each seasonal cycle. The bottom hole

temperature of the SRTES reservoir showed an increasing temperature decline with higher temperatures, affecting the enthalpy production.

The SRTES efficiency was analyzed at different temperatures during the 10-year seasonal cycling. At 100°C, 150°C, and 200°C, the SRTES efficiency increased with time and became steady near year 10. AT these temperatures, the decline in temperature was reduced over time, indicating that the initial cycles helped in charging the reservoir and increasing the enthalpy production cycle after cycle. However, at 250°C and 300°C, the efficiency initially increased but was not sustained over time, resulting in a loss of efficiency. At lower temperatures, such as 100°C, 150°C, and 200°C, the SRTES system operates within a range where the thermal properties of the storage medium and other system components are conducive to efficient energy storage and retrieval. As the system undergoes more cycles, it becomes better optimized, and the efficiency stabilizes near year 10. However, at higher temperatures, specifically 250°C and 300°C, the system encounters challenges that affect its efficiency. Higher temperatures can result in increased thermal losses from the system. This can occur through conduction, convection, and radiation, leading to a reduced overall efficiency. As the temperature rises, the rate of heat transfer to the surroundings becomes more significant, resulting in a higher proportion of thermal energy being lost rather than stored or utilized.

The buoyancy effect can also influence the temperature decline and enthalpy production in the SRTES system through various mechanisms. It can induce mixing or stratification within the system, affecting temperature distribution. Mixing blends fluids with different temperatures, while stratification separates fluids into layers with distinct temperatures. The buoyancy effect can hinder mixing and stratification, impacting temperature decline and overall enthalpy production. As this effect is exacerbated with temperature, that it is a factor to consider in the loss of efficiency with temperature.

7. Summary, Conclusions and Future Work

7.1 Summary

This dissertation studies the interactions between petrophysical and thermal properties in sandstones, and how the natural heterogeneity of the rock properties affects the performance of sandstone reservoir in utility scale thermal energy storage. 30 sandstone samples with different thermal properties were used in the study. Porosity, permeability, density, mineralogy, thermal conductivity, diffusivity and specific heat were obtained and calculated using laboratory equipment. The experimental results obtained were analyzed to find the intercorrelation between mineral content, petrophysical, and thermal properties of core samples. Textural properties were analyzed in a SEM study. Images were obtained from rock samples to examine various surface roughness properties. The objective was to quantitatively evaluate and characterize the roughness features of the rock surfaces, and gain insights into the micro-structural defects, crack types, and other surface characteristics that impact the thermal properties of sedimentary rocks. Finally, numerical simulation was performed to use the results of the experimental study to build a 3D model that captures the heterogeneity of porous media for SRTES applications. The properties required for model construction, including porosity, permeability, thermal conductivity, and volumetric heat capacity, are obtained through the laboratory experiments conducted on 30 sandstone rock samples. These samples represent a wide range of geological formations and exhibit distinct physical properties. The objective was to generate a reservoir model that reflects the heterogeneity in petrophysical and thermal properties of sedimentary rocks. Multiple simulations allowed to perform a sensitivity analysis that reflects factors such as heterogeneity, temperature change and seasonal cycling affect the efficiency of a thermal energy storage. The findings of this experimental study

aim to contribute to the selection of sandstone reservoirs with the appropriate mineral composition for thermal energy storage, leading to more efficient and effective energy production.

7.2 Conclusions

1. The configuration of a sandstone reservoir bounded by shales makes a good option for thermal energy storage. Sandstones can be used as the SRTES reservoir because of their higher porosity and permeability compared with other sedimentary rocks. Porosity provides capacity storage, while permeability gives flow capacity to allow the heat transfer fluids to flow through the reservoir. Sandstones have a relatively high heat capacity, thermal conductivity and thermal diffusivity, meaning they can store large amounts of thermal energy per unit mass, making them an effective storage medium. Shale provides sealing to confine the fluids in the sandstone reservoir, and their lower thermal diffusivity regulates the heat losses.
2. For utility scale applications, water seems to be an ideal heat transfer fluid. The combination of high heat capacity, high thermal conductivity, non-toxic and widely available, low cost, and environmental sustainability make water a good heat transfer fluid for thermal energy storage systems.
3. Among the 4 mineralogy groups analyzed in the experimental study; quartz, clays, carbonates and feldspars, quartz was the mineral that presents the highest positive correlation with respect of thermal conductivity (0.51), thermal diffusivity (0.53), and specific heat (0.61).
4. Carbonates were the second most abundant mineral group in the sandstone samples, with an average content of 15.4%. Carbonates showed a negative correlation with thermal properties,

reducing thermal conductivity, diffusivity, and specific heat by an average of -0.43, -0.43, and -0.42 respectively.

5. Clay minerals were present in the sandstone samples at an average concentration of 10.0%. The study found that clay mineral content was uncorrelated with both thermal and petrophysical properties of the samples.
6. Feldspars were present in the sandstone samples at a mean value of 12.4%. Feldspars showed a somewhat negative correlation with thermal properties but were uncorrelated with petrophysical properties. The average negative correlation of feldspars with thermal conductivity, diffusivity, and specific heat was around -0.3.
7. The analysis of 150 SEM images of rock samples found that the average surface roughness (Ra) values had a strong negative correlation of -0.59 with the thermal conductivity of the rocks. This indicates that as the surface roughness increases, the ability of the rock to conduct heat efficiently decreases significantly.
8. The average surface roughness (Ra) values extracted from the 150 SEM rock images showed a robust negative correlation of -0.6 with the thermal diffusivity of the samples. Thermal diffusivity is a measure of how quickly heat propagates through a material. The high negative correlation suggests that rocks with rougher surfaces have a markedly lower ability to transfer heat rapidly.
9. The quantitative measurement of the pore, crack, and void surface areas from the 150 SEM rock images revealed a moderate negative correlation of -0.18 with the thermal conductivity values. As the combined surface area of pores, cracks, and voids increased, the thermal conductivity decreased, implying these empty spaces impeding heat transfer.

10. The pore area values extracted from the 150 SEM images exhibited a negative correlation of -0.17 with thermal diffusivity of the rock samples. This moderate correlation indicates that as the proportion of non-conductive pore space increases, the ability of the rock to propagate heat quickly reduces.
11. The numerical simulation results showed that at 300°C, the homogeneous reservoir model had 2.12 Terajoules or 16.95% higher cumulative enthalpy production compared to the heterogeneous model after 10 years of operation. This indicates that heterogeneity in reservoir properties like thermal conductivity and heat capacity significantly reduces efficiency at higher temperatures.
12. At a lower temperature of 100°C, the difference in total enthalpy production between the homogeneous and heterogeneous numerical reservoir models was minimal at just 0.0323 Terajoules or 0.79% after 10 years. This implies that heterogeneity has a smaller effect on performance at lower operating temperatures.
13. Analysis of the seasonal underground thermal energy storage (SRTES) efficiency over 10 years found that at relatively lower temperatures of 100°C, 150°C and 200°C, the efficiency steadily increased over time and stabilized around year 10 of operation as the reservoir became thermally charged.
14. However, at higher temperatures of 250°C and 300°C, the SRTES efficiency initially increased but then declined after approximately 7 cycles of seasonal operation. This indicates reduced performance at higher temperatures.
15. Examination of the bottom hole temperature data showed that the temperature decline during cycling was significantly higher at 300°C compared to 100°C. This implies increased heat losses at higher operating temperatures, contributing to lower efficiency.

16. The presence of heterogeneity in key reservoir rock properties such as thermal conductivity and volumetric heat capacity creates variations in the ability of the underground medium to conduct and store thermal energy. This results in uneven heat distribution and barriers to efficient heat transfer, significantly reducing the efficiency of heat extraction in the heterogeneous storage reservoir compared to a homogeneous reservoir.
17. As the operating temperature increases, the rate of heat transfer and the mobility of thermal energy within the reservoir medium also increases. This exacerbates the impact of heterogeneity in rock thermal properties on the performance of the seasonal reservoir thermal energy storage (SRTES) system. Heterogeneities become more pronounced barriers to uniform heat transfer at higher temperatures.
18. The numerical modeling indicates that there is an optimal temperature range for efficient operation of the SRTES system. At relatively lower temperatures, the efficiency improves over cycles as the underground reservoir charges up thermally. However, at very high temperatures beyond 200°C, increased heat losses occur, resulting in a decline in system efficiency over time. This highlights the importance of designing the SRTES to operate within a suitable temperature range.

7.3 Recommendations and Future Work

- Quartz was the most abundant mineral present in the samples analyzed. This is to be expected, as the study was focused on sandstones, which are composed primarily of quartz. However, expanding the study to other rock types would provide a more complete perspective of how mineralogy affects the thermal properties of sedimentary rocks. For example, claystones, carbonates, and limestones are also common rock types in sedimentary rocks, and their thermal properties are likely to be different from those of sandstones.

- The experimental work on sandstones has provided valuable data on the thermal properties of these rocks. However, the data is limited to a relatively small number of samples. Expanding the experimental work to include mora samples would provide more data points, which would allow machine learning solutions to be used to expand the results. This would provide a more comprehensive understanding of the thermal properties of sandstones and would be useful for developing models to predict the sandstones' thermal properties.
- The experimental values obtained in the laboratory are often limited to the number of samples. However, well logs can provide information on the thermal properties of rocks at a much larger scale. By using data analytics, it is possible to generate a model that can connect the experimental values with the well log data. This would allow the model to be upscaled to generate 3D models that reflect the heterogeneity of the SRTES reservoirs. This would be useful for developing models to predict the thermal properties of these reservoirs.
- Machine learning using drilling parameters has been used to generate synthetic thermal properties of rocks. By using data analytics, it is possible to generate synthetic data that reflects the thermal properties of rocks. This data can then be used to upscale the synthetic properties to generate 3D models. This would be useful for developing models to predict the thermal properties of these rocks.
- The buoyancy effect can have a significant impact on thermal efficiency, as it can cause hot fluids to rise to the surface and cold fluids to sink to the bottom. A higher resolution numerical study will be performed to analyze the influence of the buoyancy effect on thermal efficiency at the micro-scale. This study will provide a better understanding of how the buoyancy effect affects thermal efficiency and will be useful for developing models to predict the thermal efficiency of SRTES reservoirs more accurately.

Nomenclature and Acronyms

Symbols

λ	Thermal conductivity
κ	Thermal diffusivity
c	Specific heat capacity
ρ	Density

Nomenclatures:

^{o}C	Celsius Degrees
CO_2	Carbon Dioxide
BPD	Barrels per Day
J	Joule
kWh	Kilowatts-hour
K	Permeability
l/s	Production in liters per second
$m/m^2/m^3$	Meters/ square meters/ cubic meters
mD	Millidarcies
MWh	Megawatts-hour
TJ	Tera Joules
TVD	True Vertical Depth

Abbreviations:

ATES	Aquifer Thermal Energy Storage

BTES	Borehole Thermal Energy Storage
DOE	Department of Energy
EGS	Enhanced Geothermal System
EIA	Energy Information Administration
FTIR	Fourier Transform Infrared Spectroscopy
GB	Geothermal Battery
GeoTES	Geological Thermal Energy Storage
HT	High Temperature
HTHP	High Temperature High Pressure
LCA	Life Cycle Assessment
LCOE	Levelized Cost of Energy
LFA	Laser Flash Apparatus
MTES	Mine Thermal Energy Storage
O&G	Oil and Gas
ORC	Organic Rankine Cycle
PTES	Pit Thermal Energy Storage
SI	International System of Metric Units
SRTES	Sedimentary Reservoir Thermal Energy Storage
TES	Thermal Energy Storage
UTES	Underground Thermal Energy Storage

References

Abbas, Z., Chen, D., Li, Y., Yong, L., Wang, R.Z., 2020. Experimental investigation of underground seasonal cold energy storage using borehole heat exchangers based on laboratory scale sandbox. Geothermics 87, 101837. https://doi.org/10.1016/J.GEOTHERMICS.2020.101837

Ahmed, S., Patel, H., Salehi, S., Ahmed, R., Teodoriu, C., 2020. Numerical and Experimental Evaluation of Liner Dual Barrier System in Geothermal Wells, in: 45th Workshop on Geothermal Reservoir Engineering . Stanford University, Stanford, California, USA.

Allen, R., 1979. Thermal energy storage in aquifiers: Preliminary information. Richland, WA, USA.

AlRatrout, A., Blunt, M.J., Bijeljic, B., 2018. Wettability in complex porous materials, the mixed-wet state, and its relationship to surface roughness. Proc Natl Acad Sci U S A 115, 8901–8906. https://doi.org/10.1073/PNAS.1803734115

Alva, G., Lin, Y., Fang, G., 2018. An overview of thermal energy storage systems. Energy 144, 341–378. https://doi.org/10.1016/J.ENERGY.2017.12.037

Anand, J., Somerton, W.H., Gomaa, E., 1973. Predicting Thermal Conductivities of Formations From Other Known Properties. Society of Petroleum Engineers Journal 13, 267–273. https://doi.org/10.2118/4171-PA

Anderson, T.C., 2013. Geothermal Potential of Deep Sedimentary Basins in the United States, in: URTeC (Ed.), Unconventional Resources Technology Conference (URTeC). SPE-URTeC, Denver, CO, USA.

Andersson, O., 2007. ATES FOR DISTRICT COOLING IN STOCKHOLM. Thermal Energy Storage for Sustainable Energy Consumption 239–243. https://doi.org/10.1007/978-1-4020-5290-3_15

Andersson, O., 1990. Hydrochemistry and energy storage in aquifers - Scaling And Corrosion in Subsurface Thermal Energy Storage Systems. TNO Committee on Hydrological Research, The Hague, Netherlands.

Angelini, G., Lucchini, A., Manzolini, G., 2014. Comparison of Thermocline Molten Salt Storage Performances to Commercial Two-tank Configuration. Energy Procedia 49, 694–704. https://doi.org/10.1016/J.EGYPRO.2014.03.075

Ataer, Ö.E., 2009. Storage of Thermal Energy | ENERGY STORAGE SYSTEMS – Vol. I –. Gazi University, Mechanical Engineering Department, Maltepe, 06570 Ankara, Turkey.

Bai, B., Elgmati, M., Zhang, H., Wei, M., 2013. Rock characterization of Fayetteville shale gas plays. Fuel 105, 645–652. https://doi.org/10.1016/J.FUEL.2012.09.043

Baiyegunhi, C., Liu, K., Gwavava, O., 2017. Diagenesis and Reservoir Properties of the Permian Ecca Group Sandstones and Mudrocks in the Eastern Cape Province, South Africa. Minerals 88. https://doi.org/10.3390/min7060088

Bakema, G., 2001. Well and Borehole Failures and Solutions in Underground Thermal Energy Storage.

Bakema, G., Drijver, B., 2019. State of the art HT-ATES in the Netherlands Evaluation of thermal performance and design considerations for future projects.

Bakr, M., van Oostrom, N., Sommer, W., 2013. Efficiency of and interference among multiple Aquifer Thermal Energy Storage systems; A Dutch case study. Renew Energy 60, 53–62. https://doi.org/10.1016/J.RENENE.2013.04.004

Banks, J., Poulette, S., Grimmer, J., Bauer, F., Schill, E., 2021. Geochemical Changes Associated with High-Temperature Heat Storage at Intermediate Depth: Thermodynamic Equilibrium Models for the DeepStor Site in the Upper Rhine Graben, Germany. Energies 2021, Vol. 14, Page 6089 14, 6089. https://doi.org/10.3390/EN14196089

Bartels, N., Bussmann, G., Ignacy, R., 2019. Geothermal energy in the context of the energy transition process, in: CANDO-EPE 2018 - Proceedings IEEE International Conference and Workshop in Obuda on Electrical and Power Engineering. Institute of Electrical and Electronics Engineers Inc., pp. 103–108. https://doi.org/10.1109/CANDO-EPE.2018.8601144

Bauer, D., Marx, R., Nußbicker-Lux, J., Ochs, F., Heidemann, W., Müller-Steinhagen, H., 2010. German central solar heating plants with seasonal heat storage. Solar Energy 84, 612–623. https://doi.org/10.1016/J.SOLENER.2009.05.013

Beckers, K.F., McCabe, K., 2019. GEOPHIRES v2.0: updated geothermal techno-economic simulation tool. Geothermal Energy 7, 1–28. https://doi.org/10.1186/S40517-019-0119-6/TABLES/4

Bernal, S.A., Rodríguez, E.D., Mejía de Gutiérrez, R., Provis, J.L., 2015. Performance at high temperature of alkali-activated slag pastes produced with silica fume and rice husk ash based activators. Materialesde Construccion 65. https://doi.org/10.3989/mc.2015.03114

Bershaw, J., Burns, E.R., Cladouhos, T.T., Horst, A.E., Van Houten, B., Hulseman, P., Kane, A., Liu, J.H., Perkins, R.B., Scanlon, D.P., Streig, A.R., Svadlenak, E.E., Uddenberg, M.W., Wells,

R.E., Williams, C.F., 2020. An Integrated Feasibility Study of Reservoir Thermal Energy Storage in Portland, Oregon, USA, in: Stanford University (Ed.), PROCEEDINGS 45th Workshop on Geothermal Reservoir Engineering. Stanford University, Stanford, CA, USA.

Blackwell, D.D., Steele, J.L., 1989. Thermal Conductivity of Sedimentary Rocks: Measurement and Significance, in: In: Naeser N.D., M.T.H. (eds). (Ed.), Thermal History of Sedimentary Basins. Springer, New York, NY, pp. 13–36. https://doi.org/10.1007/978-1-4612-3492-0_2

Bonte, M., Stuyfzand, P.J., Hulsmann, A., Van Beelen, P., 2011. Underground Thermal Energy Storage: Environmental Risks and Policy Developments in the Netherlands and European Union. Ecology and Society 16.

Bonte, M., Van Breukelen, B., Stuyfzand, P., 2013. Environmental impacts of aquifer thermal energy storage investigated by field and laboratory experiments. Journal of water and climate change 4.

Borysenko, A., Clennell, B., Sedev, R., Burgar, I., Ralston, J., Raven, M., Dewhurst, D., Liu, K., 2009. Experimental investigations of the wettability of clays and shales. J Geophys Res Solid Earth 114, 7202. https://doi.org/10.1029/2008JB005928

Bouguila, A., Said, R., 2020. Performance investigation of a 100-kWhth thermocline packed bed thermal energy storage system: Comparison between synthetic oil and vegetable oil. Advances in Mechanical Engineering 12, 1–10. https://doi.org/10.1177/1687814020905746/ASSET/IMAGES/LARGE/10.1177_1687814020905746-FIG2.JPEG

Bowman, E.T., Soga, K., Drummond, W., 2001. Particle shape characterisation using Fourier descriptor analysis. Geotechnique 51, 545–554.

Bridger, D.W., Allen, D.M., 2014. Influence of geologic layering on heat transport and storage in an aquifer thermal energy storage system. Hydrogeol J 22, 233–250. https://doi.org/10.1007/s10040-013-1049-1

Brown, D.W., 2000. A Hot Dry Rock Geothermal Energy Concept Utilizing Supercritical CO2 Instead of Water, in: PROCEEDINGS, Twenty-Fifth Workshop on Geothermal Reservoir Engineering. Stanford, CA, USA.

Brown, K., 2013. Mineral Scaling in Geothermal Power Production. Reykjavik, Iceland.

Bücken, D., Meier, T., Backers, T., 2022. Geomechanical effects of seasonal heat storage in abandoned mines. Geomechanics and Tunnelling 15, 82–90. https://doi.org/10.1002/GEOT.202100085

Buscheck, T.A., Bielicki, J.M., Edmunds, T.A., Hao, Y., Sun, Y., Randolph, J.B., Saar, M.O., 2016. Multifluid geo-energy systems: Using geologic CO2 storage for geothermal energy production and grid-scale energy storage in sedimentary basins. Geosphere 12, 678–696. https://doi.org/10.1130/GES01207.1

Buscheck, T.A., Bielicki, J.M., Randolph, J.B., 2017. CO2 Earth Storage: Enhanced Geothermal Energy and Water Recovery and Energy Storage, in: Energy Procedia. Elsevier Ltd, pp. 6870–6879. https://doi.org/10.1016/j.egypro.2017.03.1615

Cárdenas, B., León, N., 2013. High temperature latent heat thermal energy storage: Phase change materials, design considerations and performance enhancement techniques. Renewable and Sustainable Energy Reviews 27, 724–737. https://doi.org/10.1016/J.RSER.2013.07.028

Cengel, Y., 1997. Heat And Mass Transfer By Cengel 2nd Edition, 2nd Edition. ed. McGraw-Hill.

Chang, C., Nie, B., Leng, G., Li, C., She, X., Peng, X., Deng, J., 2017. Influences of the key characteristic parameters on the thermal performance of a water pit seasonal thermal storage. Energy Procedia 142, 495–500. https://doi.org/10.1016/J.EGYPRO.2017.12.077

Chekhonin, E., Parshin, A., Pissarenko, D., Popov, Y., Romushkevich, R., Safonov, S., Chertenkov, M. V, Stenin, V.P., 2012. When rocks get hot: thermal properties of reservoir rocks. Oilfield Review 24, 20–37.

Chen, Y., Ma, G., Wang, H., Li, T., Wang, Y., 2019. Application of carbon dioxide as working fluid in geothermal development considering a complex fractured system. Energy Convers Manag 180, 1055–1067. https://doi.org/10.1016/j.enconman.2018.11.046

Clauser, C., 2011. Thermal storage and transport properties of rocks, ii: Thermal conductivity and diffusivity. Encyclopedia of Earth Sciences Series Part 5, 1431–1448. https://doi.org/10.1007/978-90-481-8702-7_67/TABLES/7

Collignon, M., Klemetsdal, Ø.S., Møyner, O., Alcanié, M., Rinaldi, A.P., Nilsen, H., Lupi, M., 2020. Evaluating thermal losses and storage capacity in high-temperature aquifer thermal energy storage (HT-ATES) systems with well operating limits: insights from a study-case in the Greater Geneva Basin, Switzerland. Geothermics 85, 101773. https://doi.org/10.1016/J.GEOTHERMICS.2019.101773

Collins, E., 1977. Underground Storage of Solar Energy, in: Proceedings Of Second Annual Thermal Energy Storage Contractors' Information Exchange Meeting. pp. 253–258.

Cruickshank, A.C., Baldwin, C., 2016. Sensible Thermal Energy Storage: Diurnal and Seasonal. Storing Energy: With Special Reference to Renewable Energy Sources 291–311. https://doi.org/10.1016/B978-0-12-803440-8.00015-4

Dahash, A., Ochs, F., Tosatto, A., Streicher, W., 2020. Toward efficient numerical modeling and analysis of large-scale thermal energy storage for renewable district heating. Appl Energy 279, 115840. https://doi.org/10.1016/J.APENERGY.2020.115840

Diaz-Munoz, J., Farouq Ali, S.M., 1974. Simulation of cyclic hot water stimulation of heavy oil wells. AIChE Symp. Ser.; (United States) 45A.

DOE, 2023. Technology Strategy Assessment - Thermal Energy Storage.

DOE, 2021. Opportunities, Value Drivers, and Barriers for Thermal Energy Storage [Presentation].

Doughty, C., Hellström, G., Tsang, C.F., Claesson, J., 1982. A dimensionless parameter approach to the thermal behavior of an aquifer thermal energy storage system. Water Resour Res 18, 571–587. https://doi.org/10.1029/WR018I003P00571

Dow, 2022. DOWTHERM^{TM} A Heat Transfer Fluid | Technical Data Sheet.

Drijver, B., Bakema, G., Oerlemans, P., 2019. State of the art of HT-ATES in The Netherlands 11–14.

Drijver, B., van Aarssen, M., de Zwart, B., 2012. High-temperature aquifer thermal energy storage (HT-ATES): sustainable and multi-usable, in: The 12th International Conference on Energy Storage. International Energy Agency's (IEA) Energy Conservation through Energy Storage (ECES) Implementing Agreement-Innostock, Lleida, Catalonia, Spain.

Dropkin, D., Somerscales, E., 1965. Heat Transfer by Natural Convection in Liquids Confined by Two Parallel Plates Which Are Inclined at Various Angles With Respect to the Horizontal. J Heat Transfer 87, 77–82. https://doi.org/10.1115/1.3689057

Dusseault, M.B., Bruno, M.S., Barrera, J., 2001. Casing Shear: Causes, Cases, Cures. SPE Drilling & Completion 16, 98–107. https://doi.org/10.2118/72060-PA

EASE-EERA, 2017. European Energy Storage Technology Development Roadmap Towards 2030.

Eastman, 2022a. Therminol VP-1 heat transfer fluid. Kingsport, TN.

Eastman, 2022b. Therminol 55 Heat Transfer Fluid | Enhanced Reader.

Eastman, 2022c. Therminol 66 heat transfer fluid | Technical Bulletin.

Eastman, 2020. Therminol® VP1 Heat Transfer Fluid -SAFETY DATA SHEET.

El Alami, K., Asbik, M., Agalit, H., 2020. Identification of natural rocks as storage materials in thermal energy storage (TES) system of concentrated solar power (CSP) plants – A review. Solar Energy Materials and Solar Cells 217, 110599. https://doi.org/10.1016/J.SOLMAT.2020.110599

Energy Institute, 2023. Statistical Review of World Energy 2023.

Esence, T., Bruch, A., Molina, S., Stutz, B., Fourmigué, J.F., 2017. A review on experience feedback and numerical modeling of packed-bed thermal energy storage systems. Solar Energy 153, 628–654. https://doi.org/10.1016/J.SOLENER.2017.03.032

Evans, A., Strezov, V., Evans, T.J., 2012. Assessment of utility energy storage options for increased renewable energy penetration. Renewable and Sustainable Energy Reviews 16, 4141–4147. https://doi.org/10.1016/J.RSER.2012.03.048

Fallahi, A., Guldentops, G., Tao, M., Granados-Focil, S., Van Dessel, S., 2017. Review on solid-solid phase change materials for thermal energy storage: Molecular structure and thermal

properties. Appl Therm Eng 127, 1427–1441. https://doi.org/10.1016/J.APPLTHERMALENG.2017.08.161

Fathi, S.J., Austad, T., Strand, S., 2010. “Smart Water” as a Wettability Modifier in Chalk: The Effect of Salinity and Ionic Composition. Energy Fuels 24, 2514–2519. https://doi.org/10.1021/ef901304m

Fleuchaus, P., Godschalk, B., Stober, I., Blum, P., 2018. Worldwide application of aquifer thermal energy storage – A review. Renewable and Sustainable Energy Reviews 94, 861–876. https://doi.org/10.1016/J.RSER.2018.06.057

Fleuchaus, P., Schüppler, S., Bloemendal, M., Guglielmetti, L., Opel, O., Blum, P., 2020. Risk analysis of High-Temperature Aquifer Thermal Energy Storage (HT-ATES). Renewable and Sustainable Energy Reviews 133, 110153. https://doi.org/10.1016/J.RSER.2020.110153

Fuchs, S., 2018. The variability of rock thermal properties in sedimentary basins and the impact on temperature modelling-A Danish example. Geothermics 76. https://doi.org/10.1016/j.geothermics.2018.06.006

Fuchs, S., Förster, H.J., Norden, B., Balling, N., Miele, R., Heckenbach, E., Förster, A., 2021. The Thermal Diffusivity of Sedimentary Rocks: Empirical Validation of a Physically Based $\alpha - \varphi$ Relation. J Geophys Res Solid Earth 126, e2020JB020595. https://doi.org/10.1029/2020JB020595

Fuchs, S., Schütz, F., Förster, H.J., Förster, A., 2013. Evaluation of common mixing models for calculating bulk thermal conductivity of sedimentary rocks: Correction charts and new conversion equations. Geothermics 47, 40–52. https://doi.org/10.1016/J.GEOTHERMICS.2013.02.002

Gao, J., Lu, C., Zhang, Y., 2023. Study on mechanism of effect of flowing water and transferring heat on rock mass temperature in curved fracture. Sci Rep 13. https://doi.org/10.1038/S41598-023-29992-0

Garcia, G., 2017. Organic Rankine Cycle - Presentation, in: Congreso de INGENIERÍA MECÁNICA, Sistemas Ciberfísicos En Ingeniería. EAFIT, Medellin, Colombia.

García-Gil, A., Epting, J., Ayora, C., Garrido, E., Vázquez-Suñé, E., Huggenberger, P., Gimenez, A.C., 2016. A reactive transport model for the quantification of risks induced by groundwater heat pump systems in urban aquifers. J Hydrol (Amst) 542, 719–730. https://doi.org/10.1016/J.JHYDROL.2016.09.042

Gehlin, S., 2016. Borehole thermal energy storage. Advances in Ground-Source Heat Pump Systems 295–327. https://doi.org/10.1016/B978-0-08-100311-4.00011-X

Gehlin, S., Nordell, B., 2006. Promoting Tes Systems In Sweden, The Swedish Society of HVAC Engineers (SWEDVAC). Stockholm, Sweden.

Ghaebi, H., Bahadori, M.N., Saidi, M.H., 2017. Economic and Environmental Evaluations of Different Operation Alternatives of an Aquifer Thermal Energy Storage in Tehran, Iran. Scientia Iranica 24, 610–623. https://doi.org/10.24200/SCI.2017.4046

Gil, A., Medrano, M., Martorell, I., Lázaro, A., Dolado, P., Zalba, B., Cabeza, L.F., 2010. State of the art on high temperature thermal energy storage for power generation. Part 1—Concepts, materials and modellization. Renewable and Sustainable Energy Reviews 14, 31–55. https://doi.org/10.1016/J.RSER.2009.07.035

Gluyas, J.G., Adams, C.A., Wilson, I.A.G., 2020. The theoretical potential for large-scale underground thermal energy storage (UTES) within the UK. Energy Reports 6, 229–237. https://doi.org/10.1016/J.EGYR.2020.12.006

Green, S., McLennan, J., Panja, P., Kitz, K., Allis, R., Moore, J., 2021. Geothermal battery energy storage. Renew Energy 164, 777–790. https://doi.org/10.1016/J.RENENE.2020.09.083

Guglielmetti, L., Alt-Epping, P., Birdsell, D., De Oliveira Filho, F., Diamond, L., Driesner, T., Eruteya, O., Hollmuller, P., Koumrouyan, M., Makhloufi, Y., Marti, U., Martin, F., Meier, P., Meyer, M., Mindel, J., Moscariello, A., Nawratil de Bono, C., Quiquerez, L., Saar, M., Sohrabi, R., Valley, B., Van den Heuvel, D., Wanner, C., 2020. HEATSTORE SWITZERLAND: New Opportunities of Geothermal District Heating Network Sustainable Growth by High Temperature Aquifer Thermal Energy Storage Development, in: Proceedings World Geothermal Congress 2020. Reykjavik, Iceland.

Hahn, F., Bussmann, G., Jagert, F., Ignacy, R., Bracke, R., Seidel, T., 2018. Reutilization of mine water as a heat storage medium in abandoned mines, in: Wolkersdorfer, Ch., Sartz, L., Weber, A., Burgess, J., Tremblay, G. (Eds.), 11th ICARD | IMWA | MWD Conference. pp. 1057–1062.

Hahn, F., Jagert, F., Bussmann, G., Nardini, I., Bracke, R., Seidel, T., König, T., 2019. The reuse of the former Markgraf II colliery as a mine thermal energy storage, in: European Geothermal Congress 2019 . European Geothermal Congress 2019 Den Haag, Den Haag, The Netherlands, pp. 1–4.

Hahne, E., Hornberger, M., 1994. Experience With a Solar Heating ATES System for a University Building. J Sol Energy Eng 116, 88–93. https://doi.org/10.1115/1.2930503

Hamm, V., Charles Maragna, B., Camille Maurel, B., Stefan Klein, B., Hahn, F., IEG Thomas Vangkilde-Pedersen, F., Geoffroy Gauthier, G., Rey, C., Martin Bloemendal, S., Stijn Beernink, K., Koen Allaerts, K., Sigrún Tómasdóttir, V., Energy Gunnar Gunnarsson, R., Energy Andre El-Alfy, R., Energie Luca Guglielmetti, G., Meyer, M., Loic Quiquerez, S., Voirand, A., 2021. Synthesis of demonstrators and case studies - Best practice guidelines for UTES development | Geothermica ERA NET - HeatStore.

Hasan, A.R., Kabir, C.S., 2002. Fluid flow and heat transfer in wellbores. Society of Petroleum Engineers.

Heap, M.J., Kushnir, A.R.L., Vasseur, J., Wadsworth, F.B., Harlé, P., Baud, P., Kennedy, B.M., Troll, V.R., Deegan, F.M., 2020. The thermal properties of porous andesite. Journal of Volcanology and Geothermal Research 398, 106901. https://doi.org/10.1016/J.JVOLGEORES.2020.106901

Heller, L., 2013. Literature Review on Heat Transfer Fluids and Thermal Energy Storage Systems in CSP Plants STERG Report.

Herrmann, U., Kearney, D.W., 2002. Survey of Thermal Energy Storage for Parabolic Trough Power Plants. J Sol Energy Eng 124, 145–152. https://doi.org/10.1115/1.1467601

Hoffmann, J., 2015. Stockage thermique pour centrale solaire thermodynamique à concentration mettant en oeuvre des matériaux céramiques naturels ou recyclés. Université de Perpignan.

Homuth, S., Rühaak, W., Sass, I., Bär, K., 2013. Medium Deep High Temperature Heat Storage. European Geothermal Congress 3–7.

Hou, J., Han, M., Wang, J., 2021. Manipulation of surface charges of oil droplets and carbonate rocks to improve oil recovery. Scientific Reports 2021 11:1 11, 1–11. https://doi.org/10.1038/s41598-021-93920-3

Idaho National Laboratory, 2006. The Future of Geothermal Energy. Idaho Falls, ID, USA.

ISO, 2006a. 14040. Environmental management—life cycle assessment—principles and framework, International Organization for Standardization.

ISO, 2006b. 14044: 2006-10 Environmental management–Life cycle assessment–Requirements and guidelines, International Organization for Standardization.

Jahanbakhsh, A., Shahrokhi, O., Maroto-Valer, M.M., 2021. Understanding the role of wettability distribution on pore-filling and displacement patterns in a homogeneous structure via quasi 3D pore-scale modelling. Scientific Reports 2021 11:1 11, 1–12. https://doi.org/10.1038/s41598-021-97169-8

Jenne, E.A., 1990. Hydrochemistry and energy storage in aquifers - Aquifer Thermal Energy Storage: The importance of Chemical Reactions. The Hague, Netherlands.

Jenne, E.A., Andersson, O., Willemsen, A., 1992. Well, hydrology, and geochemistry problems encountered in ATES systems and their solutions, in: 27. Intersociety Energy Conversion Engineering Conference. Washington, DC (United States). https://doi.org/10.2172/10135328

Jin, W., Atkinson, T., Neupane, G., McLing, T., Doughty, C., Spycher, N., Dobson, P., Smith, R., 2022. Influence of Mechanical Deformation and Mineral Dissolution/precipitation on Reservoir Thermal Energy Storage. All Days. https://doi.org/10.56952/ARMA-2022-2068

Jouhara, H., Żabnieńska-Góra, A., Khordehgah, N., Ahmad, D., Lipinski, T., 2020. Latent thermal energy storage technologies and applications: A review. International Journal of Thermofluids 5–6, 100039. https://doi.org/10.1016/J.IJFT.2020.100039

Kadoya, K., Matsunaga, N., Nagashima, A., 1985. Viscosity and Thermal Conductivity of Dry Air in the Gaseous Phase. J Phys Chem Ref Data 14, 947–970. https://doi.org/10.1063/1.555744

Kallesøe, A.J., Vangkilde-Pedersen, T., Guglielmetti, L., 2019. HEATSTORE Underground Thermal Energy Storage (UTES) – state-of-the-art, example cases and lessons learned. Geneve, Switzerland.

Kallesøe, A.J., Vangkilde-Pedersen, T., Nielsen, J.E., Bakema, G., Egermann, P., Maragna, C., Hahn, F., Guglielmetti, L., Koornneef, J., 2021. HEATSTORE-Underground Thermal Energy Storage (UTES)-State of the Art, Example Cases and Lessons Learned, in: Proceedings World Geothermal Congress 2020+1 . Reykjavik, Iceland.

Karasu, H., Dincer, I., 2020. Life cycle assessment of integrated thermal energy storage systems in buildings: A case study in Canada. Energy Build 217, 109940. https://doi.org/10.1016/J.ENBUILD.2020.109940

Karlsruhe Institute of Technology, 2020. DeepStor-High-temperature deep-underground thermal storage Background. Karlsruhe, Germany.

Kearney, D., Herrmann, U., Nava, P., Kelly, B., Mahoney, R., Pacheco, J., Cable, R., Potrovitza, N., Blake, D., Price, H., 2003. Assessment of a Molten Salt Heat Transfer Fluid in a Parabolic Trough Solar Field. J Sol Energy Eng 125, 170–176. https://doi.org/10.1115/1.1565087

Kelly, S., El-Sobky, H., Torres-Verdín, C., Balhoff, M.T., 2016. Assessing the utility of FIB-SEM images for shale digital rock physics. Adv Water Resour 95, 302–316. https://doi.org/10.1016/J.ADVWATRES.2015.06.010

Khalifeh, M., 2021. Well Integrity and Well Abandonment for Green Transition – Geothermal Energy.

Khare, S., Dell'Amico, M., Knight, C., McGarry, S., 2013. Selection of materials for high temperature sensible energy storage. Solar Energy Materials and Solar Cells 115, 114–122. https://doi.org/10.1016/J.SOLMAT.2013.03.009

Kirch, W., 2008. Pearson's Correlation Coefficient. Encyclopedia of Public Health 1090–1091. https://doi.org/10.1007/978-1-4020-5614-7_2569

Klapper, H.S., Stevens, J., 2013. Challenges for Metallic Materials Facing HTHP Geothermal Drilling, in: CORROSION 2013. OnePetro, Orlando, Florida.

Knobloch, K., Ulrich, T., Bahl, C., Engelbrecht, K., 2022. Degradation of a rock bed thermal energy storage system. Appl Therm Eng 214. https://doi.org/10.1016/J.APPLTHERMALENG.2022.118823

Korte, D., Kaukler, D., Fanetti, M., Cabrera, H., Daubront, E., Franko, M., 2017. Determination of petrophysical properties of sedimentary rocks by optical methods. Sediment Geol 350, 72–79. https://doi.org/10.1016/J.SEDGEO.2017.01.007

Kuravi, S., Trahan, J., Goswami, D.Y., Rahman, M.M., Stefanakos, E.K., 2013. Thermal energy storage technologies and systems for concentrating solar power plants. Prog Energy Combust Sci 39, 285–319. https://doi.org/10.1016/J.PECS.2013.02.001

Labus, M., Labus, K., 2018a. Thermal conductivity and diffusivity of fine-grained sedimentary rocks. J Therm Anal Calorim 132, 1669–1676. https://doi.org/10.1007/S10973-018-7090-5/FIGURES/3

Labus, M., Labus, K., 2018b. Thermal conductivity and diffusivity of fine-grained sedimentary rocks. J Therm Anal Calorim 132, 1669–1676. https://doi.org/10.1007/S10973-018-7090-5/FIGURES/3

Lee, K.S., 2013. Chapter 2: Underground Thermal Energy Storage. Green Energy and Technology 75, 15–26. https://doi.org/10.1007/978-1-4471-4273-7_2/FIGURES/4

Leonhardt, J., 1983. Die Gebirgstemperaturen im Ruhrrevier. Das Markscheidewesen 90, 218–230.

Llanos, Ella Maria, Zarrouk, S.J., Llanos, Ella M, Hogarth, R.A., 2015. Simulation of the Habanero Enhanced Geothermal System (EGS), Australia. Proceedings World Geothermal Congress 19–25.

Mahon, H., O'Connor, D., Friedrich, D., Hughes, B., 2022. A review of thermal energy storage technologies for seasonal loops. Energy 239, 122207. https://doi.org/10.1016/J.ENERGY.2021.122207

Malmberg, M., 2017. Transient modeling of a high temperature borehole thermal energy storage coupled with a combined heat and power plant. KTH Industrial Engineering and Management.

Marx, J.W., Langenheim, R.H., 1959. Reservoir Heating by Hot Fluid Injection. Transactions of the AIME 216, 312–315. https://doi.org/10.2118/1266-G

Matos, C.R., Carneiro, J.F., Silva, P.P., 2019. Overview of Large-Scale Underground Energy Storage Technologies for Integration of Renewable Energies and Criteria for Reservoir Identification. J Energy Storage 21, 241–258. https://doi.org/10.1016/J.EST.2018.11.023

McLing, T.L., Jin, W., Neupane, G., Atkinson, T., Dobson, P., Doughty, C., Spycher, N., Smith, R.W., 2022. Dynamic Earth Energy Storage: Terawatt-year, Grid-scale Energy Storage Using Planet Earth as a Thermal Battery (GeoTES): Phase I Project Final Report. Idaho Falls, Idaho, USA.

Medrano, M., Gil, A., Martorell, I., Potau, X., Cabeza, L.F., 2010. State of the art on high-temperature thermal energy storage for power generation. Part 2—Case studies. Renewable and Sustainable Energy Reviews 14, 56–72. https://doi.org/10.1016/J.RSER.2009.07.036

Mehling, H., Cabeza, L.F., 2008. Heat and cold storage with PCM. Heat and Mass Transfer. https://doi.org/10.1007/978-3-540-68557-9

Mercer, J.W., Faust, C.R., Miller, W.J., Pearson, F.J.Jr., 1981. Review of simulation techniques for aquifer thermal energy storage (ATES). Richland, WA (United States). https://doi.org/10.2172/6069851

Mesquita, L., Mcclenahan, D., Thornton, J., Carriere, J., Wong, B., 2017. Drake Landing Solar Community: 10 Years of Operation, in: ISES Solar World Congress 2017. https://doi.org/10.18086/swc.2017.06.09

MidttØmme, K., Roaldset, E., 1999. Thermal conductivity of sedimentary rocks: uncertainties in measurement and modelling. Geol Soc Spec Publ 158, 45–60. https://doi.org/10.1144/GSL.SP.1999.158.01.04

Miller, F.G., Seban, R.A., 1955. The Conduction of Heat Incident to the Flow of Vaporizing Fluids in Porous Media. Transactions of the AIME 204, 282–284. https://doi.org/10.2118/344-G

Mindel, J., Driesner, T., 2020. HEATSTORE: Preliminary Design of a High Temperature Aquifer Thermal Energy Storage (HT-ATES) System in Geneva Based on TH Simulations Conference Paper HEATSTORE: Preliminary Design of a High Temperature Aquifer Thermal Energy Storage (HT-ATES) System in Geneva Based on TH Simulations, in: Proceedings World Geothermal Congress 2020. ETZ Zürich, Reykjavik, Iceland. https://doi.org/10.3929/ethz-b-000444531

Moeck, I., Bracke, R., Weber, J., 2021. The Energy Transition from Fossil Fuels to Geothermal Energy-a German Case Study, in: Proceedings World Geothermal Congress 2020+1.

Molz, F.J., Parr, A.D., Andersen, P.F., 1980. Experimental study of the storage of thermal energy in confined aquifers. Final report, July 1, 1977-December 31, 1979. https://doi.org/10.2172/5505872

Molz, F.J., Parr, A.D., Andersen, P.F., Lucido, V.D., Warman, J.C., 1979. Thermal energy storage in a confined aquifer: Experimental results. Water Resour Res 15, 1509–1514. https://doi.org/10.1029/WR015I006P01509

Molz, F.J., Warman, J.C., Jones, T.E., 1976. Transport of Water and Heat in an Aquifer Used for Hot Water Storage - Experimental Study. TRANSACTIONS-AMERICAN GEOPHYSICAL UNION 57, 918–918.

Moradi, A., Smits, K.M., Massey, J., Cihan, A., McCartney, J., 2015. Impact of coupled heat transfer and water flow on soil borehole thermal energy storage (SBTES) systems: Experimental and

modeling investigation. Geothermics 57, 56–72. https://doi.org/10.1016/J.GEOTHERMICS.2015.05.007

Nagano, K., Mochida, T., Ochifuji, K., 2002. Influence of natural convection on forced horizontal flow in saturated porous media for aquifer thermal energy storage. Appl Therm Eng 22, 1299–1311. https://doi.org/10.1016/S1359-4311(02)00056-X

Neupane, G., Mcling, T.L., Atkinson, T., Mclaughlin, J.F., Smith, R.W., Atkinson, T.A., Spycher, N., Dobson, P.F., 2021. Experimental Assessment of Geochemistry of Geologic Thermal Energy Storage (GeoTES) Systems Evaluation of Mineral Scaling during High-Temperature Thermal Energy Storage in Deep Saline Aquifers View project Experimental Assessment of Geochemistry of Geologic Thermal Energy Storage (GeoTES) Systems. GRC Transactions 45, 1149–1166.

Neupane, G., Smith, R.W., Mcling, T.L., Mclaughlin, J.F., Spycher, N., Dobson, P.F., 2020. Geochemistry of Geologic Thermal Energy Storage (GeoTES) systems: assessment of the Weber Sandstone, western Wyoming, USA. GRC Transactions 44, 1110–1122.

Nield, D.A., Bejan, A., 2017. Convection in porous media. Convection in Porous Media 629–982. https://doi.org/10.1007/978-3-319-49562-0/COVER

Nole, M., Daigle, H., Milliken, K.L., Prodanović, M., 2016. A method for estimating microporosity of fine-grained sediments and sedimentary rocks via scanning electron microscope image analysis. Sedimentology 63, 1507–1521. https://doi.org/10.1111/SED.12271

Nordell, B., 1994. Borehole heat store design optimization. Luleå University of Technology, Luleå, Sweden .

Novo, A. V., Bayon, J.R., Castro-Fresno, D., Rodriguez-Hernandez, J., 2010. Review of seasonal heat storage in large basins: Water tanks and gravel–water pits. Appl Energy 87, 390–397. https://doi.org/10.1016/J.APENERGY.2009.06.033

Ortega, I., Gutiérrez, M., 2020. Thermal storage: the way to optimize energy management | CIC energiGUNE [WWW Document]. CIC energiGUNE. URL https://cicenergigune.com/en/blog/thermal-storage-optimize-energy-management (accessed 10.25.22).

Pacio, J., Wetzel, T., 2013. Assessment of liquid metal technology status and research paths for their use as efficient heat transfer fluids in solar central receiver systems. Solar Energy 93, 11–22. https://doi.org/10.1016/J.SOLENER.2013.03.025

Panja, P., McLennan, J., Green, S., 2021. Influence of permeability anisotropy and layering on geothermal battery energy storage. Geothermics 90, 101998. https://doi.org/10.1016/J.GEOTHERMICS.2020.101998

Panja, P., McLennan, J., Green, S., 2020. Temperature and Pressure Profiles for Geothermal Battery Energy Storage in Sedimentary Basins, in: 54th U.S. Rock Mechanics/Geomechanics Symposium. ARMA.

Passamonti, A., Hahn, F., Strozyk, F., Bussmann, G., Seidel, T., Bracke, R., 2020. Study on HTHP Coupled with HT-MTES, in: Der Digital Geothermiekongress. Fraunhofer IEG.

Pedersen, A.S., Elmegaard, B., Christensen, C.H., Kjøller, C., Elefsen, F., Hvid, J., Hansen, J.B., Sørensen, P.A., Kær, S.K., Vangkilde-Pedersen, T., Jensen, T.F., 2014. Status and recommendations for RD&D on energy storage technologies in a Danish context.

Pereira, V. de V., 2014. Calcium Carbonate Scaling Control in Geothermal Well Pv8 In Sao Miguel, Azores, Combining Chemical Inhibition And Mechanical Reaming. Orkustofnun 9, 33.

Petrunin, G.I., Popov, V.G., Il'in, I.A., 2004. Conductive heat transfer in plagioclases. Izvestiya, Physics of the Solid Earth 40, 752–759.

Pettijohn, F.J., Potter, P.E., Siever, R., 1987. Sand and Sandstone, 2nd ed, Sand and Sandstone. Springer New York, New York, NY. https://doi.org/10.1007/978-1-4612-1066-5

Podara, C. V., Kartsonakis, I.A., Charitidis, C.A., 2021. Towards Phase Change Materials for Thermal Energy Storage: Classification, Improvements and Applications in the Building Sector. Applied Sciences 2021, Vol. 11, Page 1490 11, 1490. https://doi.org/10.3390/APP11041490

Poulsen, S.E., Bjørn, H., Mathiesen, A., Nielsen, L.H., Vosgerau, H., Vangkilde-Pedersen, T., Ditlefsen, C., Røgen, B., 2019. Geothermal Energy Use, Country Update for Denmark, in: European Geothermal Congress 2019. European Geothermal Congress 2019 Den Haag, Den Haag, The Netherlands, pp. 11–14.

Pruess, K., 2006. Enhanced geothermal systems (EGS) using CO2 as working fluid-A novel approach for generating renewable energy with simultaneous sequestration of carbon. Geothermics 35, 351–367. https://doi.org/10.1016/j.geothermics.2006.08.002

Qi, C., Zhou, R., Zhan, H., 2023. Analysis of heat transfer in an aquifer thermal energy storage system: On the role of two-dimensional thermal conduction. Renew Energy 217, 119156. https://doi.org/10.1016/J.RENENE.2023.119156

Raade, J.W., Padowitz, D., 2011. Development of molten salt heat transfer fluid with low melting point and high thermal stability. Journal of Solar Energy Engineering, Transactions of the ASME 133. https://doi.org/10.1115/1.4004243/456229

Rabbimov, R.T., Umarov, G.Y., Zakhidov, R.A., 1971. Storage of solar energy in a sandy-gravel ground. Appl. Solar Energy (USSR) (Engl. Transl.).

Rad, F.M., Fung, A.S., 2016. Solar community heating and cooling system with borehole thermal energy storage – Review of systems. Renewable and Sustainable Energy Reviews 60, 1550–1561. https://doi.org/10.1016/J.RSER.2016.03.025

Rapp, B.E., 2016. Microfluidics: Modeling, mechanics and mathematics. Microfluidics: Modeling, Mechanics and Mathematics 1–766. https://doi.org/10.1016/C2012-0-02230-2

Reyes, A.G., Trompetter, W.J., Britten, K., Searle, J., 2003. Mineral deposits in the Rotokawa geothermal pipelines, New Zealand. Journal of Volcanology and Geothermal Research 119, 215–239. https://doi.org/10.1016/S0377-0273(02)00355-4

Robertson, E.C., 1988. Thermal Properties of Rocks. Reston, VA.

Rosenbrand, E., Haugwitz, C., Jacobsen, P.S.M., Kjøller, C., Fabricius, I.L., 2014. The effect of hot water injection on sandstone permeability. Geothermics 50, 155–166. https://doi.org/10.1016/J.GEOTHERMICS.2013.09.006

Rucker, M., Naderi, M., Yesufu-Rufai, S., Lowe, S., Marcelis, F., Ryan, M.P., Pini, R., Georgiadis, A., Williams, D., Luckham, P.F., Rucker, M., Naderi, M., Yesufu-Rufai, S., Lowe, S., Marcelis, F., Ryan, M.P., Pini, R., Georgiadis, A., Williams, D., Luckham, P.F., 2019. Impact of texture

and mineralogy on the wettability of rock surfaces. American Geophysical Union, Fall Meeting 2019. 2019, H41G-1752.

Saeed, M., Jadhawar, P., Ayirala, S.C., Abhishek, R., Zhou, Y., 2022. Modelling the effects of reservoir parameters and rock mineralogy on wettability during low salinity waterflooding in sandstone reservoirs. J Pet Sci Eng 215, 110676. https://doi.org/10.1016/j.petrol.2022.110676

Sahimi, M., 1993. Flow phenomena in rocks: from continuum models to fractals, percolation, cellular automata, and simulated annealing. Rev Mod Phys 65, 1393. https://doi.org/10.1103/RevModPhys.65.1393

Salehi, S., Nygaard, R., 2011. Evaluation of new drilling approach for widening operational window: Implications for wellbore strengthening. SPE Production and Operations Symposium, Proceedings 118–133. https://doi.org/10.2118/140753-MS

Salehi, S., Vivas, C., Nygaard, R., Rehg, D., 2022. Scalable Geothermal Energy Potential from Sedimentary Basins: Opportunities for Energy Transition and Skilled Workforce Development. Geothermal Resources Council Transactions 46, 964–975.

Sanner, B., Knoblich, K., 1999. Advantages and problems of high temperature underground thermal energy storage. Bulletin d'Hydroge'ologie 17.

Sanner, B., Knoblich, K., 1998. New IEA-Activity ECES ANNEX 12 High temperature underground thermal energy storage, in: In Proceedings of the Second Stockton International Geothermal Conference. New Jersey, NJ, USA.

Sanner, B., Nordell, B., 1998. Underground thermal energy storage with heat pumps : an international overview. Newsletter / IEA Heat Pump Center 16, 10–14.

Sanyal, S.K., Butler, S.J., 2005. An Analysis of Power Generation Prospects from Enhanced Geothermal Systems. Proceedings World Geothermal Congress 24–29.

Sarbu, I., Sebarchievici, C., 2018. A Comprehensive Review of Thermal Energy Storage. Sustainability 2018, Vol. 10, Page 191 10, 191. https://doi.org/10.3390/SU10010191

Sari, A., Al Maskari, N.S., Saeedi, A., Xie, Q., 2020. Impact of surface roughness on wettability of oil-brine-calcite system at sub-pore scale. J Mol Liq 299, 112107. https://doi.org/10.1016/J.MOLLIQ.2019.112107

Saugy, B., Miserez, J.J., Matthey, B., 1988. Stockage saisonnier de chaleur dans l'aquifère,stockage pilote d'energie par ouvrage souterrain (SPEOS), Résultats de 5 ans de fonctionnement., in: Proc. 4th Int. Conf. Energy Storage Jigastock 88. AFME, Paris, France.

Schneider, B., 2013. Storing Solar Energy in the Ground.

Schüppler, S., Fleuchaus, P., Blum, P., 2019. Techno-economic and environmental analysis of an Aquifer Thermal Energy Storage (ATES) in Germany. Geothermal Energy 7, 1–24. https://doi.org/10.1186/S40517-019-0127-6/FIGURES/10

Setiawan, F.A., Rahayuningsih, E., Petrus, H.T.B.M., Nurpratama, M.I., Perdana, I., 2019. Kinetics of silica precipitation in geothermal brine with seeds addition: minimizing silica scaling in a cold re-injection system. Geothermal Energy 7, 1–16. https://doi.org/10.1186/S40517-019-0138-3/FIGURES/8

Sharma, A., Burak, T., Nygaard, R., Hellvik, S., Hoel, E., Welmer, M., 2023. Projection of Logging While Drilling Data at the Bit by Implementing Supervised Machine Learning Algorithm.

Society of Petroleum Engineers - SPE Oklahoma City Oil and Gas Symposium 2023, OKOG 2023. https://doi.org/10.2118/213070-MS

Sheikholeslami, M., Ganji, D.D., 2017. Nanofluid Natural Convection Heat Transfer. Applications of Nanofluid for Heat Transfer Enhancement 53–125. https://doi.org/10.1016/B978-0-08-102172-9.00002-2

Sheldon, H.A., Wilkins, A., Green, C.P., 2021. Recovery efficiency in high-temperature aquifer thermal energy storage systems. Geothermics 96, 102173. https://doi.org/10.1016/J.GEOTHERMICS.2021.102173

Shi, X., Jiang, S., Xu, H., Jiang, F., He, Z., Wu, J., 2016. The effects of artificial recharge of groundwater on controlling land subsidence and its influence on groundwater quality and aquifer energy storage in Shanghai, China. Environ Earth Sci 75, 1–18. https://doi.org/10.1007/S12665-015-5019-X/TABLES/3

Sibbitt, B., McClenahan, D., 2014. Seasonal Borehole Thermal Energy Storage-Guidelines for design & construction.

Skarphagen, H., Banks, D., Frengstad, B.S., Gether, H., 2019. Design Considerations for Borehole Thermal Energy Storage (BTES): A Review with Emphasis on Convective Heat Transfer. Geofluids 2019. https://doi.org/10.1155/2019/4961781

Sletcha, B., Vivas, C., Saleh, F.K., Ghalambor, A., Salehi, S., 2020. Digital Oilfield: Review of Real-time Data-flow Architecture for Upstream Oil and Gas Rigs, in: SPE (Ed.), Proceedings - SPE International Symposium on Formation Damage Control. OnePetro, Lafayette, LA, USA. https://doi.org/10.2118/199298-MS

Snijders, A.L., 2000. Lessons from 100 ATES projects The developments of aquifer storage in the Netherlands, in: Proceedings TERRASTOCK 2000. Stuttgart, Germany.

Somerton, W.H., 1958. Some Thermal Characteristics of Porous Rocks. Transactions of the AIME 213, 375–378. https://doi.org/10.2118/965-G

Sommer, W., Rijnaarts, H., Grotenhuis, T., van Gaans, P., Sommer, W., Rijnaarts, H., Grotenhuis, T., van Gaans, P., 2012. The effect of soil heterogeneity on ATES performance. EGUGA 14, 9724.

Sommer, W., Valstar, J., Van Gaans, P., Grotenhuis, T., Rijnaarts, H., 2013. The impact of aquifer heterogeneity on the performance of aquifer thermal energy storage. Water Resour Res 49, 8128–8138. https://doi.org/10.1002/2013WR013677

Sørensen, P.A., Larsen, J., Thøgersen, L., Andersen, J.D., Østergaard, C., Schmidt, T., 2013. Boreholes in Brædstrup.

Spitler, J.D., Javed, S., Ramstad, R.K., 2016. Natural convection in groundwater-filled boreholes used as ground heat exchangers. Appl Energy 164, 352–365. https://doi.org/10.1016/J.APENERGY.2015.11.041

Steel, R.J., Thompson, D.B., 1983. Structures and textures in Triassic braided stream conglomerates (‘Bunter’ Pebble Beds) in the Sherwood Sandstone Group, North Staffordshire, England. Sedimentology 30, 341–367. https://doi.org/10.1111/J.1365-3091.1983.TB00677.X

Stemmle, R., Blum, P., Schüppler, S., Fleuchaus, P., Limoges, M., Bayer, P., Menberg, K., 2021. Environmental impacts of aquifer thermal energy storage (ATES). Renewable and Sustainable Energy Reviews 151, 111560. https://doi.org/10.1016/J.RSER.2021.111560

Stryi-Hipp, G., 2015. Renewable Heating and Cooling: Technologies and Applications. Renewable Heating and Cooling: Technologies and Applications 1–274. https://doi.org/10.1016/C2013-0-16484-7

Suberu, M.Y., Wazir Mustafa, M., Bashir, N., 2014. Energy storage systems for renewable energy power sector integration and mitigation of intermittency. Renewable and Sustainable Energy Reviews 35, 499–514. https://doi.org/10.1016/J.RSER.2014.04.009

Sun, F., Yao, Y., Li, G., Li, X., 2018. Performance of geothermal energy extraction in a horizontal well by using CO2 as the working fluid. Energy Convers Manag 171, 1529–1539. https://doi.org/10.1016/j.enconman.2018.06.092

Tamme, R., Laing, D., Steinmann, W.-D., Bauer, T., 2012. Thermal Energy Storage. Encyclopedia of Sustainability Science and Technology 10551–10577. https://doi.org/10.1007/978-1-4419-0851-3_684

Tao, R., Sharifzadeh, M., Zhang, Y., Feng, X.T., 2020. Analysis of Mafic rocks Microstructure damage and failure Process under Compression Test Using Quantitative Scanning Electron Microscopy and Digital Images Processing. Eng Fract Mech 231, 107019. https://doi.org/10.1016/J.ENGFRACMECH.2020.107019

Thomas, L.K., Tinjum, J.M., Holcomb, F.H., 2020. Environmental Life Cycle Assessment of a Deep Direct-use Geothermal System in Champaign, Illinois, in: Stanford University (Ed.), 45th Workshop on Geothermal Reservoir Engineering. Stanford University, Stanford, CA, USA.

Tsang, C.F., Goranson, C.B., Lippmann, M.J., Witherspoon, P.A., 1977. Modeling Underground Storage in Aquifers of Hot Water from Solar Power Systems. Berkeley, CA, USA.

Tulus, V., Boer, D., Cabeza, L.F., Jiménez, L., Guillén-Gosálbez, G., 2016. Enhanced thermal energy supply via central solar heating plants with seasonal storage: A multi-objective optimization approach. Appl Energy 181, 549–561. https://doi.org/10.1016/J.APENERGY.2016.08.037

van Lopik, J.H., Hartog, N., Zaadnoordijk, W.J., 2016. The use of salinity contrast for density difference compensation to improve the thermal recovery efficiency in high-temperature aquifer thermal energy storage systems. Hydrogeol J 24, 1255–1271. https://doi.org/10.1007/S10040-016-1366-2/TABLES/7

Vangkilde-Pedersen, T., Kallesøe, A.J., 2019. High Temperature Underground Thermal Energy Storage: Lessons Learned from Existing and Past Underground Thermal Energy Storage Systems, in: HEATSTORE (Ed.), European Workshop on Underground Energy Storage . Paris, France.

Vidal, R., Olivella, S., Saaltink, M.W., Diaz-Maurin, F., 2022a. Heat storage efficiency, ground surface uplift and thermo-hydro-mechanical phenomena for high-temperature aquifer thermal energy storage. Geothermal Energy 10, 1–27. https://doi.org/10.1186/S40517-022-00233-3/FIGURES/23

Vidal, R., Olivella, S., Saaltink, M.W., Diaz-Maurin, F., 2022b. Heat storage efficiency, ground surface uplift and thermo-hydro-mechanical phenomena for high-temperature aquifer thermal energy storage. Geothermal Energy 10, 1–27. https://doi.org/10.1186/S40517-022-00233-3/FIGURES/23

Vidler, A., Buzzi, O., Fityus, S., 2021. The Significance of Hydrophobicity for the Water Retention Properties of Sand and Coal. Applied Sciences 2021, Vol. 11, Page 5966 11, 5966. https://doi.org/10.3390/APP11135966

Vivas, C., Salehi, S., 2022. Naturally Rechargeable Thermal Energy Storage | Unpublished Manuscript. Norman, OK, USA.

Vivas, C., Salehi, S., 2021a. Machine Learning Approach to Generate Synthetic Sonic Logs in Geothermal Wells, in: In Geothermal Rising Conference, San Diego, California. Geothermal Resources Council, San Diego, CA, USA., pp. 1335–1348.

Vivas, C., Salehi, S., 2021b. Real-Time Model for Thermal Conductivity Prediction in Geothermal Wells Using Surface Drilling Data: A Machine Learning Approach, in: Stanford University (Ed.), 46th Workshop on Geothermal Reservoir Engineering Stanford University. Stanford University, Stanford, CA.

Vivas, C., Salehi, S., Tuttle, J.D., Rickard, B., 2020. Challenges and Opportunities of Geothermal Drilling for Renewable Energy Generation. GRC Transactions 44.

Voutilainen, M., Miettinen, A., Sardini, P., Parkkonen, J., Sammaljärvi, J., Gylling, B., Selroos, J.O., Yli-Kaila, M., Koskinen, L., Siitari-Kauppi, M., 2019. Characterization of spatial porosity and mineral distribution of crystalline rock using X-ray micro computed tomography, C-14-PMMA autoradiography and scanning electron microscopy. Applied Geochemistry 101, 50–61. https://doi.org/10.1016/J.APGEOCHEM.2018.12.024

Wang, H., Alvarado, V., Smith, E.R., Kaszuba, J.P., Bagdonas, D.A., McLaughlin, J.F., Quillinan, S.A., 2020. Link Between CO2-Induced Wettability and Pore Architecture Alteration. Geophys Res Lett 47, e2020GL088490. https://doi.org/10.1029/2020GL088490

Wanner, C., Eichinger, F., Jahrfeld, T., Diamond, L.W., 2017. Unraveling the Formation of Large Amounts of Calcite Scaling in Geothermal Wells in the Bavarian Molasse Basin: A Reactive Transport Modeling Approach. Procedia Earth and Planetary Science 17, 344–347. https://doi.org/10.1016/J.PROEPS.2016.12.087

Waples, D.W., Waples, J.S., 2004. A Review and Evaluation of Specific Heat Capacities of Rocks, Minerals, and Subsurface Fluids. Part 1: Minerals and Nonporous Rocks. Natural Resources Research 13.

Welsch, B., Göllner-Völker, L., Schulte, D.O., Bär, K., Sass, I., Schebek, L., 2018. Environmental and economic assessment of borehole thermal energy storage in district heating systems. Appl Energy 216, 73–90. https://doi.org/10.1016/J.APENERGY.2018.02.011

Wendt, D., Huang, H., Zhu, G., Sharan, P., McTigue, J., Kitz, K., Green, S., McLennan, J., 2019. Geologic Thermal Energy Storage of Solar Heat to Provide a Source of Dispatchable Renewable Power and Seasonal Energy Storage Capacity, in: GRC Transactions, Vol. 43.

Willemsen, A., Weiden, M.J.J.V.D., 1991. Heat Losses and Groundwater Chemistry Of The Utrecht University ATES, in: Proceedings Thermastock, 91.

Winterleitner, G., Schütz, F., Wenzlaff, C., Huenges, E., 2018. The Impact of Reservoir Heterogeneities on High-Temperature Aquifer Thermal Energy Storage Systems. A Case Study from Northern Oman. Geothermics 74, 150–162. https://doi.org/10.1016/J.GEOTHERMICS.2018.02.005

Wu, Y., Patel, H., Salehi, S., 2021. Parametric Study of Mechanical Stresses within Cement Sheath in Geothermal Wells. Geothermics 90, 102000. https://doi.org/10.1016/J.GEOTHERMICS.2020.102000

Wu, Y., Patel, H.R., Salehi, S., 2020. Thermal Considerations of Cement Integrity in Geothermal Wells, in: PROCEEDINGS, 45th Workshop on Geothermal Reservoir Engineering Stanford University, Stanford, California, February 10-12, 2020. Stanford University, Stanford, CA, USA., pp. 1–15.

Wyman, C., 1979. Thermal Energy Storage for Solar Applications: An Overview. Golden, CO, USA.

Xiang, Y., Xie, Z., Furbo, S., Wang, D., Gao, M., Fan, J., 2022. A comprehensive review on pit thermal energy storage: Technical elements, numerical approaches and recent applications. J Energy Storage 55, 105716. https://doi.org/10.1016/J.EST.2022.105716

Xu, J., Wang, R.Z., Li, Y., 2014. A review of available technologies for seasonal thermal energy storage. Solar Energy 103, 610–638. https://doi.org/10.1016/J.SOLENER.2013.06.006

Xu, T., Pruess, K., 2004. Numerical Simulation of Injectivity Effects of Mineral Scaling and Clay Swelling in a Fractured Geothermal Reservoir (Conference) | OSTI.GOV, in: Geothermal Resources Council 2004 Annual Meeting. Geothermal Resources Council, Palm Springs, CA, USA.

Zhang, H., Baeyens, J., Cáceres, G., Degrève, J., Lv, Y., 2016. Thermal energy storage: Recent developments and practical aspects. Prog Energy Combust Sci 53, 1–40. https://doi.org/10.1016/J.PECS.2015.10.003

Zhao, B., Gedler, G., Manas-Zloczower, I., Rowan, S.J., Feke, D.L., 2020. Fluid transport in open-cell polymeric foams: effect of morphology and surface wettability. SN Appl Sci 2, 1–10. https://doi.org/10.1007/S42452-020-1983-1/FIGURES/13

Zheng, Q., 2014. Design of a High Temperature Subsurface Thermal Energy Storage System. All Theses. Clemson University.

Zhou, F., Zheng, X., Zhou, F., Zheng, X., 2015. Heat Transfer in Tubing-Casing Annulus during Production Process of Geothermal Systems. Journal of Earth Science, 2015, Vol. 26, Issue 1, Pages: 116-123 26, 116–123. https://doi.org/10.1007/S12583-015-0511-5

Zhou, M., Cho, J., Zerpa, L.E., Augustine, C., 2016. Optimization of Well Configuration for a Sedimentary Enhanced Geothermal Reservoir. GRC Transactions 40.

Zoback, M.D., 2007. Reservoir Geomechanics. Cambridge University Press, University of Cambridge, Cambridge CB2 8BS, United Kingdom.

Zotzmann, J., Vetter, A., Regenspurg, S., 2018. Evaluating efficiency and stability of calcite scaling inhibitors at high pressure and high temperature in laboratory scale. Geothermal Energy 6, 1–13. https://doi.org/10.1186/S40517-018-0105-4/FIGURES/6